1989

Computer simulation of plastic deformation in irradiated metals

Üner Çolak
Iowa State University

INFORMATION TO USERS

The most advanced technology has been used to photograph and reproduce this manuscript from the microfilm master. UMI films the text directly from the original or copy submitted. Thus, some thesis and dissertation copies are in typewriter face, while others may be from any type of computer printer.

The quality of this reproduction is dependent upon the quality of the copy submitted. Broken or indistinct print, colored or poor quality illustrations and photographs, print bleedthrough, substandard margins, and improper alignment can adversely affect reproduction.

In the unlikely event that the author did not send UMI a complete manuscript and there are missing pages, these will be noted. Also, if unauthorized copyright material had to be removed, a note will indicate the deletion.

Oversize materials (e.g., maps, drawings, charts) are reproduced by sectioning the original, beginning at the upper left-hand corner and continuing from left to right in equal sections with small overlaps. Each original is also photographed in one exposure and is included in reduced form at the back of the book. These are also available as one exposure on a standard 35mm slide or as a 17" x 23" black and white photographic print for an additional charge.

Photographs included in the original manuscript have been reproduced xerographically in this copy. Higher quality 6" x 9" black and white photographic prints are available for any photographs or illustrations appearing in this copy for an additional charge. Contact UMI directly to order.

U·M·I

University Microfilms International
A Bell & Howell Information Company
300 North Zeeb Road, Ann Arbor, MI 48106-1346 USA
313/761-4700 800/521-0600

Order Number 8920118

Computer simulation of plastic deformation in irradiated metals

Çolak, Üner, Ph.D.

Iowa State University, 1989

U·M·I
300 N. Zeeb Rd.
Ann Arbor, MI 48106

Computer simulation of plastic deformation in irradiated metals

by

Üner Çolak

A Dissertation Submitted to the
Graduate Faculty in Partial Fulfillment of the
Requirements for the Degree of
DOCTOR OF PHILOSOPHY

Major: Nuclear Engineering

Approved:

Signature was redacted for privacy.

In Charge of Major Work

Signature was redacted for privacy.

For the Major Department

Signature was redacted for privacy.

For the Graduate College

Iowa State University
Ames, Iowa
1989

TABLE OF CONTENTS

ACKNOWLEDGEMENTS viii

1 INTRODUCTION 1

2 LITERATURE REVIEW 5

2.1 Defect Clusters 5

2.2 Dislocation Channeling 8

2.3 Dislocation Mobility 14

2.4 Dislocation Pile-ups 16

3 A MODEL FOR PLASTIC DEFORMATION IN IRRADIATED METALS 21

3.1 Plastic Deformation on Microscopic Scale 21

3.2 Plastic Deformation on Macroscopic Scale 42

4 RESULTS AND DISCUSSION 53

5 SUMMARY AND CONCLUSIONS 80

6 BIBLIOGRAPHY 82

7 APPENDIX: DESCRIPTION OF COMPUTER CODES . . . 87

7.1 The PILEUP Code 87

7.2 The DEFORM Code 98

LIST OF TABLES

Table 4.1: Basic properties of niobium 54

Table 4.2: Dislocation velocity parameters for niobium single crystals . 54

Table 4.3: Dislocation velocities at the upper yield stresses in unirradiated and irradiated niobium single crystals 55

Table 4.4: Properties of dislocation channels in niobium based on TEM observations 65

Table 4.5: Effect of basic parameters on the shear displacement 68

Table 4.6: Parameters used in computer simulations 69

Table 4.7: H values used in the computer simulation 71

Table 4.8: Results of computer simulations. Shear stress as a function of the numbers of active slip planes per channel, as indicated, for S range of 1.20 to 1.25 μm 74

Table 4.9: Results of computer simulations as a function of shear displacement for n=1000 76

Table 7.1: Listing of the computer code PILEUP 91

Table 7.2: Listing of the computer code DEFORM 103

LIST OF FIGURES

Figure 2.1: A TEM micrograph of an irradiated and then plastically deformed copper single crystal showing dislocation channels 10

Figure 3.1: A schematic representation of slip bands, which are observed by transmission electron microscopy as dislocation channels, as shown in Figure 2.1 22

Figure 3.2: Schematic arrangement of a pile-up of edge dislocations . . . 28

Figure 3.3: Position of the leading dislocation as a function the dynamic parameter, Θ, for various values of the stress sensitivity of dislocation velocity, m 34

Figure 3.4: Position of the leading dislocation as a function the dynamic parameter, Θ, for various β values 35

Figure 3.5: Stress concentration on the barrier, R_B, as a function of the dynamic parameter, Θ, for various m values 37

Figure 3.6: Stress concentration on the barrier, R_B, as a function of the dynamic parameter, Θ, for various β values 38

Figure 3.7: Normalized strain parameter H as a function of the dynamic parameter, Θ, for various m values 40

Figure 3.8: Normalized strain parameter H as a function of the dynamic parameter, Θ for various β values 41

Figure 3.9: Shear displacement produced by the movements of edge dislocations in a crystal 43

Figure 3.10: Shear displacement S in a dislocation channel 47

Figure 3.11: Intersected dislocation channels in an irradiated Nb single crystal 49

Figure 4.1: Variation of the upper yield stress with the neutron fluence in niobium 56

Figure 4.2: Position of the leading dislocation in a dislocation pile-up in niobium single crystals for a 50 μm long pile-up as a function of time from the emission of the first dislocation by the source. The shear stress corresponds to the critical resolved shear stress (28.9 MPa for Sample #3 and 40.5 MPa for Sample #4) 57

Figure 4.3: Stress concentration factor R_B as a function of time in niobium single crystals. Pile-up length and shear stresses are the same as for Figure 4.2 59

Figure 4.4: Relative velocity profiles of the leading dislocations in niobium single crystals. Pile-up length and shear stresses are the same as for Figure 4.2 61

Figure 4.5: Relative velocity profiles of dislocations in the pile-up 62

Figure 4.6: Locations of dislocations as a function of time 63

Figure 4.7: Computer simulation results. Shear stress as a function of engineering strain with different number of active planes per channel as indicated and for S range of 1.20 to 1.25 μm . . 73

Figure 4.8: Shear stress-engineering strain curve for the irradiated niobium crystal, earlier experimental results and computer simulation in this study 77

ACKNOWLEDGEMENTS

I would like to thank to my major professor, Dr. Monroe S. Wechsler for his invaluable guidance, suggestions, and advice during the course of this study. I wish to thank to Dr. Otto Buck who taught me the essentials of mechanical metallurgy which is the basis for this study. Sincere thanks go to Drs. Otto Buck, Richard A. Danofsky, Alfred F. Rohach, and Thomas J. Rudolphi for their valuable suggestions as committee members. I would also thank Niyazi Sökmen for sharing his knowledge in all computer related activities without any hesitation. I would like to extend my appreciation to Zekeriya Altaç, Niyazi Sökmen, and Ramin Mikaili for their friendship and valuable suggestions. My special thanks are due to my special friend, Nur, for her support, encouragment, and patience, and to my sons, Deniz and Arda for being with us.

1 INTRODUCTION

Nuclear power is an inevitable solution for the increasing energy demand in the world. One of the major concerns associated with nuclear power is safety. Prediction of material behavior in the hostile reactor environment is an important consideration from this view. Understanding the response of materials may help the development of new materials with more desirable properties. An important consideration is the mechanical behavior of materials, or more specifically, plastic deformation.

Plastic deformation in a single crystal material is an inhomogeneous phenomenon due to the nature of the slip process. The assumption of homogeneity may be justified if deformation takes place uniformly in a large portion of the crystal. However, to make this assumption in irradiated metals is somewhat inadequate. Observations [1] show that plastic deformation takes place in regions called dislocation channels separated by undeformed regions. It has been shown that radiation produced defect clusters, i.e., planar vacancy and interstitial aggregates or small prismatic dislocation loops, are responsible for hardening the metal. Hardening is observed upon irradiation by an increase in yield strength of material, i.e., the initiation of plastic deformation is delayed until a higher stress level is reached. After the initiation, defect clusters in the channel region are cleared out so that

subsequent dislocations encounter fewer defect clusters. However, the mobility of dislocations does not significantly change because of the formation of jogs on moving slip dislocations [2].

In general, the interaction between dislocations is so complex that to account for every individual event in the whole process is almost impossible. The development of dislocation channels may be regarded as a process that involves the mutual interaction of all kinds of microstructural irregularities, like point defects, defect clusters, impurity atoms, inclusions, and dislocations. Therefore, development of a mathematical model that estimates, even approximately, the true nature of the process is formidable. There are several models proposed for the interaction of a slip dislocation and a defect cluster [3,4,5]. It should be remembered that the density of defect clusters in irradiated material is very high. For instance, it is 7.4×10^{21} m^{-3} in niobium irradiated to 1.8×10^{18} n/cm^2 [6]. The number of such interactions is so large that to deduce any conceivable model for the macroscopic response of the material in terms of single microscopic events is not feasible. Furthermore, dislocations do not act as single entities, but their behavior is correlated in a manner that depends on the arrangement of many microscopic features.

To make simplifications in a model that could account for the whole process is necessary in view of all these difficulties. The degree of simplification also depends on the scale that is considered. For instance, if the formation of a dislocation channel is analyzed on a scale of a small fraction of a micron, the interactions between individual dislocations and defect clusters may be considered. On a larger scale, say 100 μm, interactions between dislocation groups may be treated by regarding each group as a single entity. On a still larger scale, the effect of individual channels

on the macroscopic shape change during deformation may be studied based on the assumption of uniform deformation within the channel. The last idea is incorporated in the present study.

The purpose of this research is to develop a model that can relate the macroscopic deformation process (external shape change of a sheet tensile sample in two dimensions) to the motion of dislocations for a sheet metal sample deformed uniaxially at a constant macroscopic strain rate. Then, a computer program based on this model is developed to simulate the plastic deformation. The simulation is performed for an irradiated niobium single crystal. Comparison is made with the experimental observations in terms of a shear stress-engineering strain curve.

Plastic deformation is the consequence of the motion of dislocations in the channel. Dislocations are emitted by sources distributed within the channel. After the activation of these sources, a particular dislocation moves considerable distances as a result of, not only the applied stress, but also the stresses on it due to other dislocations. Then, dislocations form large arrays by piling up against some kinds of barriers, like inclusions or forest dislocations, in the matrix. Formation time for a single dislocation channel is short enough so that dislocations do not have sufficient time to produce large stress concentrations to break through these barriers. On the other hand, the time period is long enough so that dislocations move considerable distances to produce sufficient shear displacement and tensile strain. Activity of dislocations in a channel continues up to a certain local shear displacement and further development is prohibited by a large amount of local work hardening. At this point, the applied stress must be increased to maintain the prescribed tensile strain rate, and dislocation sources are activated at other locations of the crystal.

Shear displacement per channel is calculated based on the distances traveled by dislocations which form pile-ups of various lengths. Then, the microscopic shear displacement is calculated for the current applied shear stress τ_a. An appropriate value of τ_a is selected such that the crosshead speed of the tensile machine is kept constant at its prescribed value. External shape change is performed by the application of calculated displacement fields in the deforming channel. Thus, a slip step is produced on the surface of the sample. Then, the progress of plastic deformation is followed by the formation of many dislocation channels. The results of these calculations provide the information about the relation between the applied stress and macroscopic strain at a constant strain rate, thus providing strain-stress curves based on the model that can be compared with experimental strain-stress curves obtained in tensile tests.

2 LITERATURE REVIEW

Efforts to understand the mechanism of plastic deformation in metals, irradiated and unirradiated, have yielded a large number of publications. This makes it difficult to make an attempt for a complete historical review of the literature to the present date. Instead of a complete review, background information for the present study with some typical examples will be presented. This will consist of the following topics; (i) defect clusters, (ii) dislocation channeling, (iii) dislocation mobility, and (iv) dislocation pile-ups.

2.1 Defect Clusters

As the result of irradiation of metals by energetic particles, changes in the microstructure are observed. Collision of these particles with host metal atoms and, then, secondary collisions between host atoms result in the formation of collision cascades which contain dense concentrations of interstitial atoms and vacancies. If the irradiation temperature is high enough to mobilize the interstitials and vacancies, they may agglomerate and form defect clusters, which are essentially small prismatic dislocation loops.

The basic effect of defect clusters in the deformation behavior of the metal is radiation hardening. The stress required to initiate plastic deformation or yielding

increases, if defect clusters are present in the matrix. This is due to the action of defect clusters as barriers to the motion of slip dislocations. Radiation produced defect clusters serve as pinning points to slip dislocations. A dislocation impeded by defect clusters will bow between these barriers until it reaches an unstable configuration that is a semicircle. At this point, the barrier is encircled by a segment of the dislocation as in the Orowan process. The stress reaches a level, the critical shear stress τ_C, that is necessary to move dislocations through the arrays of barriers. The critical shear stress is inversely proportional to interbarrier spacing [7]. In addition, the radiation-produced barriers cause an increase in flow stress, the stress necessary to continue yielding at a constant strain rate.

The first observation of defect clusters by transmission electron microscopy (TEM) was reported in copper irradiated to fluences in the range from 6.7×10^{17} to 1.4×10^{20} neutrons/cm^2 (E > 1 MeV) by Silcox and Hirsch [8]. These defect clusters were assumed to be vacancy type. The character (vacancy or interstitial type) of defect clusters has been subject to a great controversy. Several investigators including Crump [9] and Wilkens and Rühle [10] reported vacancy type defect clusters in neutron irradiated copper. On the other hand, McIntyre and Brown [11] observed an interstitial type of defect clusters.

Irradiation fluence is an important parameter, as well as the irradiation temperature. For the formation of defect clusters, the fluence must be high enough as the first condition to ensure a sufficient number of radiation produced point defects. Tucker and Wechsler [6] analyzed the density and size distribution of defect clusters as a function of neutron fluence in single and polycrystal niobium irradiated to fluences from 2×10^{17} to 4.4×10^{18} neutrons/cm^2 (E > 1 MeV). According to their

observations, defect cluster size has a peaked distribution. At low fluences (below about 2×10^{18} neutrons/cm^2 (E > 1 MeV)), the defect clusters are small in size and the defect cluster density of all sizes is high. On the contrary, at high fluences, above 2×10^{18} neutrons/cm^2 (E > 1 MeV), the distribution shifts to larger sizes and the total density decreases.

Defect clusters may be observed after irradiation at very low temperatures. As the temperature increases smaller defect clusters will agglomerate and form larger defect clusters. Therefore, defect cluster density decreases and the size of defect clusters increases with increasing temperature. At still higher temperatures defect clusters will anneal out, i.e., dissociate into constituents. Makin and Manthorpe [12] measured the density and size of defect clusters in neutron irradiated copper as a function of post-irradiation annealing temperature. They observed that recovery takes place at 275^{o}C in two stages. First, sub-microscopic vacancy clusters thermally dissociate and a large portion of interstitial atoms in large clusters (diameter > 50 Å) are annihilated within a few tens of minutes. Meanwhile, large size vacancy clusters get more stable and larger. In the second stage, large vacancy clusters and remaining interstitial clusters disappear in about several thousand minutes.

Another important factor is the presence of impurity atoms which may serve as the nucleation sites for the defect clusters and form small impurity-defect aggregates. Impurity atoms greatly affect the structure and properties of defect clusters especially in BCC metals. The defect cluster density and size distribution were analyzed for the irradiated and post-irradiation annealed conditions in high purity single crystal vanadium containing oxygen as impurity atoms with concentrations ranging from 95 to 500 wt. ppm [13]. The results showed that the density of defect

clusters increases with increasing oxygen concentration. The size distribution of defect clusters had a peaked shape and the peak shifted toward larger sizes with increasing oxygen concentration. Furthermore, increasing oxygen concentration also caused an increase in the stability of defect clusters, i.e., the annealing of defect clusters started at higher temperatures.

The energy spectrum of the irradiating particles is also another factor since particles with higher energies will produce a greater number of point defects. For this reason, experimental observations may differ quantitatively from one reactor to another depending upon the neutron energy spectrum.

2.2 Dislocation Channeling

While radiation hardening in metals was being investigated, it was also observed that plastic deformation tends to be localized in coarse slip bands in which defect clusters have been removed, i.e., dislocation channels. One of the first observations of dislocation channeling was reported by Greenfield and Wilsdorf [14] for high purity copper which was irradiated to about 10^{17} fast neutrons/cm^2. Later, it was suggested that the slip markings on the surface of irradiated copper single crystals correspond to the dislocation channels in the interior of the crystal [15], in which the defect clusters were removed.

The first systematic study of dislocation channeling is due to Sharp [16], who analyzed the width of the dislocation channels in copper single crystals irradiated to about 10^{18} n/cm^2 as a function of temperature, dose and strain by transmission electron microscopy techniques. Then, this information was compared with surface replicas. This showed a strong correspondence between surface slip steps observed

in the replicas and dislocation channels. The correspondence can be seen for the dislocation channels in irradiated copper [17], as shown in Figure 2.1.

Even though first observations of dislocation channeling had been for copper, it has been observed in many other irradiated metals with different crystal structures. Dislocation channeling is not a unique process for irradiated crystals. Similar observations have also been made for quenched and deformed crystals [18,19].

A possible mechanism for the formation of dislocation channels was first proposed by Cottrell [20]. He suggested that dislocations moving on a slip plane sweep away radiation produced defect clusters and clear the channel. Then, subsequent dislocations move more easily on the slip plane. Later, a similar model with more details was introduced by Saada and Washburn [3]. In this model it was proposed that a part of the defect cluster (prismatic dislocation loop) becomes incorporated with the slip dislocation when the Burgers vectors of both the loop and slip dislocation are in the same direction. A smaller loop remains after the dislocation passes through. The next dislocation therefore interacts with a smaller defect cluster. When many dislocations move along the slip plane, it becomes free of defect clusters due to subsequent size reduction. Later, Foreman [4] and Foreman and Sharp [5] developed a more elaborate model based on the same idea.

A second possible mechanism is the annihilation of defect clusters by antidefects [21]. As an example for this process annihilation of interstitial type defect clusters may be given. Vacancies may be created during the nonconservative motion of jogs associated with slip dislocations. These vacancies may then be associated with defect clusters of interstitial type. This process results in mutual annihilation of defects.

Figure 2.1: A TEM micrograph of an irradiated and then plastically deformed copper single crystal showing dislocation channels (at arrows). Region S is the sample, and region E is an electroplated region that was applied after deformation and before thinning and examination in the electron microscope [17]

Tucker et al. [21] proposed still another mechanism for the removal of defect clusters which is due to the heating effect of plastic deformation. A large fraction, about 90%, of the energy of plastic deformation is transformed into heat. Since plastic deformation in irradiated metals takes place only in dislocation channels and the local strain rate is very high, there is not enough time for the conduction of heat into undeformed portions of the material. The local temperature increase in this condition was estimated to be 80^oC in irradiated and deformed Nb crystals if the energy of the plastic deformation is equally distributed among all atoms in the channel. This temperature increase greatly helps defect clusters to anneal out.

Sharp [17] indicated that partially formed slip bands are not observed and all slip bands in copper are fully developed. In general, shear strain is uniformly distributed within the central region of the slip band and is about 700%. Shear strain decreases in regions closer to the surface of the sample. It was thought to be due to the necessity of large applied stress to initiate the slip band formation. During the channel formation period the effective stress is high enough so that screw dislocations are able to cross slip to activate slip in neighboring planes.

Sharp also investigated the deformation characteristics of irradiated copper alloys and compared the results with irradiated pure copper [22]. The basic differences are the necessity of higher critical resolved shear stress for the alloys, a smaller average shear per slip line, and a reduction in the slip band spacing for alloys. The characteristics of deformation for Cu-0.8% Co crystals were similar to the irradiated copper possibly due to having a deformable second phase. However, internally oxidized Cu-0.05 wt.% Al, i.e., Cu-Al_2O_3, crystals showed great difficulty for deforming the second phase, which results in a large increase in dislocation density

and wider and more irregular channels.

Irradiation hardening and annealing in copper irradiated to high fluences (up to 8×10^{20} n/cm^2) were analyzed in connection with dislocation channeling by Howe [23]. It was reported that the slip band width, spacing, and height increased with increasing test temperature. Furthermore, radiation produced defect clusters removed in the early stages of annealing were more effective barriers to slip dislocations at low temperatures (4°K) than at 295°K. For certain annealing conditions, dislocations bowed around the defects rather than removing them.

Neuhäuser and Rodloff [24] used a high speed cinematography technique to analyze the development of slip bands in neutron irradiated copper single crystals. They emphasize the effect of local stress for the development of slip line clusters. According to their observations, many slip line clusters combine and form a slip band. Formation of a slip band also gives rise to work hardening as a result of high local strain (about $400 - 1500\%$) in the slip band. This work hardening gives some resistance to the motion of dislocations and prevents the formation of a new slip band within a certain distance from the existing one. Termination of the slip band development was attributed to local stress relaxation, work hardening, and defect production at high strain. High speed cinematography technique was also used to evaluate the velocity and local density of mobile dislocations [25] and the mean velocity of edge and screw dislocations [2] in neutron-irradiated copper crystals. It was observed that radiation-produced defect clusters are removed. However, the effect of defect clusters on the mobility of slip dislocations is balanced by the drag force produced by jogs.

Shinohara et al. [26] measured the velocity of dislocations in neutron-irradiated

copper single crystals by distinguishing edge and screw dislocations by etch-pit and microcinematography techniques. Results showed that edge dislocations move larger distances than screw dislocations do in stage I (easy glide region) as opposed to Rodloff and Neuhäuser's [2] observations.

Mughrabi et al. [27] analyzed the effect of neutron irradiation on the plastic deformation of α-iron single crystals by slip line observations, transmission electron microscopy, and x-ray topography techniques. It was observed that coarse slip lines are connected by cross slip. The average step height was 3×10^{-6} m and the average spacing of slip bands was 2×10^{-5} m. It was also noted that localized deformation in irradiated BCC crystals promotes crystallographic slip, which is not generally observed in unirradiated BCC crystals.

Dynamic formation of dislocation channels in neutron irradiated copper crystals was observed in a high voltage electron microscope by Johnson and Hirsch [28]. The active slip system was always found to be the one with the highest resolved shear stress. Formation of channels was promoted by sweeping up radiation-produced defect clusters by slip dislocations forming superjogs. Dislocations in the channels were mostly screw type. Edge dislocations were assumed to leave the crystal shortly after being emitted because of the geometry of the sample.

Nathanson et al. [29] reported etch pit and TEM observations in irradiated copper crystals. They indicated that secondary dislocation production, which takes place in the regions neighboring the slipped parts of the crystal, is the basic factor which determines the slip band spacing as an alternative to long range elastic interactions between dislocation channels. Secondary slip is associated with cross slip of screw dislocations. Secondary slip systems are activated by the local stress

concentrations due to overlapping edge dislocation arrays of opposite sign which form as a result of double cross slip.

Although observations and proposed models give some insight about dislocation channeling, detailed knowledge to account for initiation, formation, and termination of dislocation channels is still nonexistent due to the complex nature of the channels. In most cases, the formation of an irregular dislocation structure within and around the channel makes it difficult to develop an accurate mathematical model. For this reason, proposed models are oversimplified because of drastic assumptions.

2.3 Dislocation Mobility

The motion of dislocations is the necessary condition for the plastic deformation of metals. Basically, there are two types of dislocation motion. Conservative motion, or slip, is the movement of dislocations on the plane which contains the dislocation line and the Burgers vector. This is the most common mode for plastic deformation especially at low temperatures. If dislocation moves out of the slip plane normal to the Burgers vector it is called dislocation climb, which is an important process at high temperatures due to sufficient mobility of vacancy and interstitials. There is still a third process, cross slip, which is unique for screw dislocations. For screw dislocations, the Burgers vector and the dislocation line are in the same direction (and the line must be straight). In cross slip, the screw dislocation leaves the original slip plane and moves in another slip plane, where both planes contain the Burgers vector and line direction. If the cross-slipped dislocation finally returns to a plane parallel to the original slip plane, the process is called double cross slip. Cross slip is an important phenomenon for BCC metals due to the presence of several

slip systems. It is the major reason for the observation of wavy slip lines in BCC crystals.

Since dislocations are the principal ingredients of plastic deformation in metals, the velocity of dislocations is the basic parameter which determines the deformation rate. The current knowledge about the velocity of dislocations as a function of applied stress is mostly empirical and may not be very accurate, especially in the very high velocity region. In the classical work by Gilman and Johnston [30] the velocity of dislocations in LiF was measured as a function of applied shear stress by the etch-pit technique. Later, this method was used for the measurement of dislocation velocities for other materials such as Fe-Si [31] and Cu [32]. As far as dislocation mobility in irradiated metals is concerned, there are only few experimental measurements. First, Guberman [33] measured the dislocation velocity as a function of stress and neutron fluence in irradiated niobium single crystals by the etch-pit technique. Wada et al. [34] measured the stress dependency of dislocation velocity as a function of fluence and temperature in electron irradiated copper single crystals. Due to the strong temperature dependency, results were analyzed in terms of a thermal activation process.

The stress dependence of the dislocation velocity has been expressed in many different forms [35]. In the low velocity region, dislocation velocity is strongly stress dependent and thermal activation is an important factor which determines the velocity. The most commonly used relation for this region is

$$v = K\tau_a^m \tag{2.1}$$

where v is dislocation velocity, τ_a is shear stress, and K and m are material parameters. m is also known as the stress sensitivity of dislocation velocity. In the

high velocity region, the velocity-stress relation is linear and viscous drag is the rate controlling mechanism. A typical relation for this region is

$$v = b\tau_a/B \tag{2.2}$$

where b is the Burgers vector and B is drag coefficient. There is still another expression which has been used for the region of medium and high stresses

$$v = v_s e^{-D/\tau_a} \tag{2.3}$$

where v_s is the shear wave velocity and D is a material parameter with dimensions of stress.

Since plastic deformation is widely accepted as a thermally activated phenomenon, the above relations are sometimes modified to include parameters such as activation energy and temperature. In general these equations accurately represent the behavior of dislocation at low velocities. When observed velocity-stress values are plotted on log-log paper, the slope of the curve decreases in the high velocity region. Here, the velocity approaches the elastic shear wave velocity in the material which is the limiting velocity.

The motion of dislocations emitted by a source is influenced by many factors and it is very different than it is for an isolated dislocation. The basic factors which determine the velocity of dislocations are lattice friction and stress fields of other microstructural features such as other dislocations, impurity atoms, and inclusions.

2.4 Dislocation Pile-ups

When dislocations emitted from a source encounter a strong barrier that is difficult to break, they pile-up against this barrier. During the formation of the

pile-up, the leading dislocation is moved not only by the applied stress but also by the force exerted by the other dislocations in the array. Therefore, the stress concentration at the tip of the pile-up may be many times greater than the applied stress itself. The formation of a pile-up continues until the force on the leading dislocation is great enough to penetrate through the barrier. If the material has a high stacking-fault energy, screw dislocations easily cross-slip and continue to move in other planes. However, edge dislocations cannot cross-slip, and they must pile-up against the barrier. The stress concentration at the tip of the pile-up depends on the number of dislocations and their distribution.

Mathematical analyses of dislocation pile-ups are generally based on two different methods. The first method considers each dislocation as a single entity and is called the discrete method. This method provides more accurate analysis as long as adequate stress fields of dislocations are employed. If the number of dislocations in the pile-up is large, this method is not feasible due to the necessity of a separate equation for each dislocation whether under dynamic condition or equilibrium. If the pile-up is long and the distance between dislocations is short compared to the length of the pile-up, the second method, i.e., the continuum method, may be used. In this method, individual dislocations in the pile-up are replaced by a continuous distribution of smeared-out dislocations.

Eshelby et al. [36] considered a pile-up of N discrete dislocations at equilibrium under a uniform external stress and determined the positions of individual dislocations by an approximate analytical method. Under equilibrium conditions, the number of dislocations in the pile-up is

$$N = \frac{\ell \tau a}{A} \tag{2.4}$$

where ℓ is the length of the pile-up, τ_a is the shear stress, and A is $Gb/2\pi(1-\nu)$ for edge dislocations and $Gb/2\pi$ for screw dislocations. G, b, and ν are the shear modulus, the magnitude of the Burgers vector, and Poisson's ratio for the material. The stress at the tip is n times greater than τ_a.

Head and Louat [37] used the continuum approach and proposed the following singular integral equation to evaluate the distribution of dislocations in pile-ups under equilibrium in domain D.

$$\int_D \frac{f(x)}{x-x_o}dx - \frac{T(x_o)}{A} = \frac{\tau(x_o)}{A} \tag{2.5}$$

where $f(x)$ is the distribution function of dislocations, $T(x_o)$ and $\tau(x_o)$ are the appropriate short range and the applied stress at point x_o. They obtained a number of analytical solutions for this equation with different conditions by means of the inversion theorem. For instance, for a pile-up with N positive dislocations, in the region $0 < x < a$, forcing against a barrier at $x = 0$ by a constant stress $\tau(x) = -\tau_a$, $f(x)$ turns out be

$$f(x) = \frac{\tau_a}{\pi A}\sqrt{\frac{a-x}{x}} \tag{2.6}$$

a should be determined by

$$N = \int_0^a f(x)dx \tag{2.7}$$

The period of time to reach equilibrium in a pile-up depends on the mobility and stress sensitivity of dislocations. In most cases it is a very long period of time and never achieved during the testing of the material. For this reason, pile-ups may be considered as dynamic dislocation arrays. Rosenfield and Hahn [38] calculated the positions of dislocations as a function of time during the evolution of the pile-up

for up to twenty dislocations. The stress-velocity relation used in this work was the exponential form similar to Equation 2.3.

Later, Kanninen and Rosenfield [39] introduced the feature of sequential dislocation emission by the source in a single-ended pile-up against a single locked dislocation. In this work, a linear relation between the shear stress and the dislocation velocity was used. They calculated the stress exerted on the source and the barrier as a function of time for pile-ups containing up to twenty dislocations. The same investigators then used a nonlinear stress-velocity relation which is more realistic when the magnitude of internal stress is not negligible. According to their results, time required for pile-up formation increases as the stress sensitivity of dislocation velocity, m in Equation 2.1, increases, and pile-up formation is not likely to be complete especially for pure BCC metals [40].

Yokobori et al. [41] used the same nonlinear stress-velocity relation. However, the analysis was expanded to a constant stress rate instead of a constant stress. Their results show that the effective stress acting on the leading dislocation and the velocity of this dislocation are nearly equal to their values for an isolated dislocation.

Gerstle and Dvorak [42] introduced removable viscous barriers in place of the rigid barriers used in previous analyses. The stress-velocity was exponential and the stress was constant. They simulated the yielding behavior of materials. In their model, yielding starts when the viscous barrier cannot support the pile-up any longer due to the stress concentration at the tip.

Zaitsev and Nadgornii [43] analyzed the motion of dislocations in a double-ended pile-up which contains equally spaced removable barriers. Dislocations emitted by the source move for a period of time, i.e., run time, t_r. Then, they wait in

front of the barrier for the waiting time, t_w, until thermal activation takes places for the removal of the barrier. t_r was considered to be negligible compared to the waiting time. The waiting time was calculated by a Monte Carlo procedure. They found good agreement between their calculations and experimental observations for NaCl crystals.

There is not much work done for the case of the collective motion of curved dislocations. Steif and Clifton [44] simulated the expansion of dislocation loops emitted by a Frank-Read source. The expansion of loops was formulated such that the applied stress, viscous drag force and interaction forces due to the other dislocations could be taken into account. They concluded that the effect of interaction between dislocations is not very significant for the expansion of dislocations. On the other hand, nucleation time is the critical parameter for the determination of the plastic deformation rate.

Rosenfield analyzed the change with time of a continuous distribution of moving dislocations under non-equilibrium conditions [45]. He used a linear relation between dislocation velocity and stress, and applied the conservation condition

$$\frac{\partial J}{\partial x} = -\frac{\partial \rho}{\partial t} \tag{2.8}$$

where $J = \rho v$ and ρ is the linear density of dislocations. Starting with an artificial initial expression for ρ as a function of distance, x, along the slip plane, he was able to follow the shape of $\rho(x)$ as a function of time.

3 A MODEL FOR PLASTIC DEFORMATION IN IRRADIATED METALS

In this study, a simplified model for the plastic deformation of irradiated metals is developed. This model is made up of two main parts. First, plastic deformation via formation of dislocation channels will be analyzed on a microscopic scale based on the formation of dynamic dislocation pile-ups. Then, the microscopic process will be related to the macroscopic shape change for a single crystal metal sheet sample. A computer program is developed based on this model to simulate the deformation of the sample under uniaxial tension and constant strain rate for plane strain condition. Results of the calculations will be presented in Chapter 4. In this chapter, deformation characteristics of irradiated metals are discussed. Then, the model is presented.

3.1 Plastic Deformation on Microscopic Scale

Plastic deformation in irradiated metals is concentrated in coarse slip bands, known as dislocation channels. These bands are separated by undeformed regions. Each channel consists of a number of parallel slip planes. A typical dislocation channel is schematically shown in Figure 3.1. Shear displacement, and eventually a surface slip step, is produced by the movement of dislocations in the channel.

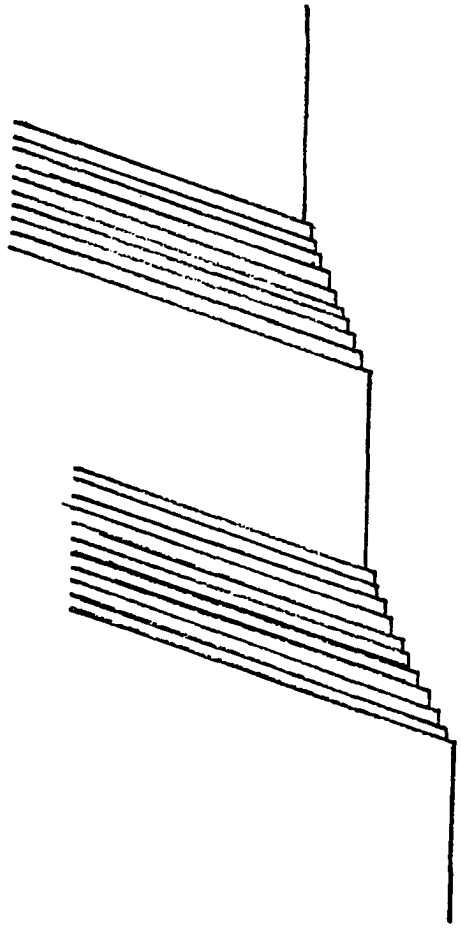

Figure 3.1: A schematic representation of slip bands, which are observed by transmission electron microscopy as dislocation channels, as shown in Figure 2.1

This also results in an axial extension of the sample. An irregular dislocation accumulation takes place at the interface of the channel and the undeformed matrix. Furthermore, dislocation tangles are frequently observed at the intersections of two dislocation channels [21].

Most dislocation channels have a uniform width and are uniformly spaced along the sample. There is not any detailed information about the initiation of dislocation channels. However, once a channel is initiated, it eventually becomes fully developed [17], i.e., partially formed dislocation channels are rarely, if ever, observed. Thus, the formation of a dislocation channel takes a short period of time. Therefore, the local shear strain is very high and can easily reach several hundred per cent. Thus, dislocation channeling is associated with high local strain rate, even if the imposed macroscopic strain rate is low [35].

Dislocations on each plane move considerable distances until they become immobilized due to the their interaction with other microstructural features. An important kind of interaction in irradiated metals takes place between slip dislocations and radiation produced defect clusters. The drastic reduction in defect cluster density upon the formation of dislocation channels suggests that defect clusters are removed by the slip dislocations [21]. However, it is difficult to observe the removal of defect clusters instantaneously in the HVEM due to the lack of dynamic recording during straining [28]. On the other hand, defect cluster counts inside and outside the channel verify that defect clusters are removed within the slip band upon post-irradiation plastic deformation. Contrary to the thought of an increase in the mobility of subsequent dislocations due to the removal of defect clusters [46], it was later suggested that the formation of jogs on the moving dislocations balances

the effect and the mobility is not greatly affected [2]. Therefore, any decrease in the flow stress following dislocation channel formation is not generally observed.

Formation of dislocation channels can be discussed on an irradiated metal sample that is a "perfect" crystal prior to the irradiation. Normally, the dislocation density in a "perfect" pure metal crystal is about 10^{10} m^{-2}. These dislocations may act as source or barrier for dislocations. Irradiation introduces defect clusters to the microstructure. If this irradiated metal is deformed beyond the yield point, dislocations start moving and cause a shear displacement in the lattice. The surface of the crystal plays an important role in the plasticity of material. Since there is a stress concentration on the surface due to the high degree of imperfection, the surface is likely to act as a dislocation source. These sources emit dislocations easier than internal dislocation sources, such as precipitates, voids, and subboundaries. Once dislocations are emitted by surface sources, the propagation of dislocations through the crystal results in stress concentrations, which help the activation of internal sources. Dislocations emitted by a source move on the same slip plane and produce an additional force on each other. If there is a barrier like a forest dislocation or a precipitate on the slip plane, dislocations pile up against the barrier. Dislocations moving on other slip planes also produce a force. However, the magnitudes of these forces are smaller and the component of the force along the glide direction becomes negligible if the slip planes are sufficiently distant.

Mobility of dislocations depends on the magnitude of the applied shear stress as well as internal stress produced by dislocations. Another important factor is the crystal structure. The force which opposes the slip of dislocations, also known as lattice friction or the Peierls-Nabarro force, is a strong function of atomic arrange-

ments in the crystal and the dislocation core structure. This force is usually low in close-packed structures like FCC and HCP. This is because of weak interatomic bonds across the slip plane so that the activation energy and the stress are low to move dislocations. However, lattice friction stress is high in BCC metals especially for screw dislocations and it may be comparable with the yield stress in magnitude. Flow stress is also strongly temperature dependent. In addition, it is difficult to reduce the interstitial impurity concentration in BCC metal crystals. Interstitial impurities also cause a strong temperature dependence and additional hardening.

Radiation produced defect clusters hinder the motion of slip dislocations by producing short range stress fields. Removal of defect clusters is due to the concentration of stress against them by collective action of slip dislocations. When the stress concentration reaches the critical stress level of defect clusters, dislocations break through defect clusters. The effect of these interactions on defect clusters is thought to be a decrease in the size of defect clusters. When the slip dislocations intersect each other, jogs and kinks are produced on the slip dislocations. Kinks are usually unstable and easily removed during the further slip of dislocations. However, jogs are more stable and immobilize dislocations.

To assess the amount of deformation produced within the channel, the total distance traveled by dislocations should be known. Although deformation is not uniform on a macroscopic scale, the uniformity of deformation may be justified within the dislocation channels. Deformation takes place in a large portion of the channel region by the simultaneous motion of dislocations over a great number of slip planes.

The formation of a dislocation channel is likely to be started by the emission

of dislocations by surface sources. The location of the channel along the sample is determined by the level of imperfection of the surface at this location and the hardening behavior of the crystal. The slip band is propagated to the interior parts of the crystal by activation of interior dislocation sources. The distance traveled by a dislocation depends on the mobility of the dislocation as well as the deformation history of the material. In the early stages of deformation, i.e., easy glide region, dislocations in FCC metals transverse a large portion of the slip plane. For BCC metals, the easy glide region is usually very limited and dislocations travel shorter distances in the work hardening region. One of the important factors that affect this distance is the presence of barriers to dislocation motion on the slip plane.

In the model that is presented in this work, the special arrangement of dislocations in the presence of a source and a barrier on the slip plane will be considered. Therefore, the traveling distance of dislocations is limited by the source-to-barrier distance. Each source is associated with a critical stress for the emission of a new dislocation. Right after the emission of the first dislocation, the distance between the source and the dislocation is so small that the stress field of the dislocation produces a large back stress on the source. The emission of the next dislocation is delayed until the previous dislocation is sufficiently far from the source. In the later stages of the pile-up formation when there are a number of dislocations in the queue, stress on the source should be evaluated by considering the stress fields of all dislocations acting on the source.

Stress on a specific dislocation in the pile-up depends on the arrangement of dislocations as well as the distance between the source and the barrier. Dislocations in metals are not perfectly straight. Bowing frequently takes place due to the applied

stress and the interactions between dislocations and other lattice defects. However, consideration of interactions between irregularly curved dislocations causes many complications in the mathematical analysis. For this kind of interaction, stress fields of small straight segments may be piecewise considered. On the other hand, this requires detailed information about the exact shape of the dislocation and it is not feasible to use this approximation for the interaction between many dislocations. To avoid extra complications, long and straight dislocations may be taken into account. Components of the stress tensor for a screw dislocation with the Burgers vector and the dislocation line along the z direction are [47]

$$\sigma_{xz} = \sigma_{zx} = -\frac{Gb}{2\pi}\frac{y}{(x^2+y^2)} \tag{3.1}$$

$$\sigma_{yz} = \sigma_{zy} = \frac{Gb}{2\pi}\frac{x}{(x^2+y^2)} \tag{3.2}$$

$$\sigma_{xx} = \sigma_{yy} = \sigma_{zz} = \sigma_{xy} = \sigma_{yx} = 0 \tag{3.3}$$

For the case of an edge dislocation along z with the Burgers vector in the x direction, the stress fields are

$$\sigma_{xx} = -\frac{Gb}{2\pi(1-\nu)}\frac{y(3x^2+y^2)}{(x^2+y^2)^2} \tag{3.4}$$

$$\sigma_{yy} = \frac{Gb}{2\pi(1-\nu)}\frac{y(x^2-y^2)}{(x^2+y^2)^2} \tag{3.5}$$

$$\sigma_{xy} = \sigma_{yx} = \frac{Gb}{2\pi(1-\nu)}\frac{x(x^2-y^2)}{(x^2+y^2)^2} \tag{3.6}$$

$$\sigma_{zz} = \nu(\sigma_{xx}+\sigma_{yy}) \tag{3.7}$$

$$\sigma_{xz} = \sigma_{yz} = \sigma_{zx} = \sigma_{zy} = 0 \tag{3.8}$$

The slip plane is considered to be the xz plane, and therefore $y = 0$. By considering the directions of the Burgers vectors of these two types of dislocations,

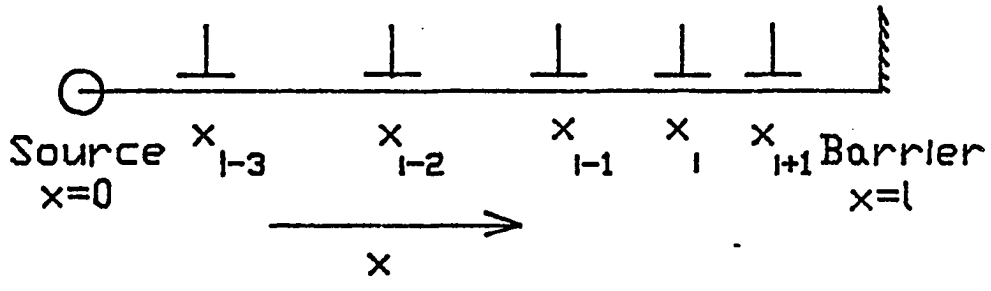

Figure 3.2: Schematic arrangement of a pile-up of edge dislocations

the slip direction may be chosen to be the x direction for edge dislocations and the z direction for screw dislocations. There is only one nonzero component of the stress tensor for each dislocation in this configuration. For screw dislocations, it is

$$\sigma_{yz} = \frac{Gb}{2\pi}\frac{1}{x} \tag{3.9}$$

and for edge dislocations

$$\sigma_{xy} = \frac{Gb}{2\pi(1-\nu)}\frac{1}{x} \tag{3.10}$$

where x is the distance between the dislocation line and the point of consideration along x direction. The only difference is the $(1-\nu)$ factor where ν is Poisson's ratio. A typical value for ν is 0.3.

The geometry of a single pile-up is shown in Figure 3.2. The source is located at $x = 0$. The length of the pile-up (source-to-barrier distance) is ℓ. The effective stress on a single dislocation may be obtained by superimposing stress fields of

dislocations and the stress field of the barrier. The effective stress, $\tau_{eff,i}$, on the ith dislocation for a general case where there are N dislocations in a single ended pile-up is [40]

$$\tau_{eff,i} = \tau_a - B(x_i) + \sum_{\substack{j=1 \\ j \neq i}}^{N} \frac{A}{x_i - x_j} \tag{3.11}$$

where A is $Gb/2\pi$ for screw and $Gb/2\pi(1-\nu)$ for edge dislocations. The second term on the right hand side of the equation is the stress field of the barrier. Depending on the choice, this term may be in different forms. For instance, Rosenfield and Kanninen considered a single locked dislocation parallel to the other dislocations in the pile-up as the barrier [40]. For this case $B(x_i)$ is

$$B(x_i) = \frac{A}{\ell - x_i} \tag{3.12}$$

In our model, a more general form is used with two adjustable parameters. This provides flexibility for simulating different cases. The form of the function is

$$B(x_i) = \frac{\alpha_1 A}{\ell - x_i}\, e^{-\alpha_2(\ell - x_i)/\ell} \tag{3.13}$$

where α_1 and α_2 are the adjustable parameters. The range of α_1 is 0 to 1. α_2 can take any value, but typically it is close to unity. The most effective barrier from the magnitude of the stress field point of view is given by Equation 3.1. This configuration may be obtained by using $\alpha_1 = 1$ and $\alpha_2 = 0$. On the other hand, if there is no stress acting on the dislocation due to the presence of the barrier, α_1 may be simply set to zero. Any other combination of α_1 and α_2 will give a configuration between these two extremes. For instance, the stress exerted by a group of forest dislocations acting as a barrier for the pile-up dislocations will be

lower than that is exerted by a single locked dislocation. Such a barrier can be represented by intermediate values of α_1, e.g., α_1=0.5.

The stress acting on the source, σ_S, and the barrier, σ_B may be expressed by

$$\sigma_S = \tau_a - \sum_{i=1}^{N} \frac{A}{x_i} \tag{3.14}$$

and

$$\sigma_B = \tau_a + \sum_{i=1}^{N} \frac{A}{\ell - x_i} \tag{3.15}$$

The velocity of dislocations depends on the stress acting on the dislocation. For low velocities, relative to the shear wave velocity in the material, an appropriate form of dislocation velocity-stress relation is the empirical power form [35]

$$v = K\tau_{eff}^{m} \tag{3.16}$$

where K and m are experimentally measured material constants. m is known as the stress sensitivity of dislocation velocity. Equation 3.16 may be transformed to a differential equation in terms of the position of the dislocations in the pile-up as a function of time. In accord with the work of Rosenfield and Kanninen [40], Equation 3.16 for the ith dislocation is written

$$\frac{dx_i}{dt} = K\tau_{eff,i}^{m}(x_i) \quad i = 1, 2, ..., N \tag{3.17}$$

where $B(x_i)$ in our model is given by Equation 3.13. Then, by Equations 3.11 and 3.13 in 3.17

$$\frac{dx_i}{dt} = K\left[\tau_a - \frac{\alpha_1 A}{\ell - x_i}\, e^{-\alpha_2(\ell - x_i)/\ell} + \sum_{\substack{j=1 \\ j\neq i}}^{N} \frac{A}{x_i - x_j}\right]^{m} \quad i = 1, 2, ..., N \tag{3.18}$$

The solution of the N coupled nonlinear differential equations provides the location of each dislocation in the pile-up as a function of time.

For the solution of Equation 3.18, the dynamic nature of pile-up formation must be considered. At the initial time step, the first dislocation is emitted. This dislocation moves away from the source due to the applied stress. The change of the stress acting on the source is followed by evaluating Equation 3.14 during the integration of Equation 3.18 for i=1. At some point, when the dislocation is sufficiently away from the source, the stress on the source reaches the critical level, σ_S^*. At this instant, the next dislocation is considered to be emitted, and, therefore, two differential equations must then be evaluated simultaneously. The same procedure is repeated as the pile-up formation evolves. As the number of dislocations increases, an equal number of equations are integrated simultaneously. This is a drawback from the computational point of view for the case of large pile-ups or high stress levels since the number of dislocations may reach several thousands. As is described in the Appendix, Section 7.1, below, a superdislocation approximation is developed for this case to avoid extremely long computations. When the distance between two neighboring dislocations is short, they are combined and replaced with one superdislocation with a strength equal to the total strength of two previous dislocations. The position of the new superdislocation is chosen such that the stress concentration at the leading dislocation remains unchanged. The results with and without these approximations did not show any significant difference, for single dislocations up to 80.

In Equation 3.18, the dislocation position is related to the stress by means of two materials constants, K and m. Rosenfield and Kanninen [40] introduced the

following dimensionless parameters:

$$\beta = \frac{A}{\tau_a \ell} \tag{3.19}$$

$$\Theta = \frac{K \tau_a^m t}{\ell} \tag{3.20}$$

$$s_i = \frac{x_i}{\ell} \tag{3.21}$$

where Θ is the dimensionless dynamic parameter, s_i is the dimensionless distance, and β is another dimensionless parameter. When these parameters are used, Equation 3.18 is converted to the following dimensionless form

$$\frac{ds_i}{d\Theta} = \left[1 - \beta \left(\frac{\alpha_1}{1 - s_i} e^{-\alpha_2 (1 - s_i)} - \sum_{\substack{j=1 \\ j \neq i}}^{N} \frac{1}{s_i - s_j} \right) \right]^m \qquad i = 1, 2, ..., N \tag{3.22}$$

One advantage of the dimensionless form of the equation is to see the effect of the stress sensitivity parameter, m. Furthermore, there is an infinite number of combinations of τ_a and ℓ. It may be necessary to obtain a solution for the system of differential equations for each combination. However, only certain values of τ_a and ℓ may be considered. Then, corresponding β values for these combinations are used and calculations are carried out by the dimensionless form of the equation. For other combinations, desired parameters may be obtained by interpolation to avoid extra computations.

A nonlinear partial integro-differential equation may be written based on the continuum approximation to analyze time dependent behavior of dislocation pile-ups. Equations 2.8 and 3.11 together with the previously defined dimensionless

parameters give

$$\frac{\partial \rho'}{\partial \Theta} = -\frac{\partial}{\partial s}\left\{\rho'\left[1+\beta\left(\frac{\alpha_1 e^{-\alpha_2(1-s)}}{s-1}+\int_0^1 \frac{\rho'(s',\Theta)}{s-s'}ds'\right)\right]^m\right\} \tag{3.23}$$

where $\rho' = \ell\rho$ and ρ, as in Equation 2.8, is the linear dislocation density. Meanwhile, the number of dislocations at any time should satisfy the following relation

$$N(\Theta) = \int_0^1 \rho(s,\Theta)ds \tag{3.24}$$

Equation 3.23 provides the advantage of using a single equation for a specific pile-up instead of solving a large number of coupled ordinary differential equations. The continuum approximation requires an initial dislocation distribution in the pile-up which may be obtained based on the solution of the equations for the discrete model. Equation 3.23 is a one dimensional hyperbolic equation. It is also known as the inviscid Burger's equation in fluid dynamics [48]. To obtain a numerical solution to this equation with the conditions described above (i.e., sequential emission of dislocations by the source when the stress acting on the source reaches a critical value), the third order Rusanov method and a time centered implicit scheme were applied [48]. However, no stable solution could be obtained because of the distortion of the distribution function by a single dislocation emitted by the source at the instant of emission. Recently, Nadgornyi [49] also indicated that this equation is not reliable for dislocation pile-ups associated with a dislocation source. Therefore, no use was made in this study of a continuum analysis.

In this part, the numerical solutions of the equation for the pile-up formation, Equation 3.22, will be presented in terms of the dimensionless parameters, β (Equation 3.19), Θ (Equation 3.20), and s (Equation 3.21). Computational results for

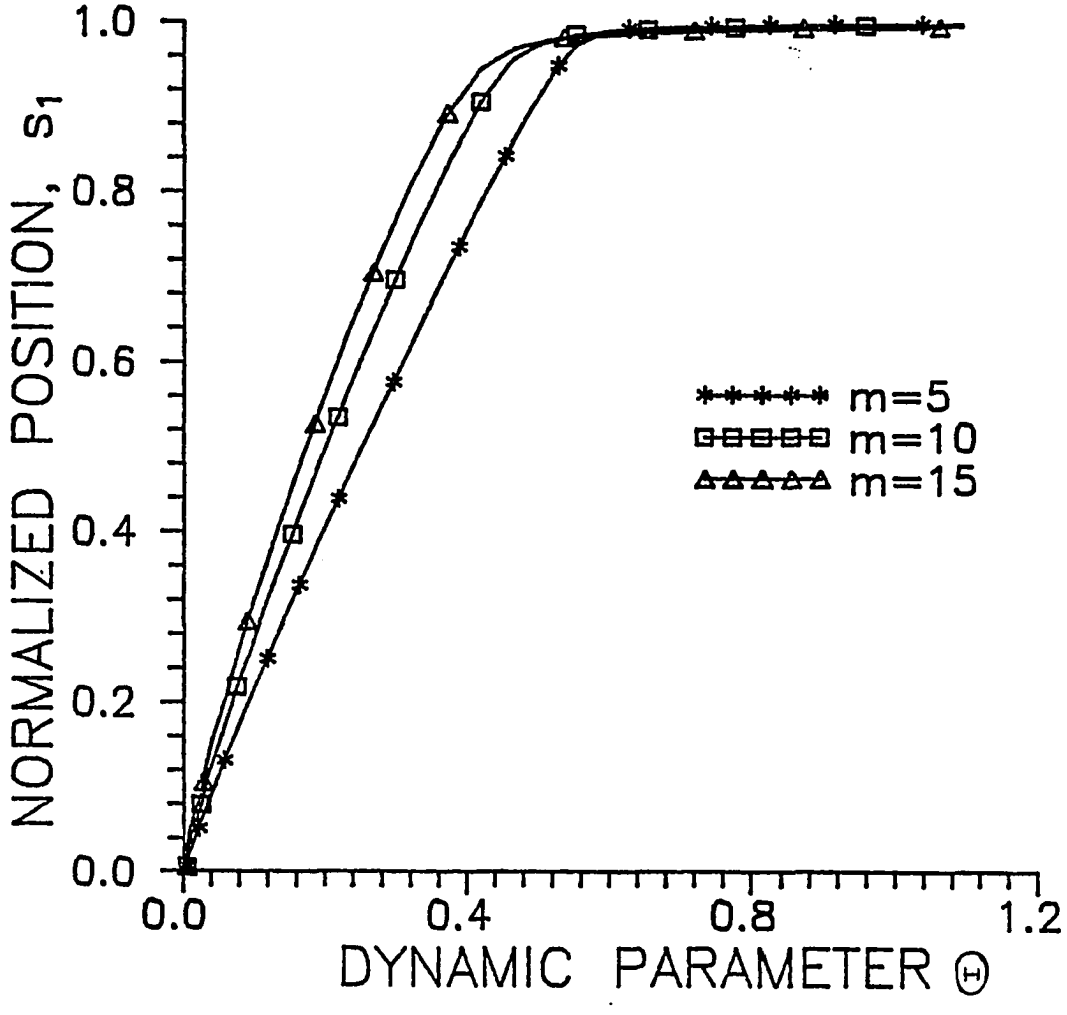

Figure 3.3: Position of the leading dislocation as a function the dynamic parameter, Θ, for various values of the stress sensitivity of dislocation velocity, m

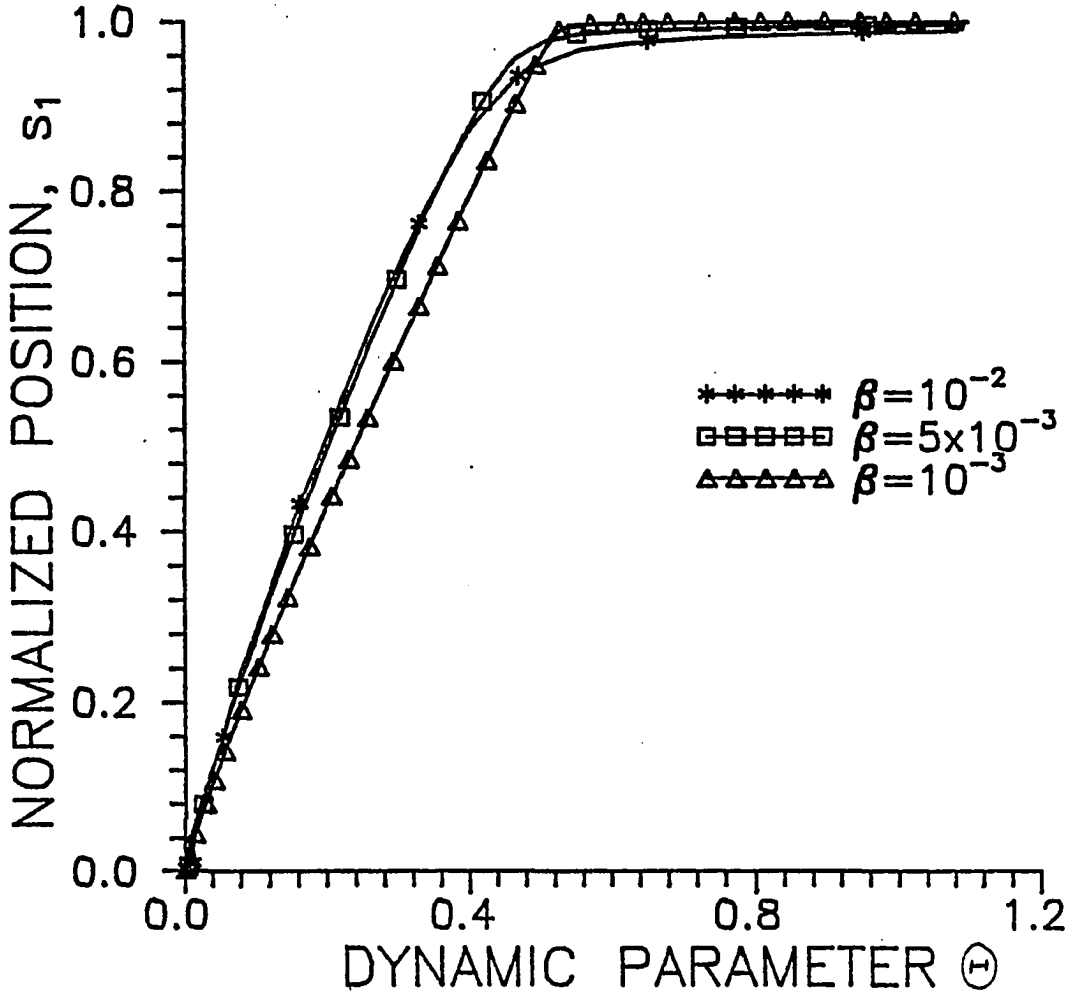

Figure 3.4: Position of the leading dislocation as a function the dynamic parameter, Θ, for various β values

the specific case of Nb single crystals are given in Chapter 4 in terms of physical parameters. The effect of m on the propagation of dislocations in the slip plane is shown in Figure 3.3. The relative position of the leading dislocation, s_1, is shown as a function of dynamic parameter, Θ, for various values of m. β is 0.001. This Θ value corresponds to a pile-up length of 90 μm in a niobium single crystal irradiated to 1.7×10^{17} n/cm^2 deformed at a shear stress of 32 MPa, which approximately corresponds to the lower yield stress of the material. Results show that the mobility of dislocations increases with increasing m value. The effect of β on the position of the leading dislocation as a function of dynamic parameter, Θ, is shown in Figure 3.4. The effect of β is not significant.

Another important parameter is the stress concentration on the barrier, R_B, which is calculated by Equation 3.15. Figures 3.5 and 3.6 show R_B versus Θ for various m and β values, respectively. If the stress concentration is high, dislocations may break through the barrier and extend the length of the slip line to the location of the next barrier on the slip plane. The position of the leading dislocation is the primary factor which determines the stress concentration. For great values of Θ, R_B increases with decreasing m and β. Increasing ℓ will decrease the value of β and cause a delay for the leading dislocation to get the vicinity of the barrier to increase the stress concentration. The choice of parameters α_1 and α_2 in Equation 3.13 is very significant for the stress concentration parameter, $R_B = \sigma_B/\tau_a$. At initial stages of the slip line formation, the increase of R_B is relatively small. A significant increase is observed when the leading dislocation approaches the barrier. If the obstacle is weak, i.e., α_1 is relatively small (about 0.1), the leading dislocation can get very close to the barrier. In this case, the increase in R_B is very sharp and

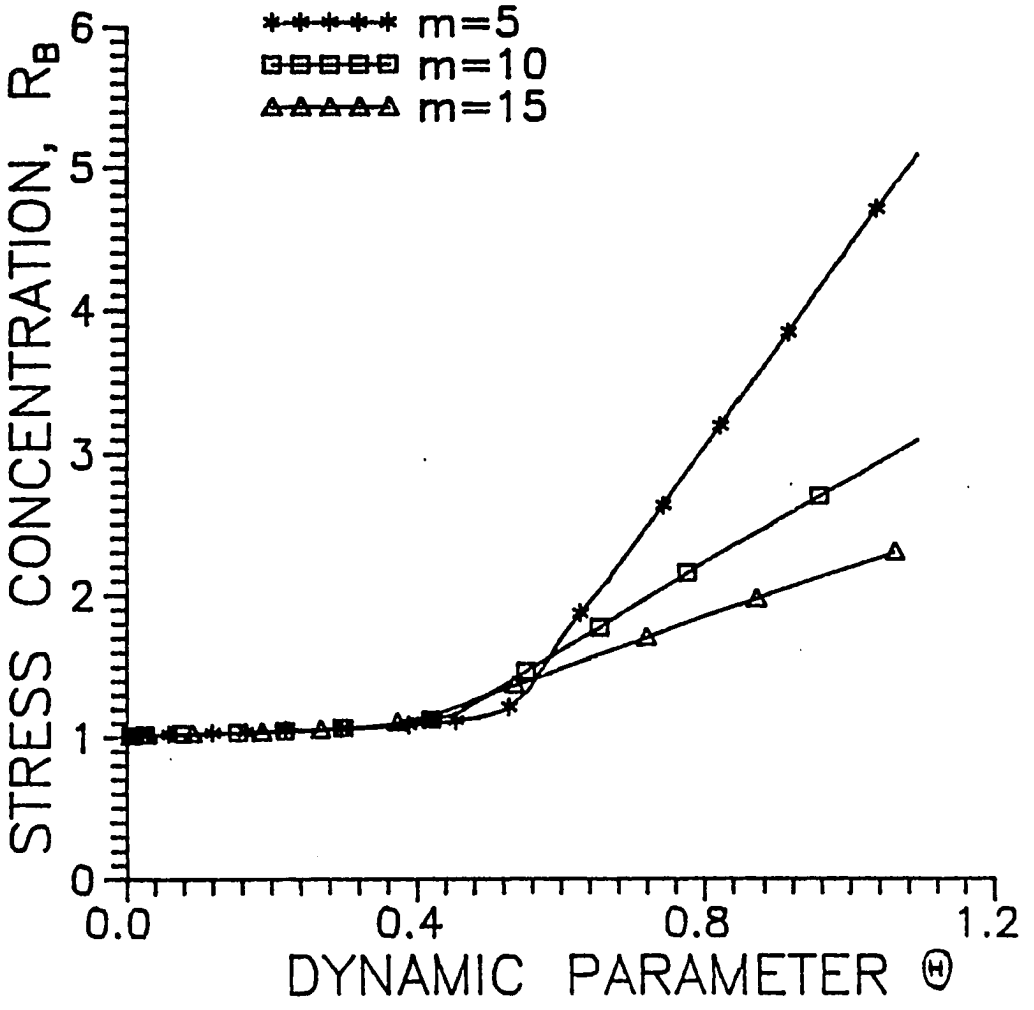

Figure 3.5: Stress concentration on the barrier, R_B, as a function of the dynamic parameter, Θ, for various m values

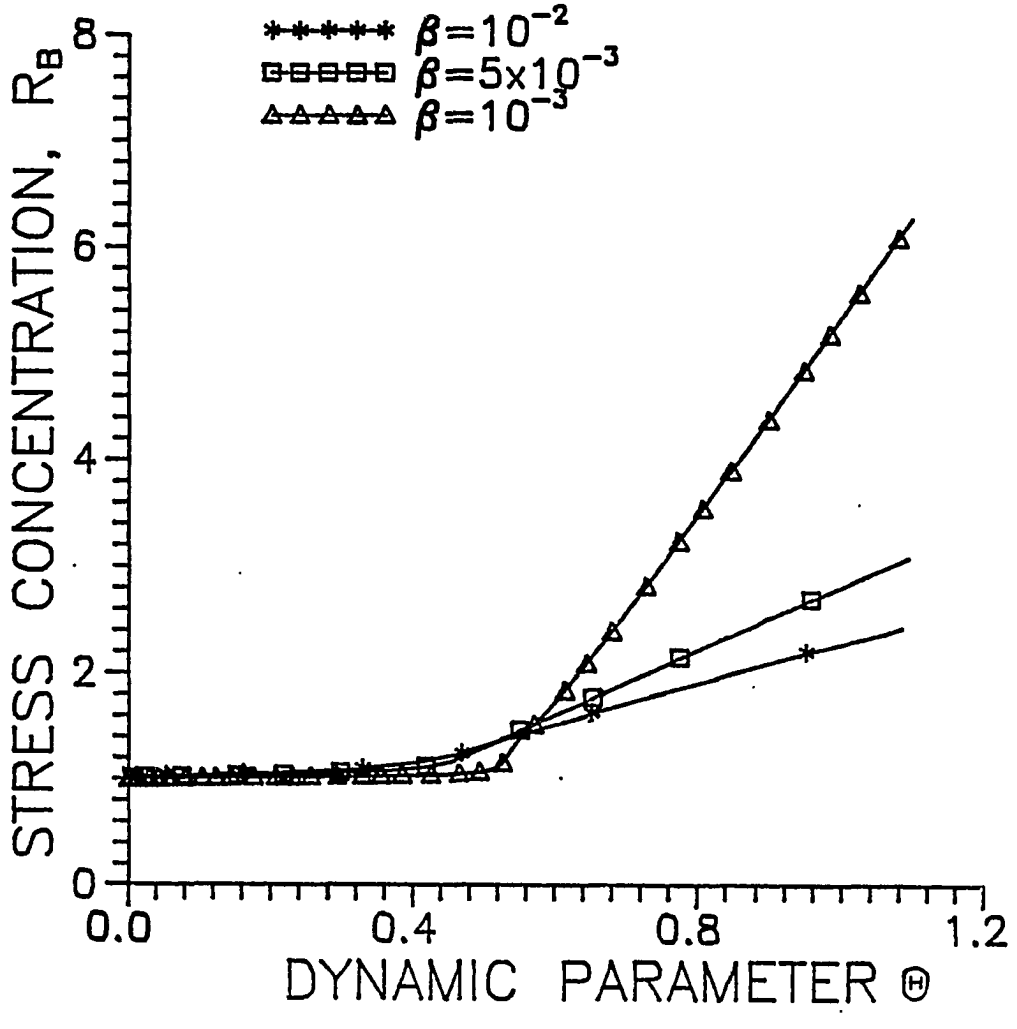

Figure 3.6: Stress concentration on the barrier, R_B, as a function of the dynamic parameter, Θ, for various β values

occurs in very short period of time. On the other hand, if the barrier is strong, i.e., α_1 is about 1, the increase is rather smooth because the strong stress field of the barrier repels or at least decelerates the leading dislocation.

The amount of plastic deformation produced in the channel region is measured by the distance traveled by dislocations. H represents this parameter for a single pile-up. H for a pile-up of N dislocations is

$$H(\beta, \Theta, m) = \sum_{i=1}^{N} s_i \tag{3.25}$$

Figures 3.7 and 3.8 show the effect of m and β on H. The strain parameter H increases with decreasing m and β values due to an increasing mobility and a longer path for dislocations to travel. Macroscopic deformation parameters may be then obtained in terms of shear displacement by means of H.

It should be kept in mind that both m and K are important for the analysis of pile-up evolution. Results obtained by the use of dimensionless equations should be converted to physical parameters to make comparison between two materials.

An interesting feature of the dislocation channeling in irradiated metals is that incompletely formed channels are rarely observed. The nature of slip band formation in unirradiated metals is different. Growth of the band is observed step by step to the final width with small increments with increasing stress. In irradiated metals cross slip lines connect existing channels with increasing stress. The termination of slip in dislocation channels is closely related to the local strain hardening. Since local strain rate is very high, accumulation of dislocations is very significant. In the absence of any other effect, dislocations in a pile-up become immobilized when the dislocations reach their equilibrium positions so that interaction forces are zero.

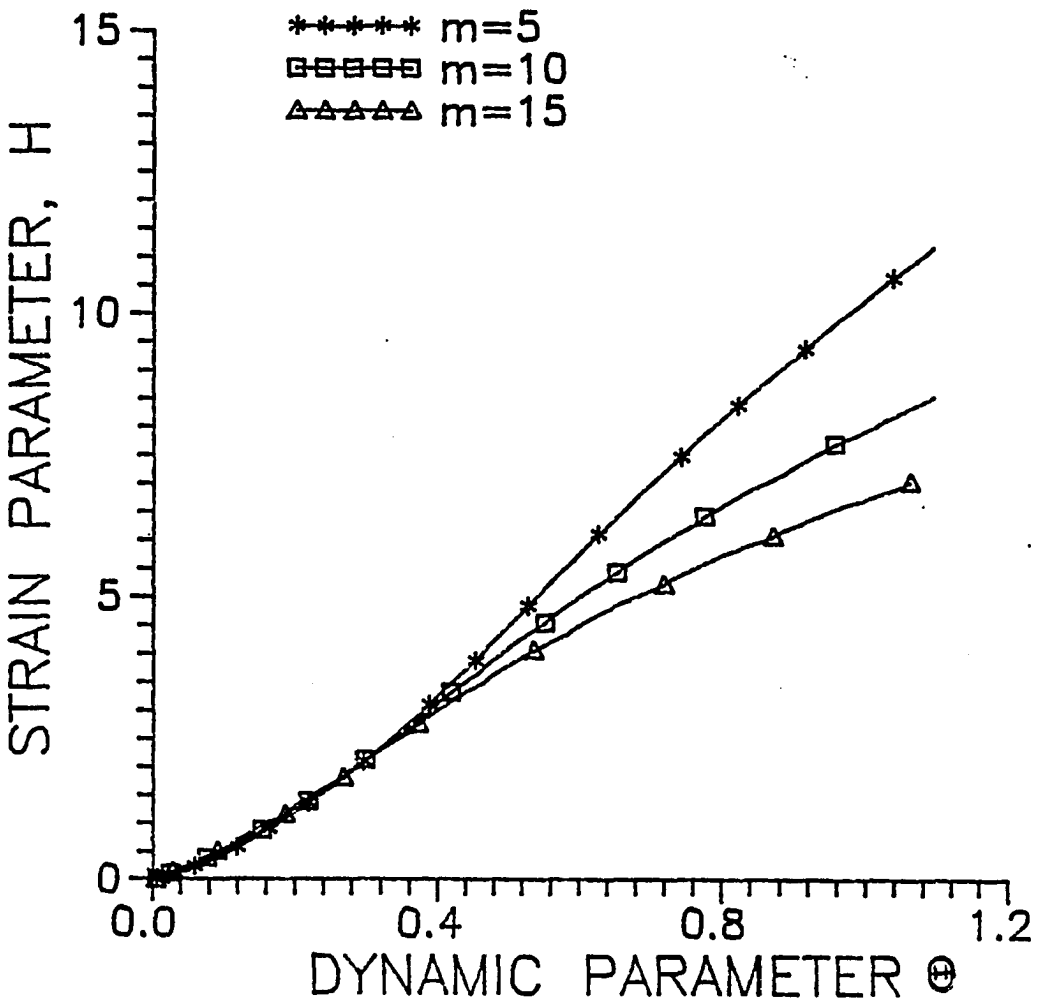

Figure 3.7: Normalized strain parameter H as a function of the dynamic parameter, Θ, for various m values

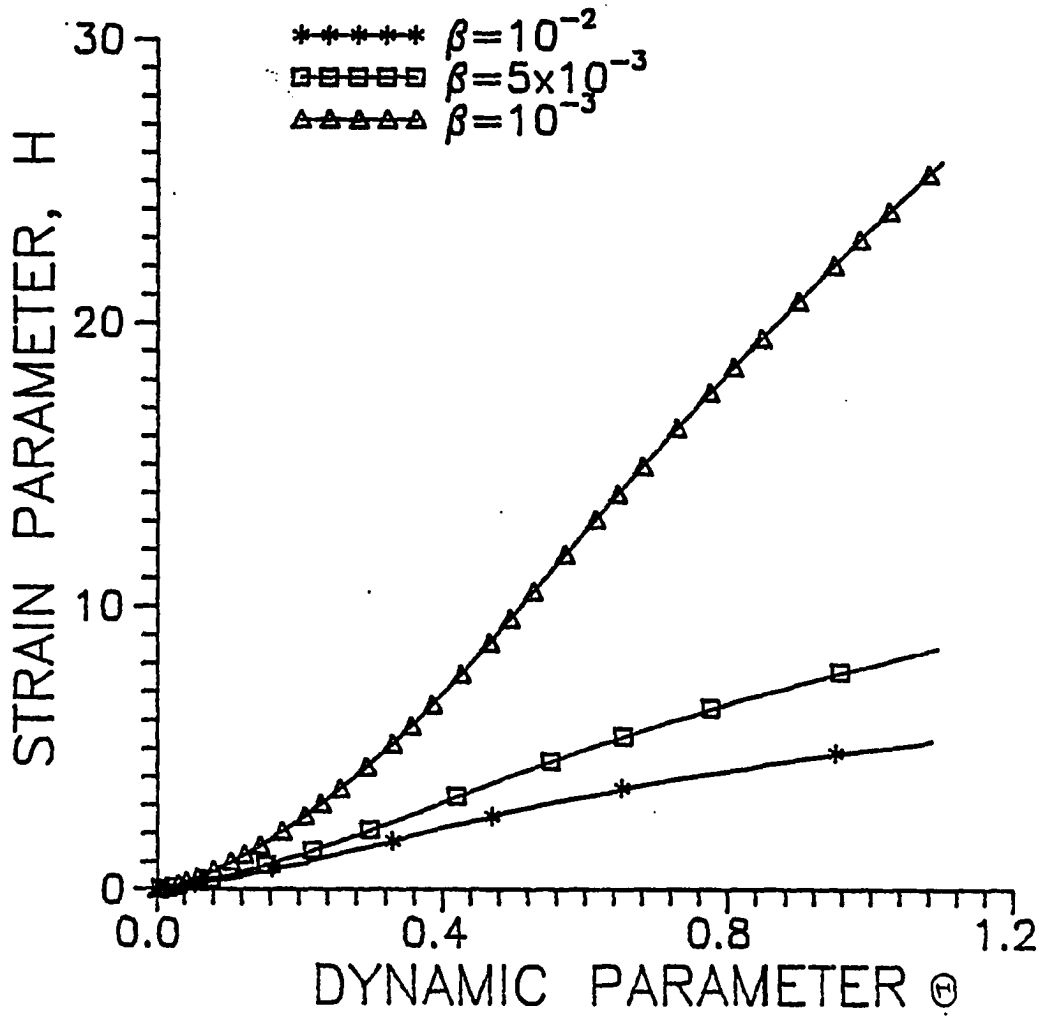

Figure 3.8: Normalized strain parameter H as a function of the dynamic parameter, Θ for various β values

The time to reach equilibrium is usually very long especially in BCC metals due the low mobility of dislocations. Therefore, the termination of dislocation channel formation may be attributed to the formation of complex dislocation structures, such as tangles and dislocation cells, in the channel region.

3.2 Plastic Deformation on Macroscopic Scale

Dislocation channels will be considered as bundles of slip lines with a uniform thickness. Shear within the channel is thought to be uniformly distributed as the result of massive motion of dislocations. Pre-existing dislocations, other forms of irregularities, and frequent cross-slip events form necessary dislocation sources, as well as barriers to moving dislocations.

Individual slip lines are considered to be a number of dynamic dislocation pile-ups with various lengths. Since formation time is usually short enough, excessive stress concentrations on barriers may be avoided. The lower limit of the pile-up length should be kept large enough so that barriers at smaller distances will be destroyed due to the high stress concentration. Barriers in pile-ups may be under a great stress produced by the dislocations in the pile-up. This stress concentration may be high enough so that dislocations break through the barrier, which effectively removes the barrier and extends the pile-up length. Since the stress fields of dislocations are inversely proportional to distance and the leading dislocation reaches the vicinity of the barrier in a shorter time for shorter pile-ups, short pile-ups are eliminated and converted to longer pile-ups in the model.

The shear displacement in the channel is a function of the distance traveled by dislocations within the channel. Surface slip step is equal to the Burgers vector

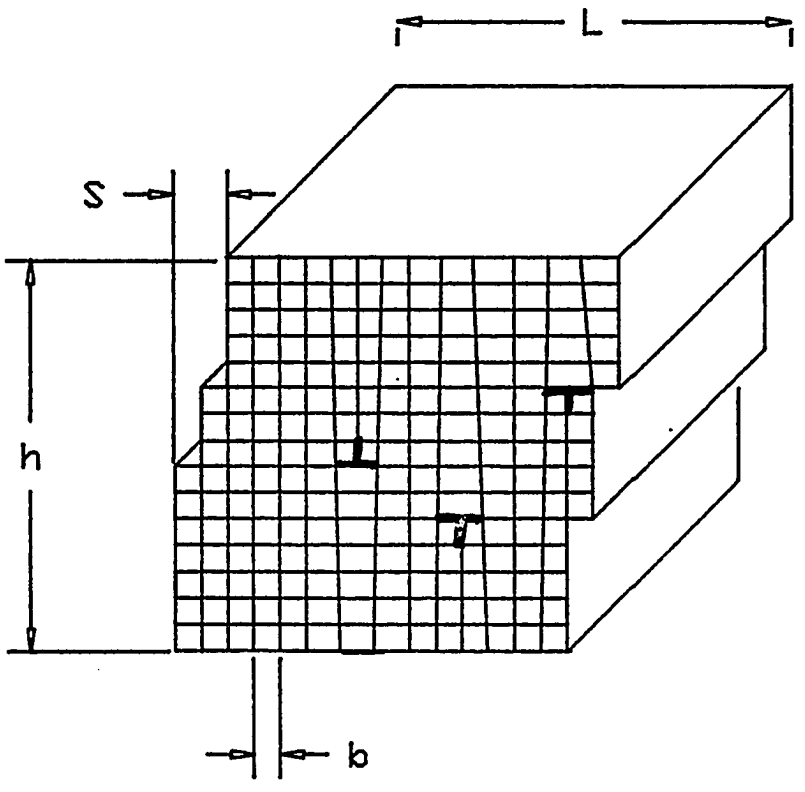

Figure 3.9: Shear displacement produced by the movements of edge dislocations in a crystal

of the dislocation if a single dislocation moves across the slip plane as shown in Figure 3.9. However, if a dislocation moves only a portion of the slip plane, L is the length of the slip plane and x is the distance traveled, the corresponding displacement is bx/L. The shear displacement due to the motion of all dislocations in the channel is

$$S = \begin{array}{c}\text{number}\\ \text{of active}\\ \text{slip planes}\end{array} \times b/L \times \begin{array}{c}\text{total distance moved by}\\ \text{all dislocations in a}\\ \text{given slip plane}\end{array}$$

Similarly, the shear displacement in a channel of length L containing n parallel active slip planes and pile-ups whose lengths are represented by a distribution function, $P(\ell)$, is

$$S(\tau_a, t) = \frac{bn}{L} \int_{\ell_{min}}^{\ell_{max}} \ell P(\ell) H(\tau_a, t, \ell) d\ell \tag{3.26}$$

where ℓ_{min} and ℓ_{max} are the minimum and maximum slip line length and H is

$$H(\tau_a, t, \ell) = \sum_{i=1}^{N} \frac{x_i}{\ell} \tag{3.27}$$

where x_i is the distance traveled by the ith dislocation in the pile-up. H is obtained from the equations of dynamic slip line formation that were discussed in Section 3.1.

For the simulation of plastic deformation, a sheet tensile sample will be assumed. Elastic strain is small compared to plastic strain and it is neglected. Simulation starts at a stress level that corresponds to the yield stress of the material. The first dislocation channel is formed at the center of the sample. Dislocation channels form in two different orientations. The first is from the upper left to lower

right diagonal and the second is from the upper right to lower left diagonal. It is assumed that dislocation channels form where the resolved shear stress is maximum. Single crystal material is assumed such that dislocation channels make a 45^o angle with the tensile axis. Dislocation channels form alternatively in these two directions. Therefore, the most recently formed channel crosses previously operated channels. Intersections of channels form dislocation tangles, which are very complex and irregular dislocation arrangements. Because of this complex structure, these regions are not considered to be ideal regions for dislocation motion. Channel boundaries also show irregular dislocation structure relative to the channel interior. Formation of a dislocation channel causes some amount of hardening around the channel region. Therefore, the subsequent channels tend to form as far as possible from the previously formed channels. The location of a new channel is chosen such that the channel will be located in the softest region of the sample.

For the selection of the new dislocation channel location, the following criteria are to be satisfied in the given order;

1. The new channel is at least a critical distance away from other channels. This distance was taken to be 2 μm, in accord with experiments [21].

2. The distance between the new channel and the existing ones is maximum, consistent with choosing the softest region in the crystal.

3. The new channel is crossed by the minimum number of oppositely oriented channels.

4. The length of the channel is a minimum to provide maximum resolved shear stress on the slip plane.

The first channel is formed in the midsection of the sample. The resulting shear displacement is calculated, as shown is Figure 3.10. u and v are displacements within the channel along x and y, directions as indicated. u an v are given by

$$u = \frac{Sy}{h} \tag{3.28}$$

$$v = 0 \tag{3.29}$$

The upper end of the sample is fixed and the lower end moves downward as dislocation channels form. The required translations for the lower part of the sample with respect to the new dislocation channel are $\Delta x'$ and $\Delta y'$ along x' and y' directions

$$\Delta x' = S\cos\varphi \tag{3.30}$$

$$\Delta y' = S\sin\varphi \tag{3.31}$$

According to the above criteria, the next four channels form at the upper and lower corner regions in two opposite directions where the distance from the first channel is the greatest. For each step, coordinates of the channel region are calculated, and then, shear displacement is applied for fully developed region as shown in Figure 3.10. After this step the selection is done as follows. The distances between neighboring channels are calculated. Channels with a distance smaller than the critical distance away from each other are eliminated. The criteria require the selection of the farthest apart location. If there is more than one possibility, the selection process is carried out by the next criterion. Before applying this criterion the location of all possible channels are calculated. Using this information and the locations of previously formed and oppositely oriented channels, the number of

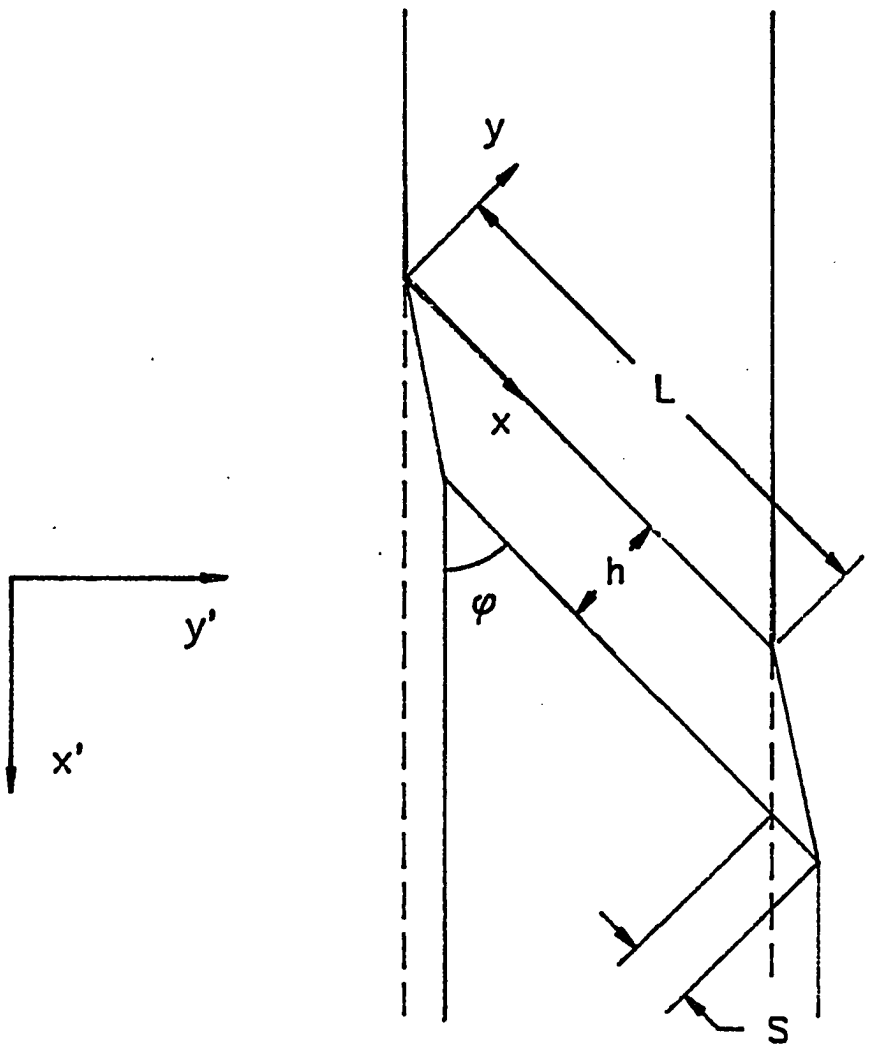

Figure 3.10: Shear displacement S in a dislocation channel

crossing channels is determined. The rules require the selection of the channel with the fewest number of crossing channels. If there is still more than one possibility, the next criterion is applied. The lengths of all possible channels are calculated. The shortest one is selected as the new dislocation channel. If there is still more than one possibility, one or more of them (up to a maximum allowable number of channels for simultaneous formation) are selected. The information obtained during the selection process is used to calculate the amount of shear displacement associated with the channel according to Equation 3.26. The required parameters are the length of the channel and the number of crossing dislocation channels to calculate the available space for dislocation motion. A typical channel width, h, is about 0.3-1 μm. The amount of shear, S/h, is observed to be as high as several hundred per cent [21,24].

When a dislocation channel is formed, it may cross a number of oppositely oriented channels as shown in Figure 3.11. Because of the shear displacement produced in the channel, previously formed channels should also be translated to their new positions if these channels are located in the lower part of the sample with respect to the new channels. As new channels form along the sample, the length of channels decreases and the number of crossing channels increases. As the result of shear displacement introduced by each channel, an axial elongation along the x'-direction is produced. The number of channels to produce a certain amount of elongation is a function of the average shear displacement and the thickness of channels. For instance, if the average shear displacement associated with each channel is 1μm and φ is 45^o, the contribution of each channel to the axial elongation is 0.707 μm. If the sample is 12 mm long, approximately 1700 channels are required to produce 10%

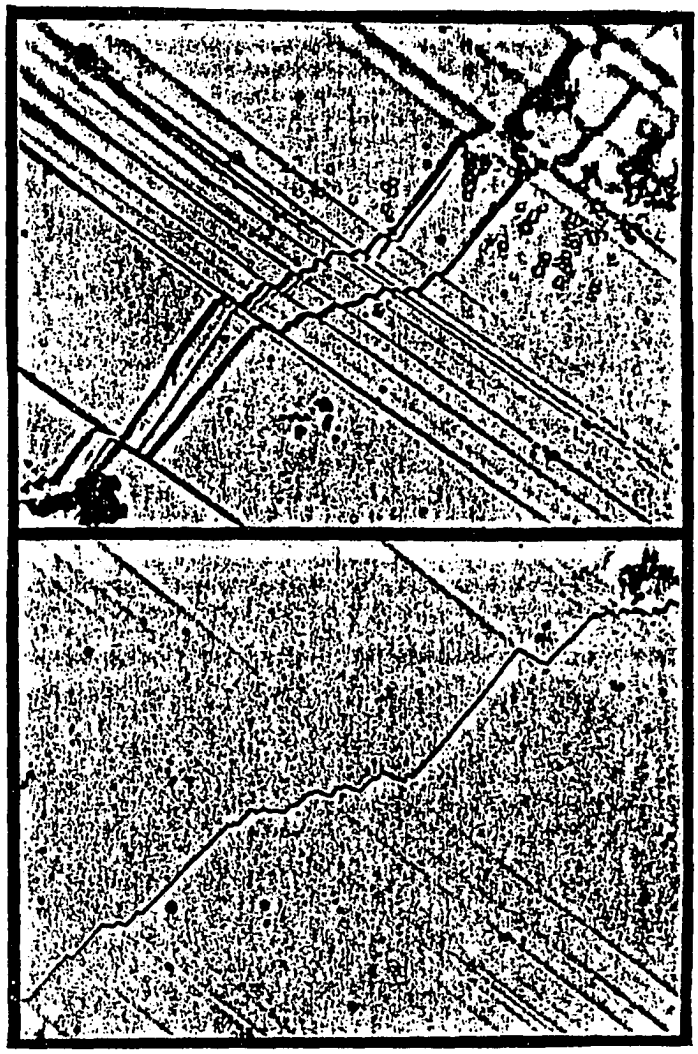

Figure 3.11: Oppositely directed and intersected dislocation channels in an irradiated Nb single crystal [50]

strain.

One of the purposes of the computer simulation is to calculate stress as a function of strain. The key equation for this purpose is Equation 3.26 which gives the shear displacement S as a function of time t, shear stress τ_a, and pile-up length ℓ. The integrand contains the normalized strain parameter, H. Instead of solving the system of differential equations for every τ_a and ℓ to obtain the necessary H value, it is calculated by interpolation using bi-cubic splines from a table prepared based on the solutions of Equation 3.22 in terms of β and Θ.

The widths of dislocation channels are assumed to remain constant throughout the deformation. The shear displacement is limited to remain within a certain range. The estimated number of simultaneously forming channels is given as an input parameter in the first step. Then, the shear displacement and the corresponding crosshead speed are calculated. One of the aims in the simulation is to keep the crosshead speed constant at a prescribed level. To calculate the shear displacement per channel to achieve the imposed crosshead speed, first the calculated shear displacement as a function of time is fitted to a second order polynomial. Then, an approximated time value to reach the critical value is calculated by finding the zeros of the polynomial. The estimated time value is then used to calculate the shear shear displacement to give the correct critical crosshead speed. If it is not correct within a given error limit the procedure is repeated until the correct value is found. If the shear displacement per channel is greater than the desired upper limit, the number of simultaneously forming channels is increased by one. This is done only in the first step to obtain the optimum number of simultaneously forming channels for given crosshead speed and shear displacement. The shear stress τ_a for the first step

is chosen to correspond to the lower yield stress of the material. Once the shear displacement and the required number of channels are determined, the locations of the channels are selected and appropriate displacements are done as previously described. The macroscopic engineering strain is determined by the current increase in length of the sample divided by the original length. After the formation of all channels is completed in a generation, the shear displacement per channel is calculated using the current information about the length and available space for the pile-up formation in the next possible channel. If the shear displacement is within the specified range, the process is repeated. To impose strain hardening, shear displacement and time for channel formation are controlled to make necessary adjustments in the shear stress level. It is assumed that the formation time for the same number of channels in one generation should be shorter than the time period in the preceding generation. Otherwise, stress is increased by a small amount until it becomes adjusted. This operation also causes a decrease in the shear displacement. The number of channels is kept constant until the shear displacement drops below the minimum acceptable value. If this occurs, the number of simultaneously forming channels is decreased by one.

Because of the complexity of the real physical nature of inhomogeneous plastic deformation in irradiated metals, many simplifications have been made in the computer model. First of all, the orientation of channels with respect to the tensile axis may not be exactly 45^o. In general several degree deviations may be observed. The axis of the sample remains aligned in normal tensile tests. This causes a lattice rotation during the deformation. This is not considered here. The width of channels and the spacing between channels may not be entirely uniform along the

sample. Implementation of the deviations requires a systematic experimental study of surface morphology for irradiated metals containing dislocation channels. Another important aspect is the cross slip process. Experimental observations show that neighboring dislocation channels are connected by short cross slip lines [50]. The effect of cross slip processes is not taken into account.

4 RESULTS AND DISCUSSION

The model discussed in Chapter 3 is applied to a specific case, namely the plastic deformation of irradiated niobium single crystals. First, the plastic deformation behavior of niobium is discussed and then the results of plastic deformation simulation are presented. One of the reasons for the selection of niobium as the example is the availability of measured dislocation velocity parameters for irradiated niobium. These parameters for an irradiated metal were first reported by Guberman [33] for niobium in 1968. There are several other reports for dislocation mobility in electron and neutron irradiated copper single crystals [2,25,34]. Niobium has fairly high strength and melting point (2468^{o}C). In addition to desirable mechanical properties, low thermal neutron cross section and good corrosion resistance and formability make niobium a special material for nuclear applications. The only undesirable properties are the presence of a ductile-to-brittle transition and the strong temperature dependence of yielding. Irradiation strongly affects the behavior of the material. The yield stress increases and the rate of the work hardening decreases upon irradiation. In irradiated metals the ductile-to-brittle transition takes place at higher temperatures and the fracture energy decreases. Basic properties of niobium are listed in Table 4.1.

Guberman measured the velocity of dislocations in niobium single crystals,

Table 4.1: Basic properties of niobium

Crystal structure	BCC
Lattice constant	0.33 nm
Major slip system	$< 111 > \{110\}$
Shear modulus	46.9 GPa
Poisson's ratio	0.28
Burgers vector	0.286 nm

Table 4.2: Dislocation velocity parameters for niobium single crystals [33]. K in Equation 2.1 is $K = v_L(1/\tau_L)^m$. v_L is 1 m/s

Sample #	Condition	Fluence n/cm^2 (E > 1 MeV)	Temperature ^oK	m	τ_L (MPa)
1	Unirradiated	-	77	18	797.90
2	Unirradiated	-	194	15	159.96
3	Unirradiated	-	300	15	58.65
4	Irradiated	1.6×10^{17}	300	10	119.67
5	Irradiated	8.3×10^{17}	300	7	454.40

in irradiated and unirradiated conditions, by the etch pitting technique [33]. The results are expressed in the form of a power relation, Equation 2.1, between shear stress and dislocation velocity. The related parameters for different conditions are given in Table 4.2. The effect of temperature is clearly seen from the parameters. Mobility of dislocations decreases with decreasing temperature. On the other hand, the stress sensitivity of dislocation velocity increases with decreasing temperature. The effect of impurity content is the opposite of temperature effect, i.e., mobility increases and stress sensitivity decreases with decreasing impurity content.

For the analysis of plastic deformation the effect of irradiation on the yielding behavior of the metal should be taken into account. Tucker and Wechsler analyzed

Table 4.3: Dislocation velocities at the upper yield stresses in unirradiated and irradiated niobium single crystals [33]. K is $v_L(1/\tau_L)^m$ and v_L is 1 m/s

	m	τ_L MPa	τ_y MPa	$v_y = K\tau_y^m$ m/s
Sample #3	15	58.65	28.9	2.49×10^{-5}
Sample #4	10	119.67	40.5	1.97×10^{-5}

the effect of irradiation on the yield stress of single crystal niobium [6]. Their observations are shown in Figure 4.1. The relation between the fluence and the yield stress is given by

$$\sigma_y = \sigma_u + C_1 \left[1 - \exp\left(-C_2\Phi\right)\right]^{1/2} \tag{4.1}$$

where σ_y is the upper yield stress of the metal irradiated to fluence Φ. σ_u is the yield stress of unirradiated metal. C_1 and C_2 are experimentally measured saturation parameters. C_1 and C_2 for single crystal niobium are reported to be 5.6 kg/mm^2 (54.9 MPa) and 0.151×10^{-17} cm^2, respectively.

Resolved shear stresses corresponding to the upper yield stresses for unirradiated (Sample #3) and low fluence irradiated (Sample #4) samples are given by Guberman [33] as 28.9 MPa and 40.5 MPa, respectively. It is interesting to note that dislocation velocities in both materials at the critical resolved shear stress are not significantly different, as shown in Table 4.3. The formation of dislocation pile-ups in irradiated and unirradiated niobium is analyzed using the model described in Chapter 3. This analysis is based on the solution of the system of nonlinear differential equations given by Equation 3.18. For each case, the K and m values shown in Table 4.3 were used. The barrier parameters α_1 and α_2 are taken to be

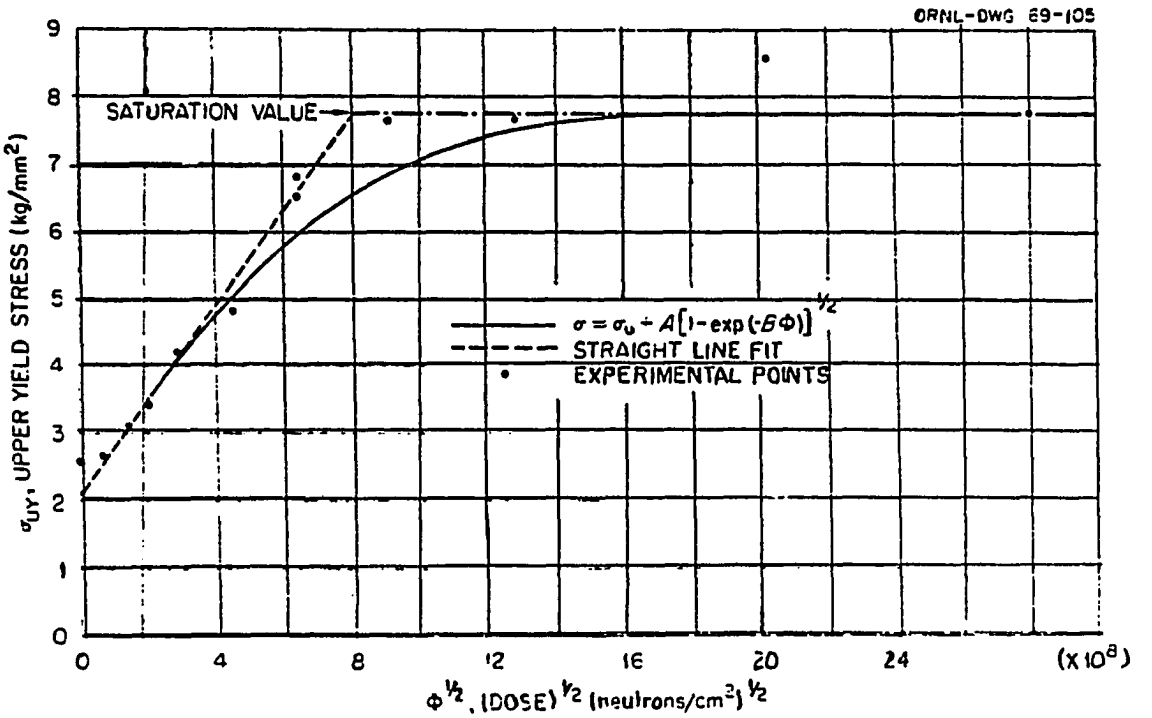

Figure 4.1: Variation of the upper yield stress with neutron the fluence in niobium single crystals [6]

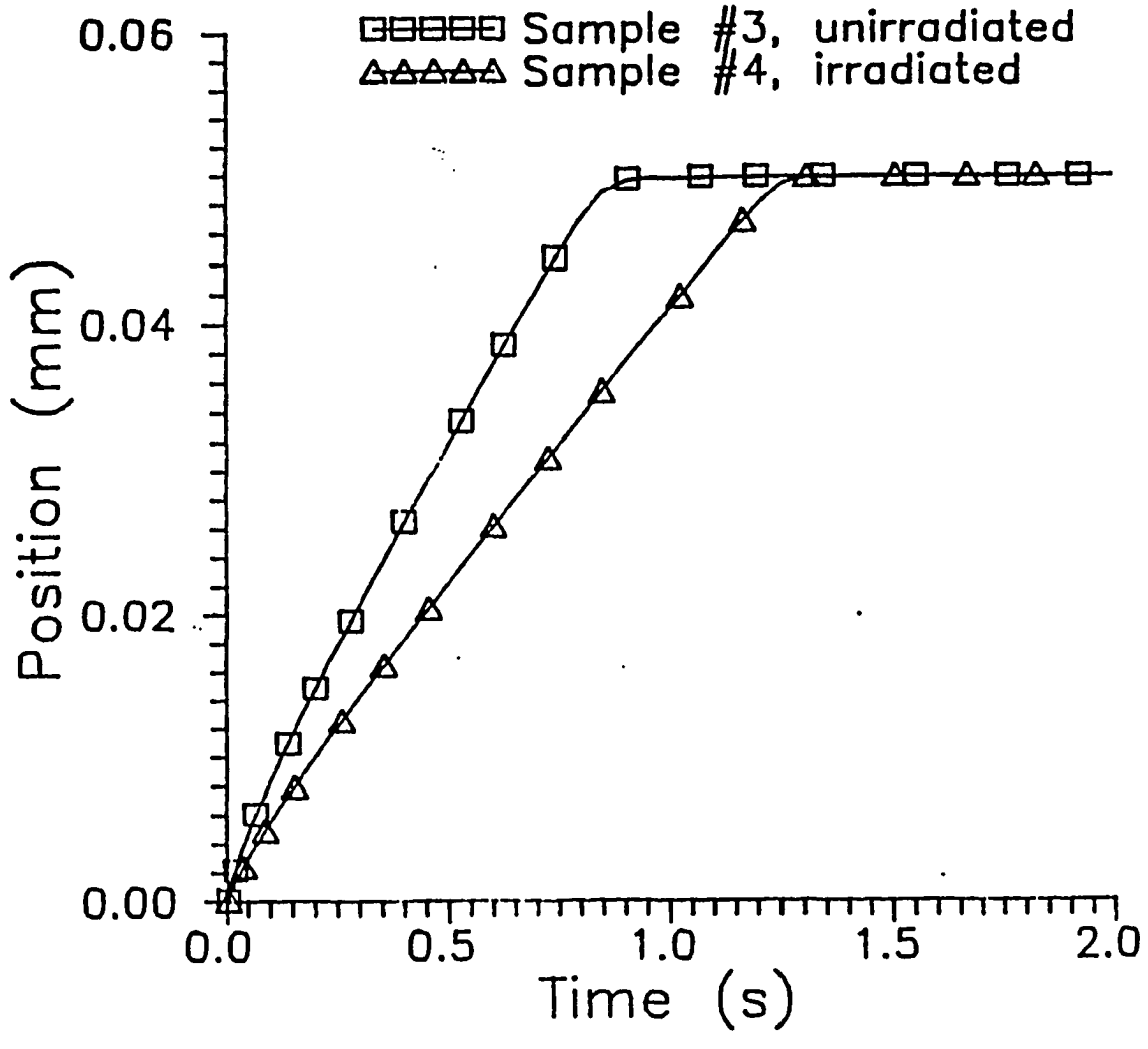

Figure 4.2: Position of the leading dislocation in a dislocation pile-up in niobium single crystals for a 50 μm long pile-up as a function of time from the emission of the first dislocation by the source. The shear stress corresponds to the critical resolved shear stress (28.9 MPa for Sample #3 and 40.5 MPa for Sample #4)

0.5 and 1, respectively. Figure 4.2 shows the position of the leading dislocation in a 50 μm long pile-up as a function of time, where t=0 corresponds to the emission of the first dislocation by the source. The leading dislocation in the unirradiated sample (Sample #3) reaches the vicinity of the barrier at about 0.8 seconds. The leading dislocation in the irradiated sample (Sample #4) travels only 70% of the total pile-up length during the same time period. The difference may be attributed to the stress sensitivity of dislocation velocity, m. The velocity of the leading dislocation increases a greater amount due to the forces exerted by the other dislocations in the pile-up as a result of an increase in m. For this reason, the time period for the leading dislocation to reach the barrier is shorter for Sample #3 since its m is larger than for Sample #4 (Table 4.3).

The second parameter related to pile-ups is the stress concentration at the barrier $R_B(= \sigma_B/\tau_a)$, which is shown in Figure 4.3. While there is no significant stress concentration on the barrier for 1.2 seconds in Sample #4, the stress concentration drastically increases in Sample #3 less than 1 second after the first dislocation is emitted from the source. In Figure 4.3, the sharp upturn in R_B is an indication of the time when the leading dislocation arrives close to the barrier (within 1% of the total pile-up length).

Relative velocity profiles of leading dislocations in the pile-up in unirradiated and irradiated samples are shown in Figure 4.4. The immobilization of the leading dislocation in the unirradiated sample takes place in a shorter time period. This indicates less frequent dislocation emission by the source due to the increasing back stress. Therefore, the number of dislocations in the pile-up in the irradiated sample is greater. After 2 seconds, the number of dislocations is 22 and 28 in unirradiated

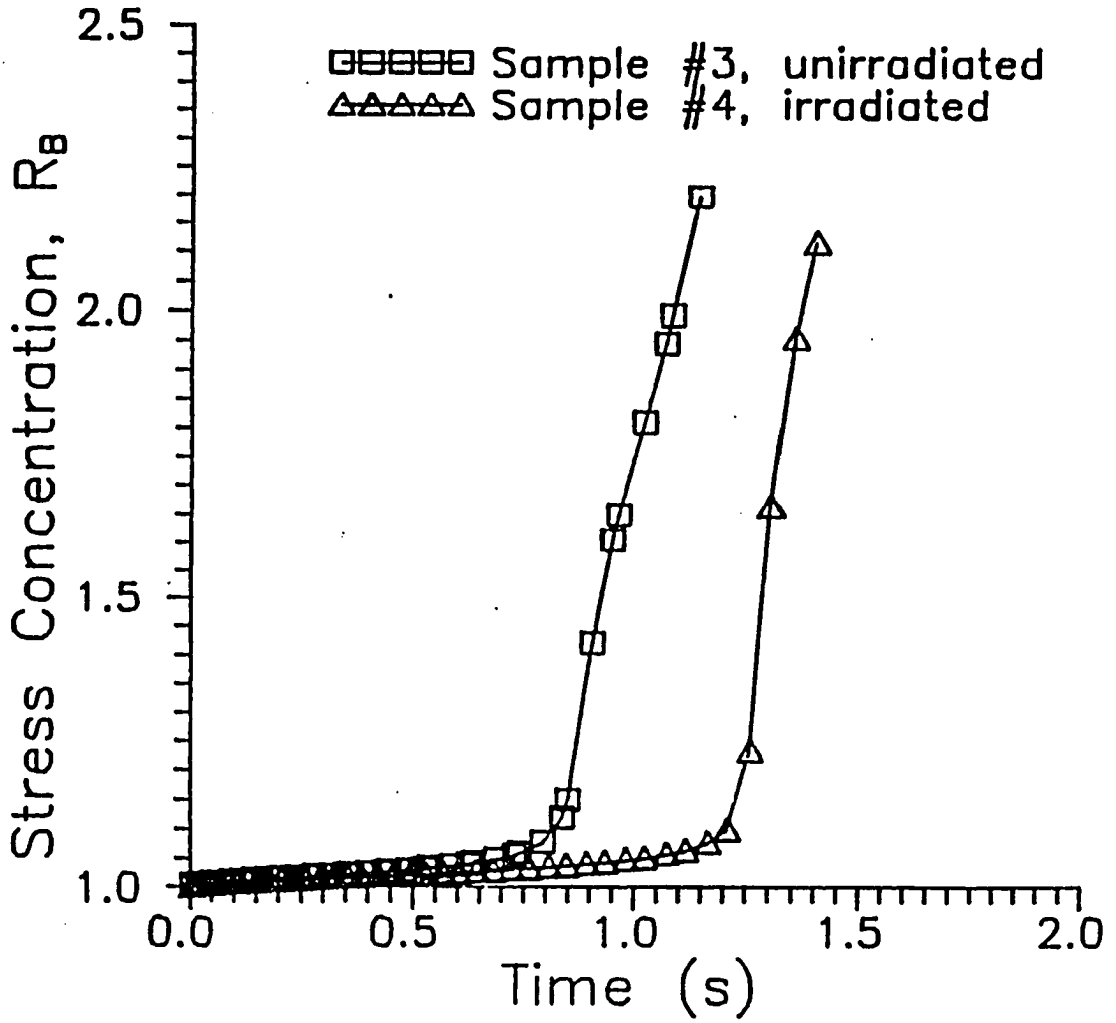

Figure 4.3: Stress concentration factor R_B as a function of time in niobium single crystals. Pile-up length and shear stresses are the same as for Figure 4.2

and irradiated samples, respectively. This results in a greater shear displacement in the irradiated sample for a similar pile-up and the same time period.

Figure 4.5 shows the relative velocity profiles of dislocations for Sample #4, again as a function of time in a 50 μm long pile-up at 40.5 MPa shear stress. Relative velocity is defined as $R_v = v/v_o$, where v is the velocity of a dislocation in a pile-up and v_o is the velocity of an isolated dislocation under the same shear stress. Upon the activation of the source, the first dislocation to be emitted moves due to only the applied shear stress. At this time, $R_v = 1$. After a short period of time, this dislocation is some distance away from the source and the second dislocation is emitted. At this instant, two dislocations are close to each other. The leading dislocation is rapidly accelerated by the applied stress, as well as by the force exerted by the second dislocation. The emission of the third dislocation is somewhat delayed since the back-stress on the dislocation source produced by two dislocations is greater than the stress due to only one dislocation in the previous case, and the second dislocation must move farther to reduce the stress to the critical value σ_S^* for the next dislocation to be emitted. The leading dislocation starts slowing down due to increasing separation distance from the other dislocations in the pile-up and the effect of the barrier. In the vicinity of the barrier a sharp decrease in mobility is observed. Figure 4.6 shows the location of four dislocations as a function of time. This figure also indicates the arrangements of dislocations in later stages of pile-up formation when the dislocations are located close to each other in the vicinity of the barrier. Separation distance increases as we go towards the source.

Equation 3.26 is used for the calculation of shear displacement as a function shear stress and time in a single dislocation channel of length L. In this equation it

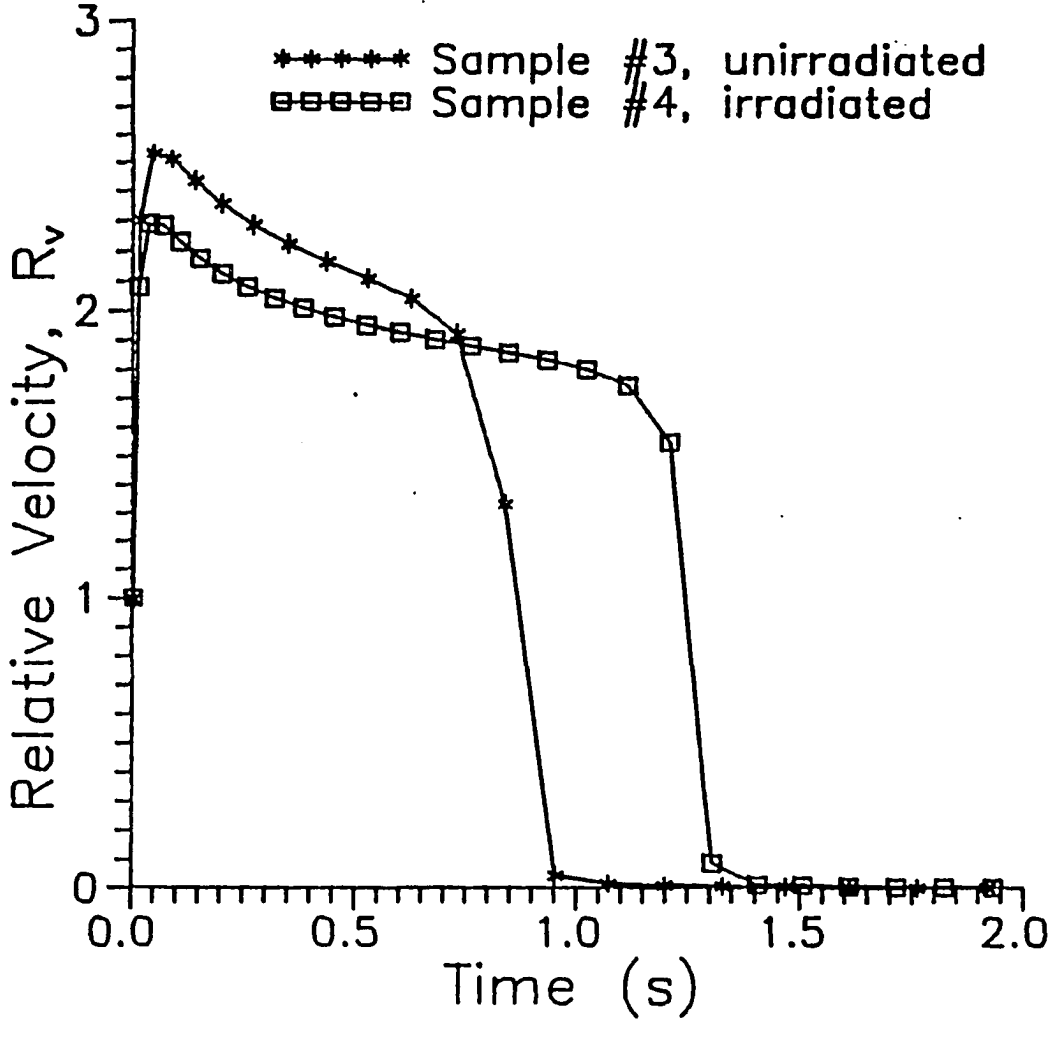

Figure 4.4: Relative velocity profiles of the leading dislocations in niobium single crystals. Pile-up length and shear stresses are the same as for Figure 4.2

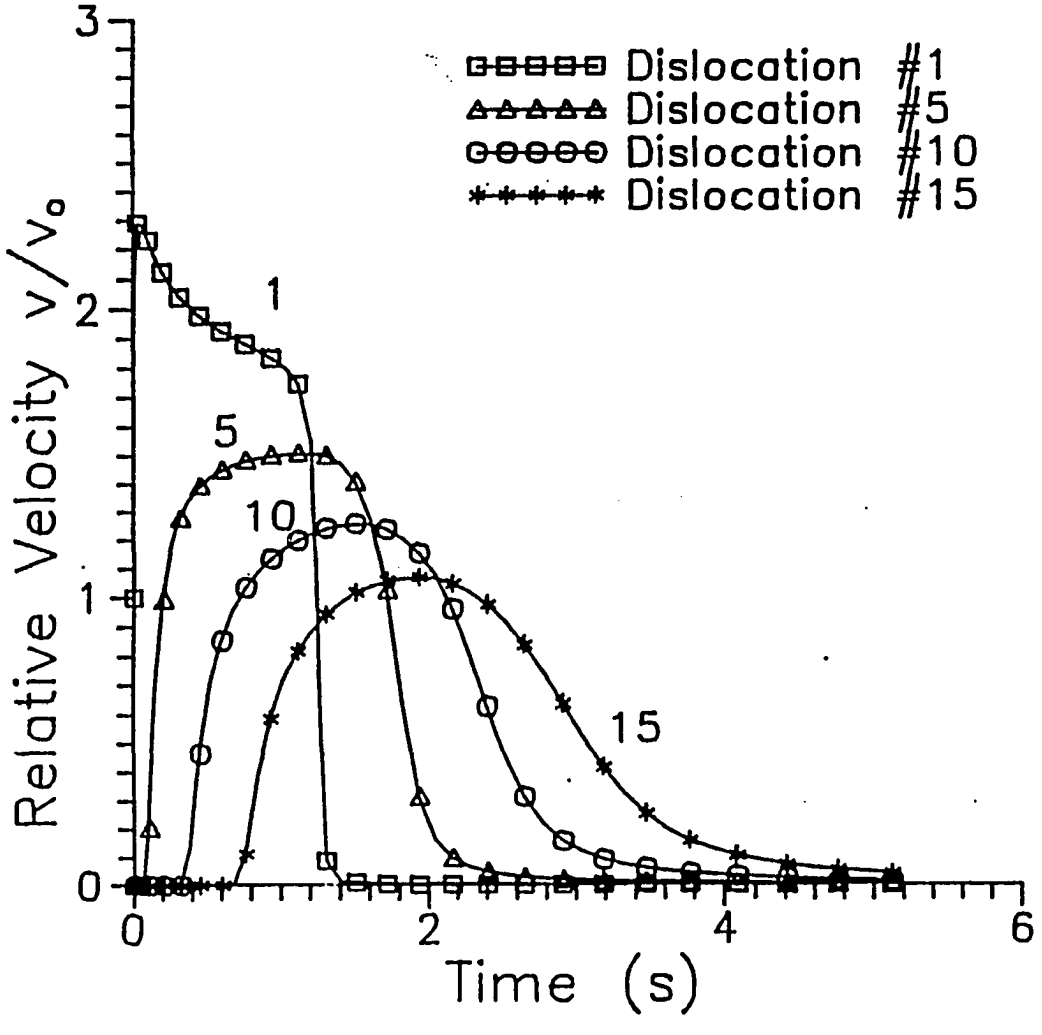

Figure 4.5: Relative velocity profiles of dislocations in the pile-up for irradiated Sample #4 (see, Tables 4.2 and 4.3). v_o is the velocity of an isolated dislocation due to only the applied shear stress. Pile-up length and applied shear stress are 50 μm and 40.5 MPa, respectively

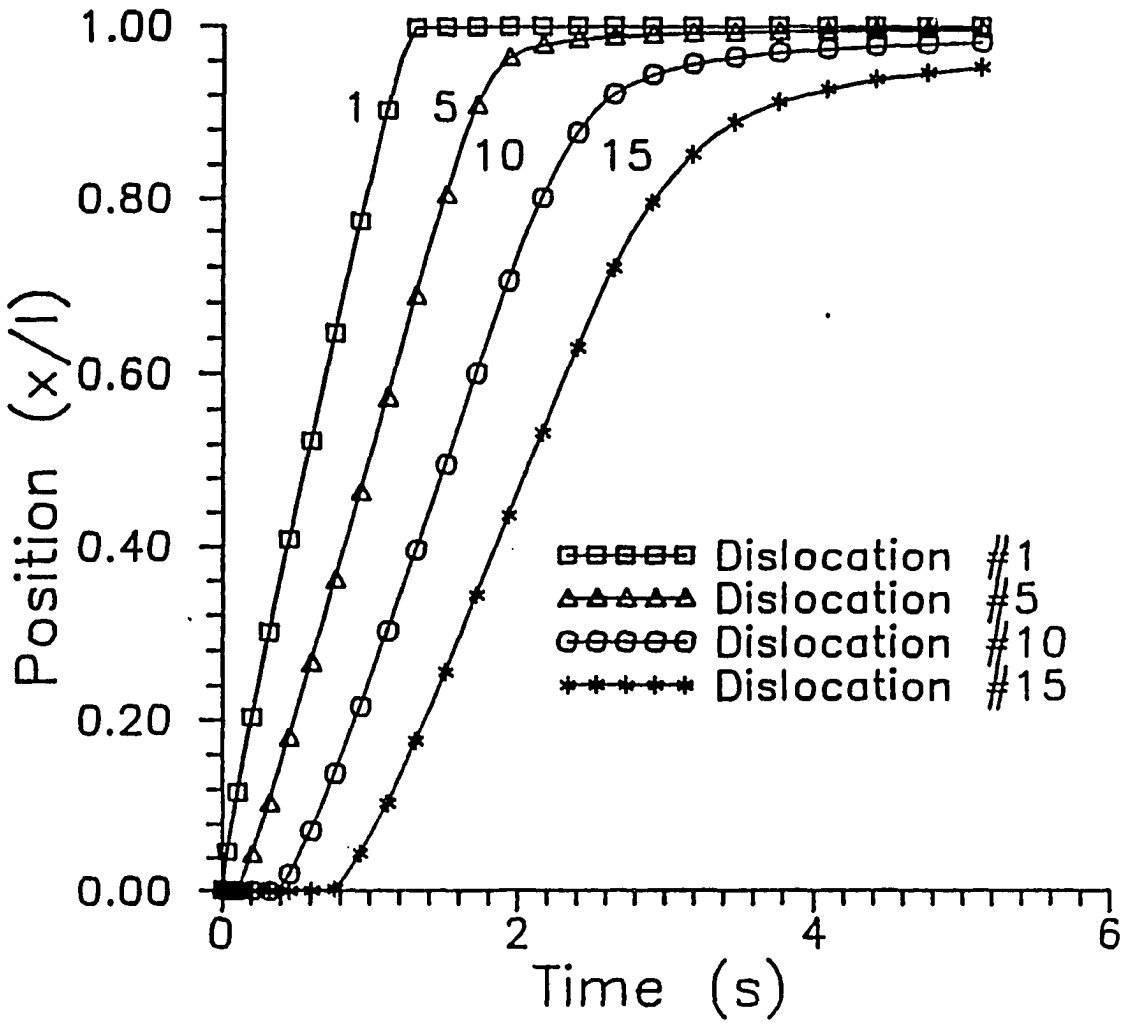

Figure 4.6: Locations of dislocations as a function of time for irradiated Sample #4 (see, Tables 4.2 and 4.3). Pile-up length and applied shear stress are 50 μm and 40.5 MPa, respectively

is assumed that dislocation channels are formed by a number of dynamic dislocation pile-ups. The length of these pile-ups is between specified limits, ℓ_{min} and ℓ_{max}. The length of pile-ups is represented by a distribution function $P(\ell)$, i.e., the number of dynamic pile-ups whose lengths are between ℓ and $\ell + d\ell$ is $P(\ell)d\ell$. Due to the absence of any experimental evidence to develop such a distribution function, it is assumed that this function is represented by a Gaussian distribution function

$$P(\ell)d\ell = \frac{n_\ell}{\sqrt{2\pi}p} \exp\left[-\frac{1}{2}\left(\frac{\ell - \bar{\ell}}{p}\right)^2\right] d\ell \tag{4.2}$$

where n_ℓ is the total number of pile-ups in one slip plane. $\bar{\ell}$ is the average length of slip lines and p is the standard error associated with pile-up lengths. Function $H(\tau_a, \ell, t)$, Equation 3.27, is the total fractional distance traveled by dislocations in a pile-up of length ℓ. Once the required shear displacement per channel is known, the crosshead speed of the tensile machine can be calculated from the total shear displacement as a function of time. Tucker made slip line observations in irradiated and unirradiated niobium single crystals [50]. The orientation of crystals for the tensile test was chosen such that $(\bar{1}01)$ [111] slip system had the maximum resolved shear stress. For this orientation, both the $(\bar{1}01)$ plane normal and the [111] direction make an angle of 45 degrees with the rod axis. Tensile tests were carried out with cylindrical samples with 1.905 cm gage length.

A detailed analysis of dislocation channeling in niobium is reported by Tucker et al. [21] based on transmission electron microscopy observations of irradiated and deformed samples. The tensile sample was polycrystalline niobium of 0.13 mm thick, 4.2 mm wide, and 12.7 mm in gage length. The neutron fluence was 4.4×10^{18} n/cm^2. The samples were strained to 6.6% at a constant strain rate of 1.3×10^{-4} s^{-1}. Observations for six different cases are given in Table 4.4.

Table 4.4: Properties of dislocation channels in niobium based on TEM observations [21]

	Slip plane	Channel width (μm)	Shear displacement (μm)
Case I	$(\bar{1}10)$	0.333	0.33
Case II	$(\bar{1}01)$	0.330	0.30
Case III	$(01\bar{1})$	0.450	0.95
Case IV	$(01\bar{1})$	0.450	0.671
Case V	$(01\bar{1})$	0.396	1.210
Case VI	$(\bar{1}10)$	0.555	0.594

The measurement of individual pile-up lengths is difficult in niobium due to the waviness of slip planes. Neuhäuser, however, gives a collection of typical slip line data for several selected materials. For instance, slip line length in copper single crystals is 11-600 μm for single slip orientation [35]. 600 μm long pile-ups are observed in the early stages of deformation (strain below 5.2%). For the strain range from 20% to 24.3%, the typical length is 20 μm. At higher strains (38-27.5%), 11 μm long pile-ups are observed. Shorter slip lines may be expected in niobium in the early stages of deformation due to lower mobility of dislocations. Greenman et al. [32] measured the velocity of dislocations in copper single crystals. Parameters K and m were found to be 3.25 m/s/(MPa)^m and 0.7, respectively. The velocity of dislocations at the critical resolved shear stress, 0.5 MPa, is about 2 m/s. Therefore, short pile-ups are easily eliminated and observations show long dislocation pile-ups. On the other hand, the velocity of dislocations in irradiated niobium (Sample #4) at the upper yield stress is only 1.97×10^{-5} m/s (Table 4.3). Since dislocations could not travel long distances, the lengths of pile-ups are determined by the arrangements

of possible barriers.

Parameters required for the computer simulation are selected based on experimental observations when the experimental information is available. However, in the absence of specific information for niobium, a reasonable estimate is made based on the information available for other metals. One specific example is the distribution of dynamic pile-up lengths ($P(\ell)$ in Equation 3.26) as well as the limiting values (ℓ_{max} and ℓ_{min}). The minimum pile-up length ℓ_{min} is usually dictated by the magnitude of the instantaneous shear stress. If the shear stress is low, then, the mobility of dislocations is also low which means a longer time to reach the vicinity of the barrier. Also, dislocations in shorter pile-ups reach the barrier in a shorter time at a given stress level, which can cause significant stress concentrations on the barrier. The stress concentration may be so high that dislocations can penetrate the barrier which removes the barrier and extends the length of the pile-up before the activity of dislocations is halted in the channel due to high local strain hardening. Therefore, long pile-ups will remain while short ones are converted to longer pile-ups. ℓ_{min} is chosen such that the leading dislocation does not get very close to the barrier to avoid an excessive stress concentration on the barrier during the formation period of the pile-up. The time to reach the barrier may be estimated by taking the average speed of the leading dislocation as $2v_o$ [51] where v_o is the velocity of an isolated dislocation under the same shear stress.

The upper limit for the pile-up length is usually controlled by the density of microscopic irregularities which may serve as barriers to the dislocation motion. The average length and standard error parameters are selected within reasonable limits. The standard error is chosen as a fraction of the minimum pile-up length. If this

parameter is very small, then, the exponent of the distribution function becomes a very large negative number and causes underflow during computations. The average length is between the minimum and maximum limits. The experimentally observed slip line lengths usually decrease with increasing strain [35]. At the same time, the short pile-ups are eliminated due to high stress concentration on barriers. The average length should increase due to the increase in ℓ_{min}. However, it is thought that the decrease in lengths of large pile-ups balances this effect.

The effects of basic parameters on the deformation process may be analyzed by means of the integral that appears in the shear displacement equation, Equation 3.26, i.e.,

$$I = \int_{\ell_{min}}^{\ell_{max}} \frac{\ell}{\sqrt{2\pi}p} \exp\left[-\frac{1}{2}\left(\frac{\ell-\bar{\ell}}{p}\right)^2\right] H(\tau_a, \ell, t) d\ell \tag{4.3}$$

where H is given by Equation 3.27. The variation of I with different parameters is shown in Table 4.5 as a function of time. Shear displacement in two similar dislocation channels (with the same length, thickness, the number of active planes, and the number of pile-ups per channel) increases with increasing shear stress. The effect of pile-up length is directly related to the distribution function. Without considering the distribution of pile-up lengths, the effect of pile-up length can be analyzed easily. As the pile-up length increases, dislocation sources will produce more dislocations. As dislocations move away from the source, the back stress becomes negligible. Therefore, dislocation emission frequency is greater. The presence of more dislocations results in larger strain contribution. However, it should be kept in mind that the number of pile-ups in the slip plane decreases with increasing pile-up length. For the case of the integral function, I decreases if the limits of the integral are

Table 4.5: Effect of basic parameters on the shear displacement for Sample#4

τ_a (MPa)	34.0	34.1	34.2	34.2	34.2	34.2
$\ell(\mu m)$	25	25	25	25	25	30
$\ell_{min}(\mu m)$	10	10	10	15	10	10
$\ell_{max}(\mu m)$	80	80	80	80	75	80
$p(\mu m)$	5	5	5	5	5	5
Time (s)	Integral parameter, I (mm)					
0.20	3.386	3.502	3.622	3.376	3.549	3.327
0.40	7.595	7.875	8.166	7.612	8.006	7.474
0.60	12.52	13.01	13.51	12.58	13.24	12.33
0.80	18.04	18.75	19.48	18.14	19.09	17.77
1.00	23.99	24.94	25.91	24.18	25.40	23.70
1.20	30.34	31.56	32.84	30.70	32.22	30.09
1.40	37.25	38.80	40.41	37.67	39.68	36.97
1.60	44.66	46.55	48.51	45.10	47.60	44.38
1.80	52.49	54.71	57.02	52.98	55.87	52.19
2.00	60.61	63.13	65.73	61.14	64.33	60.23
2.20	68.84	71.64	74.52	69.59	72.92	68.50
2.40	77.13	80.25	83.49	78.29	81.79	77.10
2.60	85.65	89.17	92.85	87.09	91.10	86.10
2.80	94.54	98.48	102.5	95.89	100.7	95.49
3.00	103.7	108.0	112.4	104.7	110.3	105.1
3.20	113.0	117.6	122.3	113.6	119.7	114.7
3.40	122.2	127.0	131.8	122.6	128.9	124.3
3.60	131.2	136.2	141.3	131.4	138.1	133.9
3.80	140.1	145.4	150.8	140.0	147.2	143.5
4.00	149.0	154.5	160.1	148.7	156.1	153.1

Table 4.6: Parameters used in computer simulations

m	10
K	1.66×10^{-21} m/s/(MPa)^m
ℓ_{min}	20 μm
ℓ_{max}	100 μm
ℓ	40 μm
p	5 μm
h	0.5 μm
Sample length	12 mm
Sample width	3 mm
Strain rate	1.75×10^{-4} s^{-1}
Crosshead speed	2.1×10^{-3} mm/s
Minimum separation distance between channels	2 μm
Shear stress at lower yield point	31.77 MPa
Engineering strain at lower yield point	0.032

contracted.

The computer simulation of dislocation channeling is performed for Sample #4. It is chosen as the specific example because the strain-stress curve and the velocity parameters (K and m, Table 4.3) have been experimentally determined [33]. The simulation is carried out for a sheet tensile sample of 3 mm wide and 12 mm in gage length. The constant strain rate is taken as 1.75×10^{-4} s^{-1}, which is the same strain rate used by Tucker [50]. The corresponding crosshead speed of the tensile machine is 2.1×10^{-3} mm/s. The sample is assumed to have such an orientation that the tensile axis makes a 45^o angle with the slip direction, $< 111 >$, and slip plane, $\{110\}$, as in the case of tensile tests performed by Tucker [50]. Parameters used in computer simulations are summarized in Table 4.6.

As a part of the input to the computer code DEFORM, a table of H values is supplied, as shown in Table 4.7, where H is defined by Equation 3.27. This table is prepared using the results obtained by the computer code PILEUP. Information about these codes is given in the Appendix. Table 4.7 contains values of H as a function of β and Θ, which can be used for a number combinations of τ_a and ℓ. For instance, the range of ℓ values when τ_a is 32 MPa (which is approximately the stress used in this simulation) is approximately 9 to 230 μm.

The initial values of the minimum and the maximum dislocation pile-up lengths, as shown in Table 4.6, are taken to be 20 and 100 μm, respectively. The value of ℓ_{max} remains constant at 100 μm, but ℓ_{min} may increase during the course of the calculations, as discussed above. The average length, $\bar{\ell}$ is assumed to be 40 μm. The standard error associated with pile-up lengths is taken as p =5 μm. The lower limit of the pile-up length is internally adjusted during the simulation by approximating the position of the leading dislocation in the pile-up. The average velocity of the leading dislocation is about twice the velocity of an isolated dislocation under the same applied shear stress [51]. The stress concentration on the barrier rapidly increases as the leading dislocation comes closer to the barrier, and it becomes exceedingly high in a very short period of time as the second term in Equation 3.15 becomes dominant in comparison with τ_a. The minimum pile-up length for a specific shear stress is calculated in such a way that the leading dislocation does not reach the location of the barrier if it moves with the average velocity. This is done by estimating the time period for the leading dislocation moving with the average velocity to reach the vicinity of the barrier (within 1% of the pile-up length). If it is shorter than the formation time of the dislocation channel, barriers with this

Table 4.7: H values used in the computer simulation

β	4.E-4	6.E-4	8.E-4	1.E-3	2.E-3	4.E-3	6.E-3	8.E-3	1.E-2
Θ									
0.000	0.000	0.000	0.000	0.000	0.000	0.000	0.000	0.000	0.000
0.050	0.051	0.436	0.396	0.367	0.298	0.253	0.234	0.216	0.190
0.100	1.395	1.159	1.022	0.935	0.728	0.591	0.532	0.501	0.440
0.150	2.561	2.091	1.830	1.662	1.256	0.921	0.881	0.772	0.798
0.200	3.977	3.217	2.785	2.511	1.864	1.445	1.267	1.163	1.047
0.250	5.617	4.510	3.892	3.479	2.552	1.944	1.654	1.550	1.464
0.300	7.471	5.960	5.112	4.560	3.302	2.487	2.142	1.939	1.744
0.350	9.528	7.557	6.463	5.749	4.118	3.051	2.627	2.364	2.203
0.400	11.77	9.300	7.936	7.040	4.991	3.670	3.108	2.770	2.517
0.450	14.22	11.19	9.514	8.426	5.914	4.289	3.586	3.118	2.848
0.500	16.84	13.20	11.20	9.894	6.851	4.872	4.017	3.513	3.203
0.550	20.36	15.33	12.94	11.37	7.763	5.434	4.450	3.851	3.434
0.600	23.42	17.47	14.68	12.86	8.658	5.977	4.846	4.199	3.720
0.700	29.38	21.71	18.08	15.73	10.38	6.998	5.596	4.769	4.240
0.750	32.31	23.77	19.74	17.14	11.20	7.464	5.919	5.081	4.424
0.800	35.18	25.82	21.36	18.49	12.00	7.943	6.285	5.333	4.720
0.850	38.01	27.82	22.95	19.84	12.77	8.385	6.607	5.582	4.496
0.900	40.78	29.78	24.51	21.13	13.52	8.820	6.907	5.835	5.107
0.950	43.50	31.72	26.02	22.41	14.25	9.223	7.213	6.067	5.254
1.000	46.17	33.60	27.51	23.64	14.95	9.636	7.499	6.293	5.496

specific length are destroyed by the dislocations and the length of the pile-up is extended. Otherwise, if the time period is longer than the formation time of the dislocation channel, pile-ups survive at this stress level.

It is assumed that dislocation channels have a uniform width of 0.5 μm. Tucker et al. [21] reported dislocation channels in niobium with widths varying between 0.33 and 0.55 μm based on TEM observations (Table 4.4). Since the spacing between {110} planes in Nb is about 0.23 nm, the number of parallel slip planes in the channels is approximately between 1400 and 2400. The minimum separation

distance between dislocation channels is taken to be 2 μm. This may be justified by examining the TEM micrographs obtained in niobium [21].

Available space for pile-up formation on an active slip plane is evaluated at each step by subtracting the area used up by intersecting channels from the total channel length. Then, the number of pile-ups, n_ℓ, is calculated by dividing the total available channel length by the average pile-up length, $\bar{\ell}$. Thus,

$$n_\ell = \frac{(1-f)L}{\bar{\ell}} \tag{4.4}$$

where f is the fraction of the channel length used up by intersecting channels. For values of the parameters ℓ_{min}, ℓ_{max}, and p used in the computer simulation (Table 4.6), the average pile-up length $\bar{\ell}$ is very close to 40 μm.

The simulation is started at the lower yield stress. The resolved shear stress at that point is 31.77 MPa [33]. During the simulation the applied shear stress is increased by small amounts so that it is adjusted to the level necessary to maintain the crosshead velocity corresponding to the imposed strain rate, 1.75×10^{-4} s^{-1}. The increments are 0.001 MPa.

Computer simulations for the plastic deformation on a macroscopic scale are performed for several different conditions. The effects of two parameters, n the number of active slip planes per channel and S the shear displacement per channel, on the strain-shear stress curve are analyzed. S is kept within the range of 1.20-1.25 μm in the first series of calculations. Four simulations are performed with different numbers of active slip planes per channel. The results of simulations are summarized in Table 4.8. Shear stress as a function of engineering strain is shown in Figure 4.7. The effect of the increasing number, n, of active slip planes in the channel is a decrease in the number of simultaneously operating dislocation channels. As the

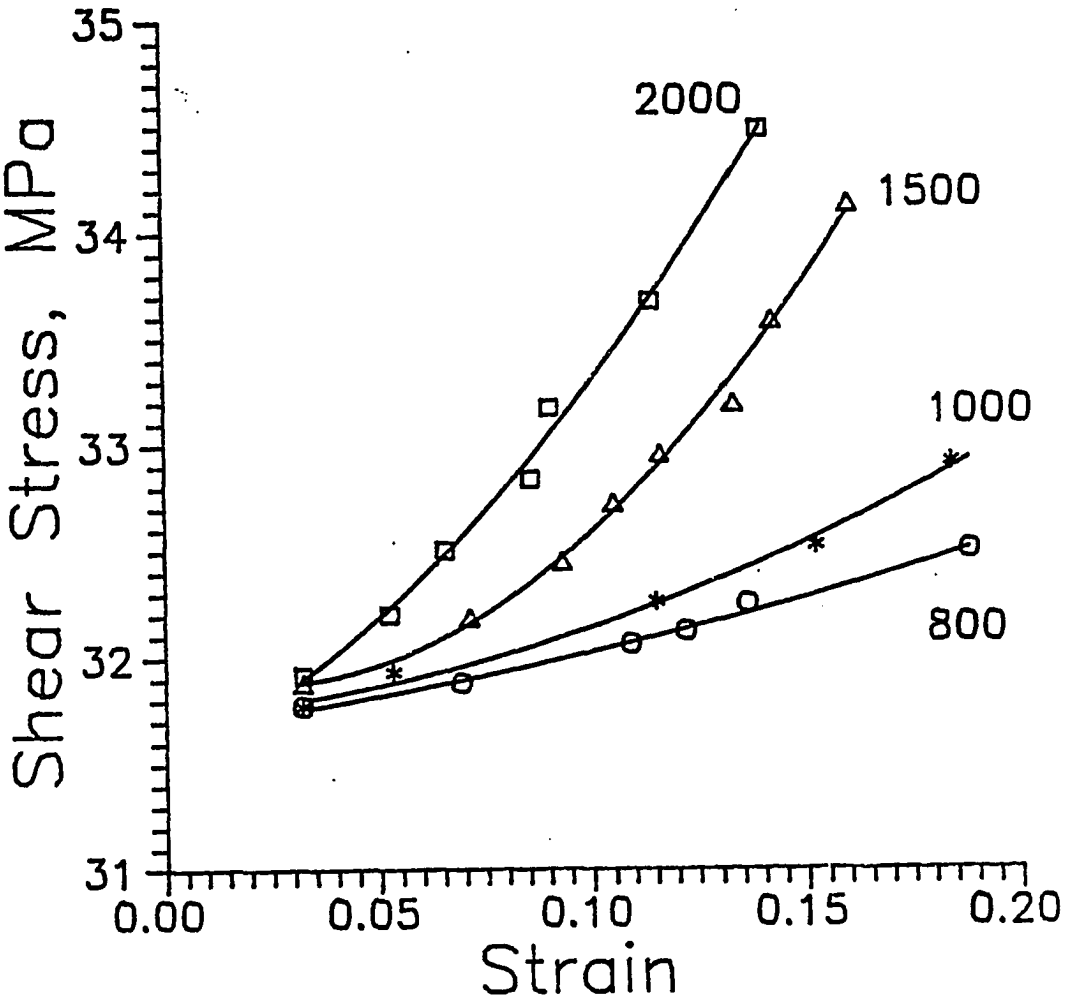

Figure 4.7: Computer simulation results. Shear stress as a function of engineering strain with different number of active planes per channel as indicated and for S range of 1.20 to 1.25 μm

Table 4.8: Results of computer simulations. Shear stress as a function of the numbers of active slip planes per channel, as indicated, for S range of 1.20 to 1.25 μm

Engineering strain	Shear stress (MPa)	Number of simultaneously operating channels	Channel formation time (s)
n=800			
0.032	31.77	24	10.40
0.069	31.88	23	10.07
0.109	32.06	22	9.65
0.122	32.12	21	8.82
0.136	32.25	20	8.32
n=1000			
0.032	31.77	20	8.67
0.053	31.93	19	8.40
0.115	32.26	18	7.96
0.152	32.52	17	7.54
0.184	32.91	16	7.29
n=1500			
0.032	31.88	14	6.35
0.071	32.18	13	5.90
0.093	32.45	12	5.51
0.105	32.72	11	5.04
0.116	32.95	10	4.65
0.133	33.19	9	4.20
0.142	33.58	8	3.80
0.160	34.12	7	3.34
n=2000			
0.032	31.91	11	5.10
0.052	32.20	10	4.69
0.066	32.50	9	4.24
0.086	32.83	8	3.85
0.090	33.17	7	3.39
0.114	33.67	6	2.95
0.140	34.48	5	2.66

deformation proceeds, the number of simultaneously operating channels remains the same until the shear displacement falls below the prescribed range. At this point, the number of active channels is reduced by one. Meanwhile, the applied shear stress increases to obtain the same axial extension rate in a smaller active volume, i.e., the part of the sample where plastic deformation takes place. A fractional decrease in the active volume is more significant when more slip planes are active in the channel. As a consequence of this, strain hardening increases with increasing n. This result may be expected due to a greater dislocation density in the channel as the result of increasing number of active slip planes.

The experimentally obtained shear stress-engineering stress curve [33] indicates that strain hardening is not significant at low strains. The best agreement with the experimental curve is obtained for the case of n=1000. Another simulation is performed using a different range of shear displacement(1.45 to 1.50 μm) to analyze the effect of the shear displacement per channel on the shear stress-strain curve. Figure 4.8 shows the experimentally observed curve [33] and the results of two simulations with n=1000. Results show that variation of shear displacement per channel does not significantly affect the response of the material. A slight increase is observed in the strain hardening upon a decrease in S. The applied stress varies almost linearly with the engineering strain in the strain range used in simulations. The relation between the shear stress and the engineering strain may be calculated by a least square fit to a straight line. The following relations are obtained from the computer simulation results and the experimentally obtained shear stress-strain curve given by Guberman [33].

S=1.20-1.25 μm, n=1000 : $\quad \tau_a = 31.53 + 7.02\,\epsilon$

Table 4.9: Results of computer simulations as a function of shear displacement for n=1000

Engineering strain	Shear stress (MPa)	Number of simultaneously operating channels	Channel formation time (s)
S= 1.20-1.25 μm			
0.032	31.77	20	8.67
0.053	31.93	19	8.40
0.115	32.26	18	7.96
0.152	32.52	17	7.54
0.184	32.91	16	7.29
S= 1.45-1.50 μm			
0.032	31.79	20	10.07
0.070	31.95	19	9.57
0.093	32.10	18	9.07
0.125	32.25	17	8.56
0.144	32.42	16	8.05
0.177	32.61	15	7.55
0.202	32.84	14	7.06

S=1.45-1.50 μm, n=1000 : $\tau_a = 31.54 + 6.15\,\epsilon$

Experimental : $\tau_a = 31.56 + 6.63\,\epsilon$

where ϵ is engineering strain and τ_a is the applied shear stress in MPa. Relative errors in estimated instantaneous shear stress are less than 1%. The greatest absolute error in the shear stress is 0.26 MPa in the smaller shear displacement case at 12.5% engineering strain.

A computer simulation is carried out for an engineering strain up to 20%. The number of dislocation channels in the sample at this strain level is of the order of 2500. The required run time for this simulation in 10 CPU minutes on a NAS-

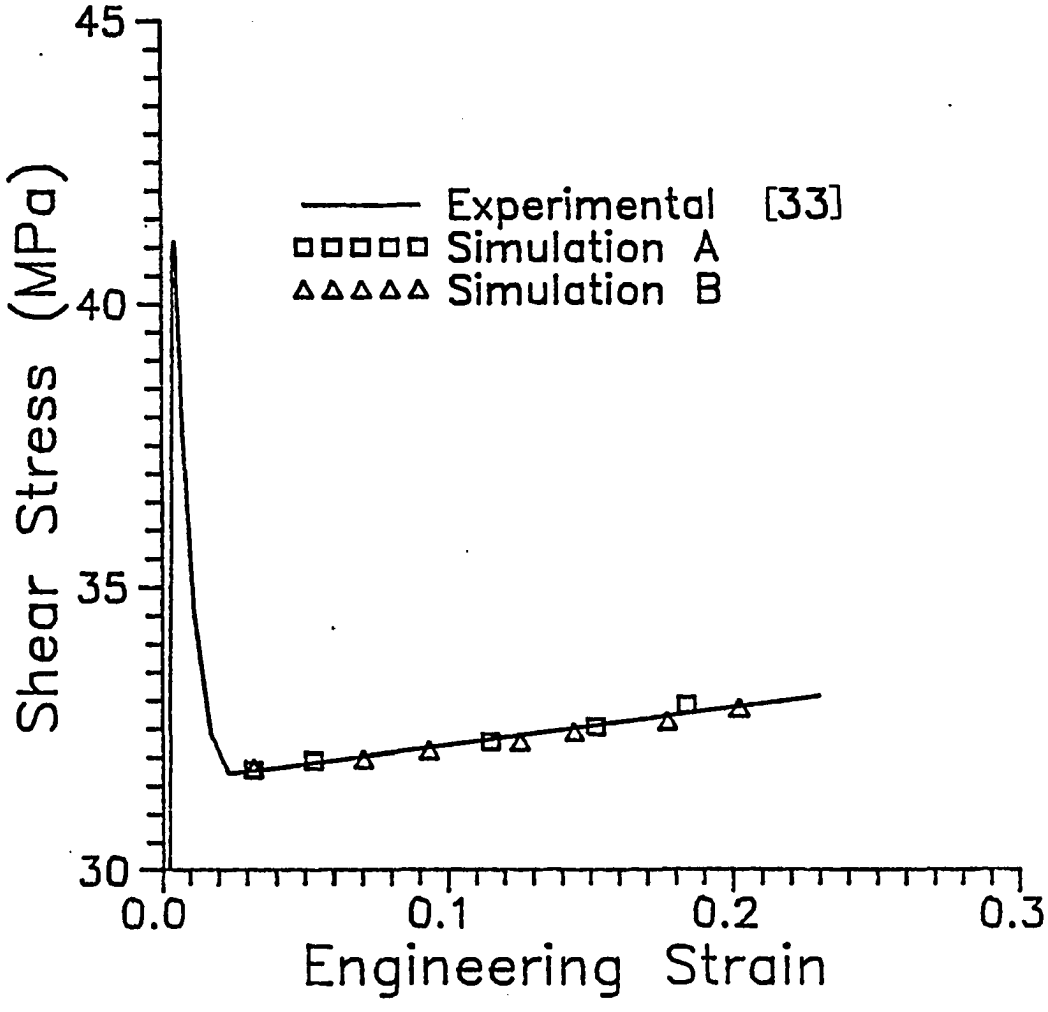

Figure 4.8: Shear stress-engineering strain curve for irradiated niobium single crystal, earlier experimental results [33] and computer simulations in this study. n is 1000. Shear displacement per channel is 1.20-1.25 and 1.45-1.50 μm in Simulation A and B, respectively

AS/9160 mainframe computer. The required memory size is about 7 megabytes. Extension of the simulation for further deformation requires larger computer memory and a longer CPU time. Another problem associated with further deformation is the round-off error in the calculations. Single precision operation is used throughout the computations to reduce the required memory size. Since the code usually deals with small differences between large numbers, the errors associated with the calculations may build up and cause some instabilities in the calculations. The work hardening region (Stage II deformation) is expected to start at a strain level of about 25%. One way to simulate plastic deformation in this region with a similar model may be to start with a smaller number of simultaneously forming dislocation channels and to limit shear displacement per channel to a smaller value. Therefore, the number of simultaneously forming channels is decreased more often. To obtain the same amount of axial extension with a smaller active volume, the shear stress should increase more rapidly.

The computer simulation may be used to follow the shape of the sample as a function of deformation. It should be remembered that each dislocation channel introduces four new exterior points in the sample. Each channel is also associated with a very small displacement (less than 1 μm). For the sample deformed to 20% strain, there are approximately 2500 dislocation channels, 10^4 exterior points, and 2×10^4 numbers for x and y coordinates of these points. It is difficult to obtain a graphical representation showing the deformed state of the sample using all points.

Because of the nature of the process, the simulation of plastic deformation in an unirradiated sample by a similar model is not feasible without the availability of high speed and memory capacity computers. Slip bands in unirradiated metals

are close to each other and consist of a smaller number of parallel slip planes. The shear displacement associated with each band is quite small. Thus, an excessively large number of slip bands in an unirradiated sample is required to obtain the same macroscopic strain in an irradiated sample. For instance, if slip bands in an unirradiated sample are made of 20 parallel slip planes, it is necessary to create about 125,000 slip bands to obtain 20% strain in a sample similar to the one considered in this work. This requires very large computer memory and long computer time. Simplifications are necessary to reduce these requirements.

5 SUMMARY AND CONCLUSIONS

A model is developed for localized plastic deformation in irradiated metals. The formation of dislocation channels on a microscopic scale is described by dynamic dislocation pile-ups. Local shear displacement is calculated by the total distance traveled by dislocations in dynamic pile-ups of various lengths om closely-spaced parallel slip planes. The dislocation motion is obtained from the solution of a set of coupled differential equations. The macroscopic distribution of the slip bands is governed by a series of postulated criteria. Computer codes are developed to simulate the plastic deformation on microscopic and macroscopic scales under a constant macroscopic strain rate. Simulations are performed based on parameters obtained from the literature for irradiated niobium single crystals.

Computational results show that the distribution of dislocations in the pile-up does not reach equilibrium, with the exception of very short pile-ups. This is due to the low mobility of dislocations in niobium. It is observed that dislocations in the unirradiated sample become immobilized in a shorter period of time. The number of dislocations and the contribution to the shear displacement for a specific pile-up in a given time period increases upon irradiation.

The simulation of the plastic deformation on a macroscopic scale is performed for engineering strains up to 20%. It is observed that strain hardening increases with

an increasing number of active slip planes in the channel. The optimum number of active planes for agreement with experiment is found to be 1000, which is about one-half of the total number of slip planes in the channel. Computer simulation results agree with the experimentally obtained stress-strain curve within an 8% error in strain hardening rate. Relative errors in instantaneous shear stress are less than 1%. It is observed that the effect of the shear displacement per channel on the strain hardening is not significant. However, decreasing the active volume of plastic deformation can cause a considerable increase in strain hardening rate.

More accurate parameters, such as the pile-up length distribution function as a function of the applied shear stress, shear displacement per channel, and channel width may improve the simulation results. A more detailed analysis of dislocation channel formation on a microscopic scale is also needed. Interactions between dislocation pile-ups as well as other microstructural features may be included in the microscopic model in future work. The analysis of dislocation channels in different orientations may be easily performed with the current computer code.

6 BIBLIOGRAPHY

[1] M. S. Wechsler. "Dislocation Channeling in Irradiated and Quenched Metals". p. 19 in *Inhomogeneity of Plastic Deformation*, edited by R. B. Pond (American Society for Metals, Metals Park, 1973).

[2] R. Rodloff and H. Neuhäuser. "Mean Velocity of Edge and Screw Dislocation Groups in Neutron-Irradiated Copper Single Crystals". Phys. Status Solidi *(a)49*, 445 (1978).

[3] G. Saada and J. Washburn. "Interaction between Prismatic and Glissile Dislocations". J. Phys. Soc. Japan *18*, Supp. I, 43 (1963).

[4] A. J. E. Foreman. "Junction Reaction Hardening by Dislocation Loops". Phil. Mag. *17*, 353 (1968).

[5] A. J. E. Foreman and J. V. Sharp. "A Mechanism for the Sweeping-up of Loops by Glide Dislocations during Deformation". Phil. Mag. *20*, 931 (1969).

[6] R. P. Tucker and M. S. Wechsler. "Radiation Hardening in Niobium - Dependence of the Yield Stress on Neutron Dose". Rad. Eff. *3*, 73 (1970).

[7] M. S. Beck. "Dispersed Barrier Hardening in Irradiated Metals". Ph. D. Dissertation, Iowa State University (1978).

[8] J. Silcox and P. B. Hirsch. "Dislocation Loops in Neutron Irradiated Copper". Phil. Mag. *4*, 1356 (1959).

[9] J. C. Crump, "Dislocation Loops in Neutron-Irradiated Copper". Bull. Amer. Phys. Soc. *13*, 462 (1968).

[10] M. Wilkens and M. Rühle. "Observations of Point Defect Agglomerations in Copper by Means of Electron Microscopy". p. 365 in *The Nature of Small Defect Clusters* Vol. 2, edited by M. J. Makin, AERE, Harwell, Report AERE-R5269 (H.M.S.O., London, 1966).

[11] K. G. McIntyre and L. M. Brown. "Diffraction Contrast from Small Defect Clusters in Irradiated Copper". p. 351 in *The Nature of Small Defect Clusters* Vol. 2, edited by M. J. Makin, AERE, Harwell, Report AERE-R5269 (H.M.S.O., London, 1966).

[12] M. J. Makin and S. A. Manthorpe. "The Annealing of Dislocation Loops in Neutron Irradiated Copper". Phil. Mag. *8*, 1725 (1963).

[13] R. Bajaj and M. S. Wechsler. "Defect Clusters in Neutron Irradiated Vanadium Containing Oxygen". Metall. Trans. *7A*, 351 (1976).

[14] I. G. Greenfield and H. G. F. Wilsdorf. "Effect of Neutron Irradiation on the Plastic Deformation of Copper Single Crystals". J. Appl. Phys. *32*, 827 (1961).

[15] A. Seeger. "Work Hardening of Metal Single Crystals, Slip Lines, and Transmission Electron Microscopy". p. 3 in *The Relation Between the Structure and Mechanical Properties of Metals* Vol. 1 (H.M.S.O., London, 1963).

[16] J. V. Sharp. "Deformation of Neutron-Irradiated Copper Single Crystals". Phil. Mag. *16*, 77 (1967).

[17] J. V. Sharp. "Correlation between Cleared Channels and Surface Slip Steps in Neutron-Irradiated Copper Crystals". Rad. Eff. *14*, 71 (1972).

[18] M. Meshii. "The Structure and Mechanical Properties of Quenched Face Centered Cubic Metals". p. 387 in *Lattice Defects in Quenched Metals*, edited by R. M. Cotterill, M. Doyama, J. J. Jackson, and M. Meshii (Academic Press, New York, 1965).

[19] T. Mori and M. Meshii. "Plastic Deformation of Quench-Hardened Aluminum Single Crystals". Acta Metall. *17*, 167 (1969).

[20] A. H. Cottrell. "Point Defects and the Mechanical Properties of Metals and Alloys at Low Temperatures". p. 1 in *Vacancies and Other Point Defects in Metal and Alloys* (The Institute of Metals, London, 1958).

[21] R. P. Tucker, M. S. Wechsler, and S. M. Ohr. "Dislocation Channeling in Neutron-Irradiated Niobium". J. Appl. Phys. *40*, 400 (1969).

[22] J. V. Sharp. "Deformation of Neutron Irradiated Copper Alloys". Acta Metall. *22*, 449 (1974).

[23] L. M. Howe. "Irradiation Hardening and Annealing in Copper at High Neutron Fluences". Rad. Eff. *23*, 181 (1974).

[24] H. Neuhäuser and R. Rodloff. "Study of Slip Band Development on Neutron-Irradiated Copper Single Crystals by High Speed Cinematography". Acta Metall. *22*, 375 (1974).

[25] H. Neuhäuser and R. Rodloff. "Determination of the Velocity and Local Density of Mobile Dislocations within Slip Bands in Neutron-Irradiated Copper by High Speed Cinematography". Phys. Status Solidi *(a)24*, 549 (1974).

[26] K. Shinohara, S. Kitajima, and H. Kurishita. "Dislocation Motion in FCC Metal Crystals". p. 95 in *Strength of Metal and Alloys* Vol. 1, edited by R. C. Gifkins (Pergamon Press, New York, 1982).

[27] H. Mughrabi, D. Ströhle, and M. Wilkens. "Irradiation Hardening and Localized Deformation of Neutron-Irradiated α-Iron Single Crystals". Z. Metallk. *72*, 300 (1981).

[28] E. Johnson and P. B. Hirsch. "In Situ Straining in the HVEM of Neutron-Irradiated Copper Crystals". Phil. Mag. *43A*, 157 (1981).

[29] P. D. K. Nathanson, P. J. Jackson, and D. R. Spalding. "Secondary Slip in Neutron-Irradiated Crystals". Acta Metall. *28*, 823 (1980).

[30] J. J. Gilman and W. G. Johnston. "The Origin and Growth of Glide Bands in Lithium Flouride Crystals". p. 116 in *Dislocations and Mechanical Properties of Crystals*, edited by J. C. Fisher, W. G. Johnson, R. Thomson, and T. Vreeland, Jr. (John Wiley & Sons, New York, 1957).

[31] D. F. Stein and J. W. Low. "Mobility of Edge Dislocations in Silicon Iron Crystals". J. Appl. Phys. *31*, 362 (1960).

[32] W. E. Greenman, T. Vreeland, and D. S. Wood. "Dislocation Mobility in Copper". J. Appl. Phys. *38*, 3595 (1967).

[33] H. D. Guberman. "Stress Dependence of Dislocation Velocity in Single Crystal Niobium". Acta Metall. *16*, 713 (1968).

[34] M. Wada, M. Meshii, and K. Marukawa. "Dislocation Velocity in Copper Electron Irradiated at 100°K". Phys. Status Solidi *(a)57*, 345 (1980).

[35] H. Neuhäuser. "Slip-Line Formation and Collective Dislocation Motion". p. 323 in *Dislocations in Solids* Vol. 6, edited by F. R. N. Nabarro (North-Holland Pub. Co., Amsterdam, 1983).

[36] J. D. Eshelby, F. C. Frank, and F. R. N. Nabarro. "The Equilibrium of Linear Arrays of Dislocations". Phil. Mag. *42*, 351 (1951).

[37] A. K. Head and N. Louat. "The Distribution of Dislocations in Linear Arrays". Aust. J. Phys. *8*, 1 (1954).

[38] A. R. Rosenfield and G. T. Hahn. "Linear Arrays of Moving Dislocations Piling-Up Against an Obstacle". Acta Metall. *16*, 755 (1967).

[39] M. F. Kanninen and A. R. Rosenfield. "The Dynamics of Dislocation Pile-Up Formation". Phil. Mag. *20*, 569 (1969).

[40] A. R. Rosenfield and M. F. Kanninen. "The Dynamics of Dislocation Pile-Up Formation with a Non-Linear Stress-Velocity Relation for Dislocation Motion". Phil. Mag. *21*, 143 (1970).

[41] T. Yokobori, A. T. Yokobori Jr., and A. Kamei. "Computer simulation of Dislocation Emission from a Stressed Source". Phil. Mag. *30*, 367 (1974).

[42] F. P. Gerstle and G. J. Dvorak. "Dynamic Formation and Release of a Dislocation Pile-up Against a Viscous Obstacle". Phil. Mag. *29*, 1337 (1974).

[43] S. I. Zaitsev and E. M. Nadgornii. "The Movement of Double-Ended Dislocation Arrays through Discrete Obstacles". Phys. Status Solidi *(a)28*, 49 (1975).

[44] P. S. Steif and R. J. Clifton. "On the Kinetics of a Frank-Read Source". Mater. Sci. Eng. *41*, 251 (1979).

[45] A. R. Rosenfield. "A Continuous Distribution of Moving Dislocations". Phil. Mag. *23*, 63 (1972).

[46] M. J. Makin and J. V. Sharp. "A Model of Lattice Hardening in Irradiated Copper Crystals with External Characteristics of Source Hardening". Phys. Status Solidi *9*, 109 (1965).

[47] J. P. Hirth and J. Lothe. *Theory of Dislocations* (J. Wiley & Sons, New York, 1982) pp. 59-96.

[48] D. A. Andersen, J. C. Tannehill, and R. H. Pletcher. *Computational Fluid Dynamics and Heat Transfer* (Hemisphere Pub. Co., Cambridge, 1984) pp. 138-154.

[49] E. Nadgornyi. *Dislocation Dynamics and Mechanical Properties of Crystals* (Pergamon Press, New York, 1988) p. 469.

[50] R. P. Tucker. "The Effect of Neutron Irradiation on Plastic Deformation in Niobium Single Crystals". ORNL-TM-1583 (Oak Ridge National Laboratory, Oak Ridge, 1966).

[51] A. R. Rosenfield and G. T. Hahn. "Linear Arrays of Moving Dislocations Emitted by a Source". p. 255 in *Dislocation Dynamics*, edited by A. R. Rosenfield, G. T. Hahn, A. L. Bement, Jr., and R. I. Jaffee (McGraw-Hill, Inc., New York, 1968).

[52] G. E. Forsythe, M. A. Malcolm, and C. B. Moler. *Computer Methods for Mathematical Computations* (Prentice-Hall, Englewood Cliffs, 1977) p. 77.

7 APPENDIX: DESCRIPTION OF COMPUTER CODES

7.1 The PILEUP Code

The PILEUP code is written according to FORTRAN77 standards. It is used to evaluate the parameters related to the dynamic dislocation pile-up formation. It is based on the solution of N number of coupled nonlinear differential equations, Equations 3.18 or 3.22. The solutions are obtained by the subroutine LSODA from the ODEPACK subroutine package. LSODA utilizes the Adams algorithm.

The PILEUP code contains a main program and four subroutines. The main program also calls LSODA. Calculations start with a single differential equation. The number of equations increases with increasing number dislocations in the pile-up. The approximate time for the emission of a new dislocation is estimated by an extrapolation process. First, LSODA is called three consecutive times with very small time increments. The time increments are selected as a fraction of the time period between the emission two consecutive dislocations in the subsequent step. Therefore, these time increments are adjusted with respect to the activation frequency of the source. The values of the stress acting on the source corresponding to these three time increments are stored. The time period to reach the critical stress for source activation is estimated by the subroutine GUESS3 by extrapolation using

the time and stress values. Extrapolated parameters are then used by LSODA in the next call and the worst estimates are replaced by the parameters evaluated by LSODA. This is repeated until the critical stress is reached on the source within a certain amount of error. At this stage, the number of dislocations is increased by one. Arguments required by LSODA are also updated according to new conditions.

An approximation, may be called a superdislocation approximation, is used in the PILEUP code to avoid exceedingly long computations for conditions required for the presence of a large number of dislocations in the pile-up (i.e., very long pile-up or high applied stress). If the number of dislocations is greater than a specified value (which was chosen to be 50), then, two dislocations with the smallest separation distance are selected, except that the first and last five dislocations are excluded. These two dislocations are replaced by a single superdislocation with a strength equal to the sum of the strengths of the two dislocations being combined into the superdislocation. The location of the new superdislocation is selected such that the stress on the leading dislocation by the superdislocation is the same as the total stress applied by the two former dislocations. Normally, dislocations close to the source at the early stages and dislocations close to the barrier at the late stages of the pile-up formation are separated by small distances.

The subroutines combined with the PILEUP code are:

F: contains differential equations and called by LSODA.

REL: checks whether equilibrium conditions are reached. This is done by monitoring the current velocity of each dislocation in the pile-up. If they move slower than a prespecified speed, the equilibrium condition is assumed to be

fulfilled.

GUESS3: provides an estimated time value for the reactivation of dislocation source. This is done by finding the zeros of a second order equation constructed with the result obtained by LSODA in previous calls.

JACOB: contains derivatives of the differential equations with respect to dependent parameters. To supply this subroutine is an option of LSODA. However, computations are considerable faster if this subroutine is provided.

The following parameters and typical values are used as input to the PILEUP code in the given order.

NVP: The power of the stress-dislocation velocity relation, 10

VELCO: The coefficient of the stress-dislocation velocity relation, 1.66×10^{-18} mm/s/(MPa)^m.

TAU: The applied shear stress, 32 MPa

PLEN: The length of the pile-up, 0.05 mm

EPS: maximum dislocation velocity to reach equilibrium, 10^{-10} mm/s

CONV: Convergence criterion, 10^{-4}

DELT: Error parameter, 10^{-6}

FAC: Factor for time increments

CRS: Critical stress for dislocation emission, 0 MPa

TIMAX: Maximum time value to stop the computation, 10 s

DIVID: The fraction of dislocation emission frequency to evaluate time increments, 10

ACO: The material constant A, 2.96×10^{-3} MPa mm

SMAX: Shear wave velocity in the material, 8×10^{5} mm/s

ALP1: Parameter α_1, 0.5

ALP2: Parameter α_2, 1

NF: Number of dislocations in the front end of the pile-up to be excluded from the superdislocation formation consideration, 5

NB: Number of dislocations in the back end of the pile-up to be excluded from the superdislocation formation consideration, 5

NUP: Maximum number of dislocations in the pile-up before the formation of superdislocations, 50

The output of the program consists of the number of dislocations, the total distance traveled by dislocations, stress concentration on the barrier, position of the leading dislocation, and the velocity of the leading dislocation as a function of time. The different combinations of parameters may be obtained by small modifications.

Table 7.1: Listing of the computer code PILEUP

```
C*********************************************************************
C                        PILEUP
C       DISLOCATION PILE-UP CALCULATIONS
C
C*********************************************************************
        EXTERNAL F,JACOB
        IMPLICIT REAL*8 (A-H,O-Z)
        DIMENSION S(100),RWORK(12000),IWORK(120)
        DIMENSION RV(100),XG(3),YG(3)
        DIMENSION SO(100),NDO(100),DST(100)
        COMMON/BL1/NVP,NDI(100),INT(100),BETA,SMAX,
     *  ALP1,ALP2,OM,FRDC
        OPEN(5,FILE='IN2.DAT',STATUS='OLD')
        OPEN(7,FILE='PGR2.DAT',STATUS='UNKNOWN')
        OPEN(8,FILE='DET2.DAT',STATUS='UNKNOWN')
        open(9,FILE='VEL2.DAT',STATUS='UNKNOWN')
        OPEN(10,FILE='POS2.DAT',STATUS='UNKNOWN')
        READ(5,*) NVP,VELCO,TAU,PLEN,EPS,CONV
        READ(5,*) DELT,FAC,CRS,TIMAX,DIVID,ACO
        READ(5,*) IN,SMAX,ALP1,ALP2,NF,NB,NDSR
        READ(5,*) NUP,RCR,OM,FRDC
        READ(5,*) ATOL,RTOL
        WRITE(8,510)
        WRITE(8,520) NVP,TAU,CRS,OM
        WRITE(8,540) DELT,FAC,PLEN
        WRITE(8,594) ALP1,ALP2,FRDC

C
        CALL UNDFL('TRUE')
        CALL OVEFL('TRUE')
C
C       PARAMETERS RELATED WITH THE LSODA SUBROUTINE
        DELTIN=DELT
        BETA=ACO/TAU/PLEN
        VO=VELCO*TAU**NVP
        TMAX=VO*TIMAX/PLEN
        ITOL=1
        ITASK=1
        ISTATE=1
        IOPT=1
        JT=1
C        INITIAL PARAMETERS
        RBOLD=0.D0
        TETA=0.D0
        S(1)=0.D0
        N=1
        NR=1
        TOUT=DELT
        TETOL=0.0D0
C
        STOT=0.D0
        NOUT=0
        NDI(1)=1
        IN=0
        K=0
        ICN=0
        IPR=0
C       MIND=1
 20     K=K+1
        IN=IN+1
```

```
      ICN=ICN+1
      IPR=IPR+1
      TI=TOUT*PLEN/VO
      SL=S(1)*PLEN
      WRITE(*,570) IN,N,NR,TI,RB,SL,RV(1)
      LRW=100+N*MAXO(16,N+9)
      LIW=30+N
      IWORK(6)=1000
C
      CALL LSODA(F,N,S,TETA,TOUT,ITOL,RTOL,ATOL,ITASK,ISTATE,
     1 IOPT,RWORK,LRW,IWORK,LIW,JACOB,JT)
C
      IF(ISTATE.LT.0) THEN
      WRITE(*,*) 'ISTATE=',ISTATE
      GO TO 600
      ENDIF
C
      CALL REL(N,TETA,S,EPS,RV)
C
 16   PAR1=0.0D0
      DO 10 I=1,N
      PAR1=PAR1+NDI(I)/S(I)
 10   CONTINUE
      RS=1.D0-BETA*(ALP1*DEXP(-ALP2)+PAR1)
C
      IF(ICN.LE.3) THEN
      XG(ICN)=TETA
      YG(ICN)=CRS-RS
      TOUT=TETA+DELT
      IF(ICN.NE.3) GO TO 20
      ENDIF
C
      IF(ICN.GE.3) THEN
      DELTA=DABS(RS-CRS)
            IF(DELTA.LT.CONV) THEN
 79         STRAIN=0.D0
            PAR2=0.D0
            DO 23 I=1,N
            STRAIN=STRAIN+NDI(I)*S(I)
            PAR2=PAR2+NDI(I)/(1.D0-S(I))
 23         CONTINUE
            RB=1.D0+BETA*PAR2
            DIF=RB-RBOLD
            IF(DIF.LT.1.D-4) GO TO 275
            TI=TETA*PLEN/VO
            STR=STRAIN*PLEN
            PLEAD=S(1)*PLEN
            WRITE(9,695) TI,RV(1),RV(5),RV(10),RV(15)
            WRITE(10,695) TI,S(1),S(5),S(10),S(15)
            WRITE(7,550) TI,NR,STR,RB,PLEAD,RV(1)
            RBOLD=RB
 275        N=N+1
            NR=NR+1
            NDI(N)=1
            NDO(N)=1
            S(N)=0.D0
            SO(N)=0.D0
```

```
                DELT=(TETA-TETOL)/DIVID
                TOUT=TETA+DELT
                TETOL=TETA
                ISTATE=1
                K=0
                ICN=0
                        IF(N.GT.NDSR) THEN
                        DMIN=1.D0
                        DO 40 I=NF,N-NB
                        DST(I)=S(I)-S(I+1)
                                IF(DST(I).LT.DMIN) THEN
                                DMIN=DST(I)
                                NMIN=I
                                ENDIF
 40                     CONTINUE
                        IF(DMIN.LT.RCR) GO TO 50
                        IF(N.LT.NUP) GO TO 20
 50                     NDI(NMIN)=NDO(NMIN)+NDO(NMIN+1)
        C1=SO(1)-SO(NMIN)
        C2=SO(1)-SO(NMIN+1)
        S(NMIN)=SO(1)-(NDO(NMIN)+NDO(NMIN+1))*C1*C2/
     *  (C1*NDO(NMIN+1)+C2*NDO(NMIN))
                        DO 55 I=NMIN+2,N
                        NDI(I-1)=NDO(I)
                        S(I-1)=SO(I)
 55                     CONTINUE
                        N=N-1
                        ENDIF
        ELSE
                        IF(ICN.EQ.3) INEW=ICN
                        YG(INEW)=CRS-RS
                        CALL GUESS3(YG,XG,XNEW,INEW,DERR,DERA)
                        XG(INEW)=XNEW
                        TOUT=XNEW
                        ISTATE=2
                        K=K+1
                ENDIF
        ENDIF
C
C
                DO 60 I=1,N
                NDO(I)=NDI(I)
                SO(I)=S(I)
 60             CONTINUE
 30     IF(K.GT.5.AND.RS.LT.CRS) THEN
        STRAIN=0.D0
        PAR2=0.D0
        DO 22 I=1,N
        PAR2=PAR2+NDI(I)/(1.D0-S(I))
        STRAIN=STRAIN+NDI(I)*S(I)+STOT
 22     CONTINUE
        RB=1.D0+BETA*PAR2
        K=0

                TI=TETA*PLEN/VO
                STR=STRAIN*PLEN
                PLEAD=S(1)*PLEN

                WRITE(7,550) TI,NR,STR,RB,PLEAD,RV(1)
                WRITE(8,550) TI,NR,STR,RB,PLEAD,RV(1)
```

```
      ENDIF
      IF(TETA.LE.TMAX) GO TO 20
C
 500  FORMAT(3X,D12.6,3X,D12.6)
 510  FORMAT(//,10X,'DISLOCATION PILE-UP CALCULATIONS',//)
 520  FORMAT(3X,' m = ',I3,3X,'BETA=',D12.6,
     1 3X,'SIGS = ',D12.6,/,3X,'OMEGA=',D12.6)
 530  FORMAT(5X,I3,3X,D12.6,3X,D12.6)
 540  FORMAT(/,3X,'DEL=',D12.6,3X,'MUL=',F8.4,3X,/,
     1 3X,'PLEN=',D12.6,//)
 550  FORMAT(2X,D12.6,2X,I4,F10.5,2X,F10.5,2X,2X,F10.5
     1 ,2X,D12.6)
 560  FORMAT(2X,I5,2X,I4,2X,I3,2X,D12.6,2X,D12.6)
 570  FORMAT(2X,I5,2X,I4,2X,I4,2X,D12.6,2X,D12.6,2X,D12.6,2X,F8.4)
 580    FORMAT(2X,I5,2X,I5,3X,D12.6,3X,D12.6)
 585  FORMAT(2X,I3,2X,D12.6,3X,D12.6)
 591  FORMAT(2X,D12.6,2X,I4,4(2X,D12.6),/)
 592  FORMAT(2X,D12.6,2X,I4)
 593  FORMAT(2X,10(1X,F6.3),/)
 594  FORMAT(2X,'ALP1=',D12.6,2X,'ALP2=',D12.6,2X,'FRDC=',D12.6)
 695  FORMAT(2X,D12.6,2X,F8.4,2X,F8.4,4X,F8.4,2X,F8.4)
 600  STOP
      END
C
C
C
      SUBROUTINE F(N,T,S,SDOT)
      IMPLICIT REAL*8 (A-H,O-Z)
      DIMENSION S(1),SDOT(1)
      COMMON/BL1/NVP,NDI(100),INT(100),BETA,SMAX,
     * ALP1,ALP2,OM,FRDC
      DO 10 I=1,N
      SUM=0.DO
      DO 20 J=1,N
      IF(J.EQ.I) GO TO 20
      P1=S(I)-S(J)
      SUM=SUM+NDI(J)/P1
 20   CONTINUE
      PR=1.DO-S(I)
      SD=1.DO-BETA*(ALP1*DEXP(-ALP2*PR)/PR-SUM)
      IF(SD.GT.SMAX) THEN
      SD=SMAX
      ELSE
      SD=DABS(SD)
      ENDIF
      IF(SD.LT.O.DO) THEN
      CAR=-1.DO
      ELSE
      CAR=1.DO
      ENDIF
      SDOT(I)=CAR*SD**NVP
 10   CONTINUE
      RETURN
      END
C
      SUBROUTINE REL(N,TETA,S,EPS,RV)
      IMPLICIT REAL*8 (A-H,O-Z)
      DIMENSION S(1),RV(1)
      COMMON/BL1/NVP,NDI(100),INT(100),BETA,SMAX,
     * ALP1,ALP2,OM,FRDC
```

```
      DO 10 I=1,N
      SUM=0.DO
      DO 20 J=1,N
      IF(J.EQ.I) GO TO 20
      P1=S(I)-S(J)
      SUM=SUM+1.DO/P1
20    CONTINUE
      PR=1.DO-S(I)
      VEL=1.DO-BETA*(ALP1*DEXP(-ALP2*PR)/PR-SUM)
      IF(DABS(VEL).GT.SMAX) THEN
      VEL=SMAX
      ELSE
      VEL=DABS(VEL)
      ENDIF
      IF(VEL.GT.0.DO) THEN
      CAL=1.DO
      ELSE
      CAL=-1.DO
      ENDIF
      RV(I)=CAL*VEL**NVP
10    CONTINUE
      OO 30 I=1,N
      IF(RV(I).GT.EPS) GO TO 100
30    CONTINUE
      WRITE(8,200)
      WRITE(8,201) TETA,N
      WRITE(8,202) (J,S(J),RV(J),J=1,N)
      STOP
200   FORMAT(5X,'EQUILIBRIUM REACHED',/)
201   FORMAT(3X,'TIME=',D12.6,3X,'N=',I3,/)
202   FORMAT(5X,I3,3X,D12.6,3X,D12.6)
100   RETURN
      END

     SUBROUTINE GUESS3(F,X,XNEW,INEW,DERR,DERA)
     IMPLICIT REAL*8(A-H,O-Z)
C=============================================
C  F RIGHT HAND SIDE
C  X
C  XNEW NEW GUESS
C  INEW COMPONENT OF X WHICH HAS THE MAX ERR.
C  DERR REL ERROR MAX X(I),XNEW
C  DERA ABS DMAX1(DABS(F(I)))
C---------------------------------------------
      DIMENSION F(3),X(3)
      IO8=6
      SMALL = 1.0D-12
      DERR=0.0DO
      DERA=0.0DO
      DO 10 I=1,3
         IF(DABS(F(I)).LT.1.D-8) THEN
         XNEW=X(I)
         GO TO 101
         ENDIF
         IF(DABS(F(I)).LE.DERA) GO TO 10
         INEW=I
         DERA=DABS(F(I))
10    CONTINUE
      DX1 = X(1) - X(2)
      DX2 = X(3) - X(1)
```

```
      DX3 = X(2) - X(3)
      F12 = F(1)*F(2)*DX1
      F13 = F(1)*F(3)*DX2
      F23 = F(2)*F(3)*DX3
      FFF = F12+F13+F23
      FFT = (F(1)*F(3)-F(2)*F(3))*DX2*DX3
      IF(DABS(FFF).LT.SMALL) GO TO 100
      XNEW = FFT/FFF + X(3)
      DO 20 I=1,3
         DERR=DMAX1(DERR,DABS( (XNEW-X(I))/(XNEW-SMALL) ))
20     CONTINUE
      GO TO 99
100    XNEW = (X(1)+X(2)+X(3))/3.0D0
      WRITE(I06,*) 'N/O IN GUESS3',(X(I),I=1,3)
99    CONTINUE
101      RETURN
      END
C
C
      SUBROUTINE JACOB(N,TETA,S,ML,MU,PD,NROWPD)
      IMPLICIT REAL*8 (A-H,O-Z)
      DIMENSION S(1),PD(NROWPD,1)
      COMMON/BL1/NVP,NDI(100),INT(100),BETA,SMAX,
     *  ALP1,ALP2,OM,FRDC
      DO 10 I=1,N
      DO 15 K=1,N
      SUM1=0.D0
      DO 20 J=1,N
      IF(I.EQ.J) GO TO 20
      SUM1=SUM1+NDI(J)/(S(I)-S(J))
20    CONTINUE
      PR=1.D0-S(I)
      VEL=1.D0-BETA*(ALP1*DEXP(-ALP2*PR)/PR-SUM1)
      IF(VEL.GT.0.D0) THEN
      CAL=1.D0
      ELSE
      CAL=-1.D0
      ENDIF
      VEL=CAL*VEL**(NVP-1)
C
      IF(I.EQ.K) THEN
      SUM2=0.D0
      DO 25 J=1,N
      IF(I.EQ.J) GO TO 25
      SUM2=SUM2+NDI(J)/(S(I)-S(J))**2
25    CONTINUE
      PD(I,K)=NVP*(-BETA*(ALP1*ALP2*DEXP(-ALP2*PR)/PR+
     1  ALP1*DEXP(-ALP2*PR)/PR**2-SUM2))*VEL
      ELSE
      PD(I,K)=NVP*BETA*NDI(J)/(S(I)-S(J))**2*VEL
      ENDIF
15     CONTINUE
10    CONTINUE
      RETURN
      END
```

7.2 The DEFORM Code

The computer code DEFORM is written in FORTRAN77 language standards. The purpose of this code is to evaluate the external shape change for an irradiated single crystalline metal sheet sample as dislocation channels form along the sample in plane strain conditions and under uniaxial loading. This code also calculates shear stress as a function axial elongation by means of the data obtained from the PILEUP computer code.

The basic limitations for this code are the requirements of a large memory and a long CPU time for the amounts of plastic deformation in excess of several per cent. However, the requirements also depends on the size of the sample. The formation of each channel normally introduces four additional exterior points after the required local shear displacement is applied. In addition to exterior points of the deforming sample, the location of each dislocation channel and the intercept of the channels are necessary to be stored for the consequent calculations. Furthermore, if a previously formed is intersected by the new channel, it will be separated into two parts and the information for each part is stored. As the number of intersected channels increases, the memory for data storage also increases. To avoid excessive memory requirement, the maximum allowable parts in a dislocation channel may be specified. If the number of parts is greater than this specified value, then, the shortest piece is selected and it is connected to the next piece by altering the coordinates and the intercept values for the new piece. Thus every channel is taken into consideration for the fulfillment of the new channel selection criteria given in Section 3.2.

The computer code DEFORM consists of a main program and a number of subprograms. The function of the main program is to determine the location of new dislocation channels by checking the selection criteria. The main program also generates rectangular and triangular grid for the current external shape of the sample. The use of grid generation reduces the speed of computation and requires considerable amount of memory (depending on the number of existing channels). The grid generation section is optional and can be deactivated. The subprograms and their purposes are;

SB: to update the information related to the shear bands and apply necessary translations

COCAL: to calculate the new coordinates of exterior points after the introduction of a new channel

INCAL: to calculate the intersection point of a candidate dislocation channel and the surface of the sample

MNCSBC: to determine possible dislocation channel locations with minimum number of crossing channels

ELCAL: to calculate the equations of lines formed by connecting exterior points of the sample

RANNUM: to evaluate a random number

SELECT: to select randomly desired number of dislocation channels in case of presence greater number of possibilities after the application of all selection

criteria

FIND: to evaluate the value of a function on a two-dimensional geometry by bi-cubic spline interpolation

SPLINE: to evaluate coefficients for cubic spline interpolation [52]

SEVAL: to evaluate the function values at a desired point based and the spline coefficients evaluated by SPLINE [52]

CALINT: to integrate the given function by a 8 point Gaussian quadrature

GUESS3: to evaluate the zero of a function with a desired accuracy

SHCAL: to calculate the amount of shear displacement and the current stress level

Input parameters for DEFOR and their typical values are given in the following order;

NSTR: Initial step number, 1

NEND: Last step number, 1000

XLEN: The gage length of the sample, 12 mm

YLEN: The width of the sample, 3 mm

DISLIM: The minimum separation distance between two channels, 0.002 mm

DELTA: Error parameter, 0.001

PPN: Number of parallel plane per dislocation channel, 1000-2000

APAR: The material constant A, 2.965×10^{-3} MPa mm

TAU: The applied shear stress to be used at the first step, 31.77 MPa

DTAU: Increments of the shear stress, 0.001 MPa

ALEN: Average pile-up length, 0.04 mm

SDL: Standard error in pile-up lengths, 0.005 mm

SLMIN: Minimum length of pile-ups, 0.02 mm

SLMAX: Maximum length of pile-ups, 0.1 mm

VELP: Constant power of stress-dislocation velocity relation, 10

VELCO: Constant coefficient of stress-dislocation velocity relation, 1.66×10^{-18} mm/s/(MPa)^m.

SHMAX: Maximum allowed shear strain per channel, 2.50 μm

SHMIN: Minimum allowed shear strain per channel, 2.40 μm

ERR: Absolute error parameter to verify the magnitude of crosshead velocity, 10^{-5} mm/s

CHV: Crosshead velocity, 2.103×10^{-3} mm/s

BURV: The magnitude of the Burgers vector, 2.86×10^{-7} mm

NPMAX: The number of simultaneously forming channels at the initial step as a guess, 5-20

NX: The number of columns in the table of $H(\beta, \Theta, s)$, see Table 4.7

NY: The number of rows in the same table, see Table 4.7

X(I): β values, I=1,NX, see Table 4.7

Y(J): Θ values, J=1,NY, see Table 4.7

F(I,J): H value corresponding to X(I) and Y(I), see Table 4.7

Table 7.2: Listing of the computer code DEFORM

```
C*************************************************************
C                    DEFORM
C
C       THIS CODE IS USED FOR THE SIMULATION OF
C       PLASTIC DEFORMATION IN IRRADIATED
C       SINGLE CRYSTALS BY DISLOCATION CHANNEL FORMATION
C
C*************************************************************
C
        EXTERNAL RANNUM,FUN1,FUN2,CALINT,GUESS3,SEVAL,SPLINE
        EXTERNAL FIND,PARAM
        DIMENSION SL(2500),CI(2500),NSB(2500),NR(2500)
        DIMENSION XMAX(2500),XMIN(2500),YMAX(2500)
        DIMENSION YMIN(2500),XA(2500),XD(2500),YA(2500),YD(2500)
        DIMENSION DINT(2500),XI(2500),YI(2500)
        DIMENSION SINT(2500)
        DIMENSION XG(1000,4),YG(1000,4),RINT(2500)
        DIMENSION XSR(2500),XSL(2500),YSL(2500),YSR(2500)
        DIMENSION XL1(2500),XL2(2500),YL1(2500),YL2(2500)
        DIMENSION XR1(2500),XR2(2500),YR1(2500),YR2(2500)
        DIMENSION XTL2(2500),XTR1(2500),YTL2(2500)
        DIMENSION YTR1(2500),XRT(2500),YRT(2500),XLT(2500)
        DIMENSION YLT(2500),SLEN(2500),SLX(2500),SRX(2500)
        DIMENSION SLY(2500),SRY(2500),NPPOL(2500),PLEN(1250)
        COMMON/SB1/NPAR(1250),SBPI(1250,50),YSBMIN(1250,50),
     *  YSBMAX(1250,50)
        COMMON/SB2/NPARA(1250),SBRI(1250,50),YSRMIN(1250,50),
     *  YSRMAX(1250,50)
        COMMON/B1/XR(2500),XL(2500),YR(2500),YL(2500)
        COMMON/B2/XNR,XNL,YNR,YNL,DX,DY,DELTA,STX
        COMMON/B3/IPRINT,NT,NTR,NPMAX
        COMMON/C1/XNRC(1250),XNLC(1250),YNRC(1250),YNLC(1250)
        COMMON/C2/XNRP(1250),XNLP(1250),YNRP(1250),YNLP(1250)
        COMMON/C3/NPART,XP(1250),YP(1250)
        COMMON/PAR1/NTBP,NTBN,NPSN(1250),NPSP(1250)
        COMMON/PAR2/SBP(1250,50),SBN(1250,50),YSPN(1250,50)
     *  ,YSPX(1250,50),YSNN(1250,50),YSNX(1250,50)
        COMMON/F1/NX,NY,X(50),Y(50),F(50,50)
        COMMON/F2/W(8),XAB(8)
        COMMON/F3/AVL,SDL
        COMMON/F4/APAR,TAU,TIME,VELP,VELCO
        COMMON/F5/ALP,BURV,PPN,CHV,ERR,SHMAX,SHMIN,DTAU,DELT
        COMMON/F6/SLMIN,SLMAX,XHEIG,ALEN,EPS
        COMMON/F7/ICO,NTOT,SHOLD,DPOLD,SBM,CHOLD,TOLD
        OPEN(5,FILE='INPUT',STATUS='UNKNOWN')
        OPEN(6,FILE='OUTPUT',STATUS='UNKNOWN')
        OPEN(7,FILE='FIG.DAT',STATUS='UNKNOWN')
        READ(5,*) NSTR,NEND
        READ(5,*) XLEN,YLEN,XO,YO
        READ(6,*) DISLIM,DELTA
        READ(5,*) NOPT,XHEIG,NUP,PPN,ALP
        READ(5,*) APAR,TAU,DTAU,ALEN,SDL
        READ(5,*) SLMIN,SLMAX,VELP,VELCO
        READ(5,*) SHMAX,SHMIN,DELT,ERR,CHV,BURV
        READ(5,*) NPMAX
        READ(5,*) NX,NY
        READ(5,*) (X(I),I=1,NX)
        READ(5,*) (Y(I),(F(I,J),J=1,NX),I=1,NY)
C
```

```
C       INPUT PARAMETERS
C
C       NSTR : NUMBER OF THE FIRST STEP
C       NEND : NUMBER OF THE LAST STEP
C       XLEN : LENGTH OF THE SAMPLE
C       YLEN : WIDTH OF THE SAMPLE
C       XO : X COORDINATE OF THE UPPER LEFT CORNER
C       YO : Y COORDINATE OF THE UPPER LEFT CORNER
C       DX : X COMPONENT OF INITIAL DISPLACEMENT VECTOR
C       DY : Y COMPONENT OF INITIAL DISPLACEMENT VECTOR
C       DISLIM :
C       DELTA : MAXIMUM ALLOWABLE NUMBER FOR SMALL DIFFERENCES
C       NOPT : MAXIMUM NUMBER OF SIMULTANEOUSLY FORMING
C              SLIP BANS
C       XHEIG : WIDTH OF THE SLIP BANDS
C       NPSL : NUMBER OF PARALLEL SLIP LINES IN THE SLIP BAND
C       FRLEN : PROPORTION OF SLIP LINE COVERED WITH PILE-UPS
C       APAR : MATERIAL PARAMETER
C       TAU : INITIAL SHEAR STRESS (CRITICAL)
C       TAUDEL : INCREMENTS OF STRESS
C       AVL : AVERAGE PILE-UP LENGTH
C       SDL : STANDARD DEVIATION ASSOCIATED WITH PILE-UP LENGTH
C
  4     NTBN=0
        NTOT=NOPT
        AVL=ALEN
        ICO=0
        TOLD=100.
        SHOLD=SHMAX+3
C
C       CALCULATION OF INITIAL CORNER COORDINATES
C
        TI=0.
        SQ2=SQRT(2.)
        XR(1)=XO
        XR(2)=XO+XLEN
        XL(1)=XO
        XL(2)=XO+XLEN
        YL(1)=YO
        YL(2)=YO
        YR(1)=YO+YLEN
        YR(2)=YO+YLEN
        T=0.
        NP=2
        IS=1
        IS=IS+1
        PRINT*, IS
C       CALCULATION OF THE CENTER POINT COORDINATES
        XC=(XO+XLEN)/2.
        YC=(YO+YLEN)/2.
        IP=1
C       CALCULATION OF THE COORDINATES OF NEW POINT
C       GENERATED AFTER THE INTRODUCTION OF SHEAR BAND
        XNL=XC-YLEN/2.-XHEIG/SQ2
        XNR=XC+YLEN/2.-XHEIG/SQ2
        YNL=YO
        YNR=YO+YLEN
        SBPI(1,1)=YNL-(XC+YLEN)/2.
        NP=NP+2
C
```

```
      NPL=NP
      NPR=NP
      FRLEN=1.
      BL=SQ2*YLEN
      CALL SHCAL(IS,FRLEN,BL,SHDIS,TI,NREST,MF)
      STX=SQ2*XHEIG*(1.+SHDIS/2./XHEIG)
      DY=SHDIS/SQ2
      DX=DY
C     CALCULATION OF THE COORDINATES IF THE EDGE AND CORNER
C     POINTS AFTER THE SECOND STEP
      CALL COCAL(NPR,NPL,IP)
      NT=1
      NPAR(1)=1
      YSBMIN(1,1)=YL(2)+IP*DY/2.
      YSBMAX(1,1)=YR(2)+IP*DY/2.

      NTBP=1
      NPSP(1)=1
      SBP(1,1)=SBPI(1,1)
      YSPN(1,1)=YSBMIN(1,1)
      YSPX(1,1)=YSBMAX(1,1)
C
      DO 400 NS=3,4
      NP=NPR
      IS=IS+1
      PRINT*, IS
      IP=(-1)**IS
      IF(IP.EQ.1) THEN
      SLP=1.
      SLR=-1.
      NTR=NTBN
      DO 2 I=1,NTR
      NPARA(I)=NPSN(I)
      NBR=NPARA(I)
            DO 3 J=1,NBR
            SBRI(I,J)=SBN(I,J)
            YSRMIN(I,J)=YSNN(I,J)
            YSRMAX(I,J)=YSNX(I,J)
 3          CONTINUE
 2    CONTINUE
      NT=NTBP
      DO 14 I=1,NT
      NPAR(I)=NPSP(I)
      NBR=NPAR(I)
            DO 5 J=1,NBR
            SBPI(I,J)=SBP(I,J)
            YSBMIN(I,J)=YSPN(I,J)
            YSBMAX(I,J)=YSPX(I,J)
 5          CONTINUE
 14   CONTINUE
      ELSE
      SLP=-1.
      SLR=1.
      NT=NTBN
      IF(NTBN.EQ.0) GOTO 11
      DO 8 I=1,NT
      NPAR(I)=NPSN(I)
      NBR=NPAR(I)
            DO 9 J=1,NBR
            SBPI(I,J)=SBN(I,J)
```

```
                YSBMIN(I,J)=YSNN(I,J)
                YSBMAX(I,J)=YSNX(I,J)
9               CONTINUE
8       CONTINUE
11      NTR=NTBP
        DO 16 I=1,NTR
        NPARA(I)=NPSP(I)
        NBR=NPARA(I)
                DO 7 J=1,NBR
                SBRI(I,J)=SBP(I,J)
                YSRMIN(I,J)=YSPN(I,J)
                YSRMAX(I,J)=YSPX(I,J)
7               CONTINUE
16      CONTINUE
        ENDIF
        DO 405 I=1,2
        DO 410 J=1,NP
        IF(I.EQ.1) THEN
                IF(NS.EQ.3) THEN
                XA(J)=XL(J)
                YA(J)=YL(J)
                ELSEIF(NS.EQ.4) THEN
                XA(J)=XR(J)
                YA(J)=YR(J)
                ENDIF
        ELSEIF(I.EQ.2) THEN
                IF(NS.EQ.3) THEN
                XA(J)=XR(J)
                YA(J)=YR(J)
                ELSEIF(NS.EQ.4) THEN
                XA(J)=XL(J)
                YA(J)=YL(J)
                ENDIF
        ENDIF
410     CONTINUE
C
        IF(I.EQ.1) THEN
                IF(NS.EQ.3) THEN
                XNRC(1)=XR(1)
                YNRC(1)=YR(1)
                DINT(1)=YNRC(1)-XNRC(1)*SLP
                ELSE
                XNLC(1)=XL(1)
                YNLC(1)=YL(1)
                DINT(1)=YNLC(1)-XNLC(1)*SLP
                ENDIF
        ELSE
                IF(NS.EQ.3) THEN
                XNLC(2)=XL(NP)
                YNLC(2)=YL(NP)
                DINT(1)=YNLC(2)-XNLC(2)*SLP
                ELSE
                XNRC(2)=XR(NP)
                YNRC(2)=YR(NP)
                DINT(1)=YNRC(2)-XNRC(2)*SLP
                ENDIF
        ENDIF
        CALL ELCAL(NP,XA,YA,SL,CI,XMAX,YMAX,XMIN,YMIN)
        NL=NP-1
        IPAR=0
```

```
      CALL INCAL(IPAR,XMAX,XMIN,DINT,SLP,SL,CI,NL,NP,
     *  NPOS,XI,YI,NSB)
      IF(I.EQ.1) THEN
              IF(NS.EQ.3) THEN
              XNLC(I)=XI(1)
              YNLC(I)=YI(1)
              ELSE
              XNRC(I)=XI(1)
              YNRC(I)=YI(1)
              ENDIF
      ELSE
              IF(NS.EQ.3) THEN
              XNRC(I)=XI(1)
              YNRC(I)=YI(1)
              ELSE
              XNLC(I)=XI(1)
              YNLC(I)=YI(1)
              ENDIF
      ENDIF
405   CONTINUE
      MF=2
      BL=SQRT((XNRC(1)-XNLC(1))**2+(YNRC(1)-YNLC(1))**2)

      IF(NS.EQ.3) THEN
      FRLEN=1.
      ELSE
      FRLEN=(BL-XHEIG)/BL
      ENDIF
      CALL SHCAL(IS,FRLEN,BL,SHDIS,TI,NREST,MF)
      STX=SQ2*XHEIG*(1.+SHDIS/2./XHEIG)
      DY=SHDIS/SQ2
      DX=DY
      CALL SB(MF,SLP,SLR,IP,IS,NPR,NPL)
400   CONTINUE

      NMIN=5
      NMAX=NEND
C
C
C
  8   IPRINT=0
C
C
      DO 1 NSTEP=NMIN,NMAX
      IF(NMAX.LT.5) STOP
      IF(NSTEP.EQ.NMAX) IPRINT=1
C
C     "IS" IS STEP NUMBER
C
      IS=IS+1
      PRINT*, IS
      IP=(-1)**IS

      IF(IP.EQ.1) THEN
      SLP=1.
      SLR=-1.
      NTR=NTBN
      DO 10 I=1,NTR
      NPARA(I)=NPSN(I)
      NBR=NPARA(I)
```

```
                DO 20 J=1,NBR
                SBRI(I,J)=SBN(I,J)
                YSRMIN(I,J)=YSNN(I,J)
                YSRMAX(I,J)=YSNX(I,J)
20              CONTINUE
10      CONTINUE
        NT=NTBP
        DO 30 I=1,NT
        NPAR(I)=NPSP(I)
        NBR=NPAR(I)
                DO 40 J=1,NBR
                SBPI(I,J)=SBP(I,J)
                YSBMIN(I,J)=YSPN(I,J)
                YSBMAX(I,J)=YSPX(I,J)
40              CONTINUE
30      CONTINUE
        ELSE
        SLP=-1.
        SLR=1.
        NTR=NTBP
        DO 50 I=1,NTR
        NPARA(I)=NPSP(I)
        NBR=NPARA(I)
                DO 60 J=1,NBR
                SBRI(I,J)=SBP(I,J)
                YSRMIN(I,J)=YSPN(I,J)
                YSRMAX(I,J)=YSPX(I,J)
60                CONTINUE
50      CONTINUE
        NT=NTBN
        DO 70 I=1,NT
        NPAR(I)=NPSN(I)
        NBR=NPAR(I)
                DO 80 J=1,NBR
                SBPI(I,J)=SBN(I,J)
                YSBMIN(I,J)=YSNN(I,J)
                YSBMAX(I,J)=YSNX(I,J)
80              CONTINUE
70      CONTINUE
        ENDIF

        NPOS=NT-1
        J=0
        BD=0.
        DO 90 I=1,NPOS
        NP=NPAR(I)
        NPN=NPAR(I+1)
        IF(IP.EQ.1) THEN
        DIF=ABS(SBPI(I,NP)-SBPI(I+1,1))
        SBIN=(SBPI(I,NP)+SBPI(I+1,1))/2.
        ELSE
        DIF=ABS(SBPI(I,1)-SBPI(I+1,NPN))
        SBIN=(SBPI(I,1)+SBPI(I+1,NPN))/2.
        ENDIF
        IF(DIF.LT.DISLIM) GO TO 90
        PAR=ABS(DIF-BD)
        IF(PAR-DELTA) 91,91,92
92      IF(DIF-BD) 90,91,93
91      J=J+1
        DINT(J)=SBIN
```

```
      GO TO 90
93    BD=DIF
      J=1
      DINT(J)=SBIN
90    CONTINUE
      NPO=J
      IF(NPO.EQ.0) THEN
      WRITE(6,*) 'NO POSSIBLE SITE'
      STOP
      ENDIF
      CALL ELCAL(NPR,XR,YR,SL,CI,XMAX,YMAX,XMIN,YMIN)
      NL=NPR-1
      IPAR=0
      CALL INCAL(IPAR,XMAX,XMIN,DINT,SLP,SL,CI,NL,NPO,
     *  NPOS,XI,YI,NSB)
      DO 210 I= 1,NPL
      SINT(I)=YL(I)+XL(I)
210   CONTINUE
      NL=NPR-1
      SLOPE=-1.
      NPZ=NPL-1
      IPAR=1
      CALL INCAL(IPAR,XMAX,XMIN,SINT,SLOPE,SL,CI,NL,NPZ
     *  ,NTEM,XTR1,YTR1,NSB)
       NPT1=0
      NEPL=0
      DO 215  I=1,NTEM
      J=NSB(I)
      PAR=ABS(SINT(J)-SINT(J-1))
       IF(PAR.LT.DELTA) THEN
              NEPL=NEPL+1
              XSL(NEPL)=XL(J)
              YSL(NEPL)=YL(J)
              GO TO 215
      ENDIF
      NPT1=NPT1+1
      XR1(NPT1)=XTR1(I)
      YR1(NPT1)=YTR1(I)
      XL1(NPT1)=XL(J)
      YL1(NPT1)=YL(J)
215   CONTINUE
      CALL ELCAL(NPL,XL,YL,SL,CI,XMAX,YMAX,XMIN,YMIN)
      NL=NPL-1
      IPAR=0
      CALL INCAL(IPAR,XMAX,XMIN,DINT,SLP,SL,CI,NL,
     *  NPO,NPOS,XD,YD,NSB)
      DO 220 I=1,NPR
      RINT(I)=YR(I)+XR(I)
C 220 CONTINUE
      NL=NPL-1
      NPZ=NPR-1
      SLOPE=-1.
      IPAR=0
      CALL INCAL(IPAR,XMAX,XMIN,RINT,SLOPE,SL,CI,NL,NPZ
     *  ,NTEM,XTL2,YTL2,NSB)
      NPT2=0
      NEPR=0
      DO 230 I=1,NTEM
      J=NSB(I)
```

```
      PAR=ABS(RINT(J)-RINT(J+1))
      IF(PAR.LT.DELTA) THEN
              NEPR=NEPR+1
              XSR(NEPR)=XR(J)
              YSR(NEPR)=YR(J)
              GO TO 230
      ENDIF
 232  NPT2=NPT2+1
      XL2(NPT2)=XTL2(I)
      YL2(NPT2)=YTL2(I)
      XR2(NPT2)=XR(J)
      YR2(NPT2)=YR(J)
 230  CONTINUE
C
C
      NCUR=1
      NN=0
      NTOT=NPT1+NPT2
      DO 235 I=1,NPT1
      NM=NCUR
      DO 240 J=NM,NPT2
      NN=NN+1
      IF(XL1(I).LT.XL2(J)) THEN
      XLT(NN)=XL1(I)
      YLT(NN)=YL1(I)
      GO TO 235
      ELSE
      XLT(NN)=XL2(J)
      YLT(NN)=YL2(J)
      NCUR=NCUR+1
      ENDIF
240   CONTINUE
      IF(NCUR.GT.NPT2.AND.NN.LT.NTOT) THEN
      NC=NN+1
      DO 238 K=NC,NTOT
      NN=NN+1
      XLT(NN)=XL1(K-NPT2)
      YLT(NN)=YL1(K-NPT2)
 238  CONTINUE
      GO TO 238
      ENDIF
 235  CONTINUE
C
C
 238  NCUR=1
      NN=0
      DO 245 I=1,NPT1
      NM=NCUR
      DO 250 J=NM,NPT2
      NN=NN+1
      IF(XR1(I).LT.XR2(J)) THEN
      XRT(NN)=XR1(I)
      YRT(NN)=YR1(I)
      GO TO 245
      ELSE
      XRT(NN)=XR2(J)
      YRT(NN)=YR2(J)
      NCUR=NCUR+1
      ENDIF
 250  CONTINUE
```

```
      IF(NCUR.GT.NPT2.AND.NN.LT.NTOT) THEN
      NC=NN+1
      DO 237 K=NC,NTOT
      NN=NN+1
      XRT(NN)=XR1(K-NPT2)
      YRT(NN)=YR1(K-NPT2)
237   CONTINUE
      GO TO 241
      ENDIF
245   CONTINUE
C
C
241   IF(NTOT.NE. NN) GO TO 2200
      DO 260 I=1,NPL
      IF(XL(I).GT.XLT(1)) THEN
      NCL=I-1
      GO TO 270
      ENDIF
260   CONTINUE

270   DO 275 I=NPR,1,-1
      IF(XR(I).LT.XRT(NN)) THEN
      NCR=I
      GO TO 280
      ENDIF
275   CONTINUE

280   NTG=NN-1+NCL+NPR-NCR
      K=0
      M=1
      L=1
      N=0
      DO 290  I=1,NTG
      N1=NN-1+NCL
      IF(I.LE.NCL) THEN
      XG(I,1)=XL(I)
      XG(I,2)=XL(I+1)
      XG(I,3)=XR(1)
      YG(I,1)=YL(I)
      YG(I,2)=YL(I+1)
      YG(I,3)=YR(1)
              IF(I.EQ.NCL) THEN
              XG(I,2)=XLT(1)
              YG(I,2)=YLT(1)
              ENDIF
      NPPOL(I)=3
      ELSEIF(I.LE.N1.AND.I.GT.NCL) THEN
      J=I-NCL
      XG(I,1)=XLT(J)
      XG(I,2)=XLT(J+1)
      YG(I,1)=YLT(J)
      YG(I,2)=YLT(J+1)
      XG(I,3)=XRT(J+1)
      XG(I,4)=XRT(J)
      YG(I,3)=YRT(J+1)
      YG(I,4)=YRT(J)
      IF(M.LE.NEPL) THEN
              IF(XG(I,2).GT.XSL(M)) THEN
              XG(I,1)=XSL(M)
              YG(I,1)=YSL(M)
```

```
          M=M+1
               ENDIF
          ENDIF
          IF(L.LE.NEPR) THEN
               IF(XG(I,3).GT.XSR(L)) THEN
               IF(L.NE.1) THEN
               XG(I,3)=XSR(L)
               YG(I,3)=YSR(L)
               ENDIF
               L=L+1
               ENDIF
          ENDIF
C
          NPPOL(I)=4
          N=N+1
          SLX(N)=(XG(I,1)+XG(I,2))/2.
          SRX(N)=(XG(I,3)+XG(I,4))/2.
          SLY(N)=(YG(I,1)+YG(I,2))/2.
          SRY(N)=(YG(I,3)+YG(I,4))/2.
          SLEN(N)=SQRT((SLX(N)-SRX(N))**2+(SLY(N)-SRY(N))**2)
C
          ELSEIF(I.GT.N1.AND.I.LE.NTG) THEN
          K=K+1
          XG(I,1)=XL(NPL)
          YG(I,1)=YL(NPL)
          XG(I,2)=XR(NCR-1+K)
          YG(I,2)=YR(NCR-1+K)
          YG(I,3)=YR(NCR+K)
          XG(I,3)=XR(NCR+K)
          IF(XR(NCR-1+K).LT.XRT(NTOT)) THEN
          XG(I,2)=XRT(NTOT)
          YG(I,2)=YRT(NTOT)
          ENDIF
          NPPOL(I)=3
          ENDIF
 290      CONTINUE
C
          NTPOL=N
          DO 100 I=1,NPOS
          XNLC(I)=XD(I)
          YNLC(I)=YD(I)
          XNRC(I)=XI(I)
          YNRC(I)=YI(I)
 100      CONTINUE

          IF(NPOS.EQ.1) THEN
          MF=1
          GO TO 140
          ENDIF

          CALL MNCSBC(NPOS,NPMIN,SLP,SLR)

          DO 110 I=1,NPOS
          XI(I)=XNRC(I)
          YI(I)=YNRC(I)
          XD(I)=XNLC(I)
          YD(I)=YNLC(I)
 110      CONTINUE
```

```
      N=1
      DLT=DELTA*10.
      BL=YLEN*SQRT(2.)
      DO 120 I=1,NPOS
      T=SQRT((XI(I)-XD(I))**2+(YI(I)-YD(I))**2)
      PAR=ABS(T-BL)
      IF(PAR-DLT) 141,141,142
142   IF(T-BL) 143,141,120
141   N=N+1
      NR(N)=I
      GO TO 120
143   BL=T
      N=1
      NR(N)=I
120   CONTINUE
C
      MF=N
      DO 130 I=1,MF
      K=NR(I)
      XNRC(I)=XI(K)
      YNRC(I)=YI(K)
      XNLC(I)=XD(K)
      YNLC(I)=YD(K)
130   CONTINUE
      NPOS=MF
      IF(NUP.EQ.1) THEN
      CALL SELECT(NPOS)
      MF=NPOS
      ENDIF
      FRLEN=(BL-NPMIN*XHEIG)/BL
C
      CALL SHCAL(IS,FRLEN,BL,SHDIS,TI,NREST,MF)
C
      STX=SQ2*XHEIG*(1.+SHDIS/2./XHEIG)
      DY=SHDIS/SQ2
      DX=DY

140   CALL SB(MF,SLP,SLR,IP,IS,NPR,NPL)
      EPS=(XL(NPL)-XLEN+XO)/(XLEN-XO)
      IF(IP.EQ.1) THEN
      PLEN(1)=SQRT((XNLC(1)-XP(1))**2+(YNLC(1)-YP(1))**2)
      PLEN(NPART+1)=SQRT((XNRC(1)-XP(NPART))**2+
     *  (YNRC(1)-YP(NPART))**2)
      ELSE
      PLEN(1)=SQRT((XNRC(1)-XP(1))**2+(YNRC(1)-YP(1))**2)
      PLEN(NPART+1)=SQRT((XNLC(1)-XP(NPART))**2+
     *  (YNLC(1)-YP(NPART))**2)
      ENDIF
C
      DO 148 I=2,NPART
      PLEN(I)=SQRT((XP(I)-XP(I-1))**2+(YP(I)-YP(I-1))**2)
148   CONTINUE
C
      WRITE(6,2100) IS,T,NPO
      WRITE(6,2000) (PLEN(I),I=1,NPART+1)

C
1     CONTINUE
C
C
```

```
      DO 500 I=1,NPL
      WRITE(7,*) XL(I),YL(I)
500   CONTINUE
      DO 510 I=NPR,1,-1
      WRITE(7,*) XR(I),YR(I)
510   CONTINUE
      AA=XO
      BB=YO
      WRITE(7,*) AA,BB


      DO 460 I=1,NTG
      J=NPPOL(I)
      WRITE(6,*)
      WRITE(6,2000) (XG(I,K),K=1,J)
      WRITE(6,2000) (YG(I,K),K=1,J)
460   CONTINUE

      DO 465 I=1,NTPOL
      WRITE(8,*) SLX(I),SLEN(I)
465   CONTINUE
2000  FORMAT(3X,F10.5,3X,F10.5,3X,F10.5,3X,F10.5)
2100  FORMAT(3X,I4,3X,F8.4,3X,I4,3X,F8.4)
      STOP
      END
```

```
      SUBROUTINE SB(MF,SLP,SLR,IP,IS,NPR,NPL)
      DIMENSION SIA1(1250,50)
      DIMENSION YMIN1(1250,50),YMAX1(1250,50),SBI(1250,50)
      DIMENSION YSMI(1250,50),YSMA(1250,50)
      COMMON/SB1/NPAR(1250),SBPI(1250,50),YSBMIN(1250,50),
     *  YSBMAX(1250,50)
      COMMON/SB2/NPARA(1250),SBRI(1250,50),YSRMIN(1250,50),
     *  YSRMAX(1250,50)
      COMMON/B1/XR(2500),XL(2500),YR(2500),YL(2500)
      COMMON/B2/XNR,XNL,YNR,YNL,DX,DY,DELTA,STX
      COMMON/B3/IPRINT,NT,NTR,NPMAX
      COMMON/C1/XNRC(1250),XNLC(1250),YNRC(1250),YNLC(1250)
      COMMON/C3/NPART,XP(1250),YP(1250)
      COMMON/PAR1/NTBP,NTBN,NPSN(1250),NPSP(1250)
      COMMON/PAR2/SBP(1250,50),SBN(1250,50),YSPN(1250,50)
     *  ,YSPX(1250,50),YSNN(1250,50),YSNX(1250,50)
      COMMON/F6/SLMIN,SLMAX,H,ALEN,EPS
C     COORDINATES FOR THE NEW SHEAR INTERSECTIONS ARE
C     DETERMINED AND STORED
      SQ2=SQRT(2.)
            DO 50 I=1,MF
C
C     READING INFORMATION ABOUT PREVIOUSLY FORMED SHEAR BANDS
C
      IF(IS.EQ.3.AND.NT.EQ.0) GO TO 46
      DO 150 K=1,NT
      NBR=NPAR(K)
            DO 151 J=1,NBR
            SBI(K,J)=SBPI(K,J)
            YSMI(K,J)=YSBMIN(K,J)
            YSMA(K,J)=YSBMAX(K,J)
151   CONTINUE
150   CONTINUE

 46         IRES=I
            IF(I.EQ.1) GO TO 61
      PAR=ABS(XNRC(I)-XNRC(I-1))
      IF(PAR-DELTA) 61,61,58
58    IF(XNRC(I)-XNRC(I-1)) 61,61,59
59                  DO 60 J=IRES,MF
                    XNRC(J)=XNRC(J)+DX
                    YNRC(J)=YNRC(J)+DY*IP
                    XNLC(J)=XNLC(J)+DX
                    YNLC(J)=YNLC(J)+DY*IP
60                  CONTINUE
61          XNR=XNRC(I)-H/SQ2
            YNR=YNRC(I)
            XNL=XNLC(I)-H/SQ2
            YNL=YNLC(I)

            IF(IS.EQ.3.OR.IS.EQ.4) THEN
            IF(I.EQ.1) THEN
            XNR=XNRC(I)
            XNL=XNLC(I)
            ELSE
            XNR=XNRC(I)-1.41421356*H
            XNL=XNLC(I)-1.41421356*H
            ENDIF
            ENDIF
            NPR=NPR+2
```

```
            NPL=NPL+2
            CALL COCAL(NPR,NPL,IP)
          IF(I.EQ.2) THEN
          IF(IS.EQ.3) THEN
          NPL=NPL-1
          ELSEIF(IS.EQ.4) THEN
          NPR=NPR-1
          ENDIF
          ENDIF

          IF(IP.EQ.1) THEN
          YSR=YNR+DY/2.
          YSL=YNL+DY/2.
          XSR=XNR+DX/2.
          ELSE
          XSR=XNR+DX/2.
          YSR=YNR-DY/2.
          YSL=YNL-DY/2.
          ENDIF
          CSBI=YSR-SLP*(XSR+SQ2*H)
          IF(IS.EQ.3.AND.NT.EQ.0) THEN
          NT=1
          SBPI(1,1)=CSBI
          YSBMIN(1,1)=YSL
          YSBMAX(1,1)=YSR
          NPAR(1)=1
          NCUR=1
          GO TO 161
          ENDIF

          ICO=0
          DO 152 K=1,NT
          NZ=NPAR(K)
          IF(IP.EQ.1) THEN
                  PAR=ABS(CSBI-SBI(K,I))
                  IF(PAR-DELTA) 152,152,300
300               IF(CSBI-SBI(K,I)) 152,152,301
301               SBPI(K,1)=CSBI
                  YSBMIN(K,1)=YSL
                   YSBMAX(K,1)=YSR
                  NCUR=K
                  ICO=1
                  GO TO 153
          ELSE
                  PAR=ABS(CSBI-SBI(K,NZ))
                  IF(PAR-DELTA) 152,152,310
310               IF(CSBI-SBI(K,NZ)) 311,152,152
311               SBPI(K,1)=CSBI
                  YSBMIN(K,1)=YSL
                  YSBMAX(K,1)=YSR
                  NCUR=K
                  ICO=1
                  GO TO 153
          ENDIF
152       CONTINUE
153       NT=NT+1
                  IF(ICO.NE.1) THEN
                  NCUR=NT
                  NPAR(NT)=1
                  SBPI(NT,1)=CSBI
```

```
              YSBMIN(NT,1)=YSL
              YSBMAX(NT,1)=YSR
              GO TO 161
              ENDIF
          DO 154 J=NCUR+1,NT
          NSP=NPAR(J-1)
          DO 155 L=1,NSP
          SBPI(J,L)=SBI(J-1,L)
          YSBMIN(J,L)=YSMI(J-1,L)+DY*IP
          YSBMAX(J,L)=YSMA(J-1,L)+DY*IP
  155     CONTINUE
  154     CONTINUE
C
C         REORGANIZATION OF DATA FILES FOR SHEAR BANDS
C
  161     IF(IP.EQ.1) THEN
          NTBP=NT
          DO 375 I1=1,NTBP
          NM=NPAR(I1)
          IF(I1.EQ.NCUR) NM=1
          IF(I1.GT.NCUR) NM=NPAR(I1-1)
          NPSP(I1)=NM
          DO 376 J=1,NM
          SBP(I1,J)=SBPI(I1,J)
          YSPN(I1,J)=YSBMIN(I1,J)
          YSPX(I1,J)=YSBMAX(I1,J)
  376     CONTINUE
  375     CONTINUE
          ELSE
          NTBN=NT
          DO 377 I1=1,NTBN
          NM=NPAR(I1)
          IF(I1.EQ.NCUR) NM=1
          IF(I1.GT.NCUR) NM=NPAR(I1-1)
          NPSN(I1)=NM
          DO 378 J=1,NM
          SBN(I1,J)=SBPI(I1,J)
          YSNN(I1,J)=YSBMIN(I1,J)
          YSNX(I1,J)=YSBMAX(I1,J)
  378     CONTINUE
  377     CONTINUE
          ENDIF
C

C         CALCULATION OF REQUIRED TRANSLATION ON THE OPPOSITELY
C         DIRECTED SHEAR BANDS
C
          DO 160 J=1,NTR
          NSPA=NPARA(J)
                  DO 165  K=1,NSPA
                  SIA1(J,K)=SBRI(J,K)
                  YMIN1(J,K)=YSRMIN(J,K)
                  YMAX1(J,K)=YSRMAX(J,K)
  165             CONTINUE
  160             CONTINUE
          NPART=0
          DO 166 J=1,NTR
          NCO=1
          NSPA=NPARA(J)
                  DO 167 K=1,NSPA
```

```
              YINT=(SLP*SIA1(J,K)-SLR*CSBI)/(SLP-SLR)
              PAR=ABS(YINT-YMIN1(J,K))
              IF(PAR) 320,325,325
325           IF(YINT-YMIN1(J,K)) 320,330,330
330           PAR=ABS(YINT-YMAX1(J,K))
              IF(PAR) 320,335,335
335           IF(YINT-YMAX1(J,K)) 340,340,320
340           YIN=YINT
              XIN=(YIN-SIA1(J,K))/SLR
              KCUR=K
              NPART=NPART+1
              XP(NPART)=XIN
              YP(NPART)=YIN
              GO TO 170


320           IF(K.EQ.NSPA) THEN
              NCO=0
              ENDIF

167           CONTINUE

170     IF(NCO.EQ.0) GO TO 175
        LN=NPARA(J)+1
        IF(IP.EQ.1) THEN
                DO 180 K=1,KCUR
                YSRMIN(J,K)=YMIN1(J,K)+DY*IP
                YSRMAX(J,K)=YMAX1(J,K)+DY*IP
                DEL=SQRT((DX**2+DY**2)*2.)
                SBRI(J,K)=SBRI(J,K)+DEL
                        IF(K.EQ.KCUR) THEN
                        YSRMAX(J,K)=YIN+DY*IP
                        ENDIF
180             CONTINUE

        DO 181 K=KCUR+1,LN
        YSRMIN(J,K)=YMIN1(J,K-1)
        YSRMAX(J,K)=YMAX1(J,K-1)
        SBRI(J,K)=SIA1(J,K-1)
                        IF(K.EQ.KCUR+1) THEN
                        YSRMIN(J,K)=YIN
                        ENDIF
181     CONTINUE

        ELSE

                DO 185 K=1,KCUR
                YSRMIN(J,K)=YMIN1(J,K)
                YSRMAX(J,K)=YMAX1(J,K)
                SBRI(J,K)=SIA1(J,K)
                        IF(K.EQ.KCUR) THEN
                        YSRMAX(J,K)=YIN
                        ENDIF
185             CONTINUE

        DO 186  K=KCUR+1,LN
        YSRMIN(J,K)=YMIN1(J,K-1)+DY*IP
        YSRMAX(J,K)=YMAX1(J,K-1)+DY*IP
        DEL=SQRT((DX**2+DY**2)*2.)
        SBRI(J,K)=SIA1(J,K-1)-DEL
```

```
                    IF(K.EQ.KCUR+1) THEN
                    YSRMIN(J,K)=YIN+DY*IP
                    ENDIF
186     CONTINUE
        ENDIF
        NPARA(J)=LN
        GO TO 166

175     XMINP=(YMIN1(J,1)-SIA1(J,1))/SLR
        XMINC=(YSL-CSBI)/SLP
              PAR=ABS(XMINP-XMINC)
              IF(PAR-DELTA) 350,350,355
355           IF(XMINP-XMINC) 166,350,350
350           NSPA=NPARA(J)
              DO 187 K=1,NSPA
              DEL=SQRT((DX**2+DY**2)*2.)
              YSRMIN(J,K)=YMIN1(J,K)+DY*IP
              YSRMAX(J,K)=YMAX1(J,K)+DY*IP
              SBRI(J,K)=SIA1(J,K)+DEL*IP
187           CONTINUE

166     CONTINUE
C
        DO 400 J=1,NTR
        IF(NPARA(J).GE.NPMAX) THEN
        DMIN=YR(1)*SQ2
        NSPA=NPARA(J)
                DO 410 K=2,NSPA-2
                DIS=SQ2*(YSRMAX(J,K)-YSRMIN(J,K))
                IF(DIS.LT.DMIN) THEN
                DMIN=DIS
                NMIN=K
                ENDIF
410             CONTINUE
        SBRI(J,NMIN)=(SBRI(J,NMIN)+YSRMIN(J,NMIN+1))/2.
        YSRMAX(J,NMIN)=YSRMAX(J,NMIN+1)
                DO 420 K=NMIN+1,NSPA-2
                SBRI(J,K)=SBRI(J,K+1)
                YSRMIN(J,K)=YSRMIN(J,K+1)
                YSRMAX(J,K)=YSRMAX(J,K+1)
420             CONTINUE
        NPARA(J)=NPARA(J)-1
        ENDIF
400     CONTINUE
        IF(IP.EQ.1) THEN
        NTBN=NTR
        DO 380 J=1,NTR
        NPSN(J)=NPARA(J)
        NSPA=NPARA(J)
        DO 381 K=1,NSPA
        SBN(J,K)=SBRI(J,K)
        YSNN(J,K)=YSRMIN(J,K)
        YSNX(J,K)=YSRMAX(J,K)
381     CONTINUE
380     CONTINUE
        ELSE
        NTBP=NTR
        DO 382 J=1,NTR
        NPSP(J)=NPARA(J)
        NSPA=NPARA(J)
```

```
      DO 383 K=1,NSPA
      SBP(J,K)=SBRI(J,K)
      YSPN(J,K)=YSRMIN(J,K)
      YSPX(J,K)=YSRMAX(J,K)
 383  CONTINUE
 382  CONTINUE
      ENDIF
C
C
  50          CONTINUE
      RETURN
      END
```

```
      SUBROUTINE COCAL(NPR,NPL,IP)
C     THIS SUBROUTINE CALCULATES AND UPDATES COORDINATES
C     OF THE EXTERIOR POINTS OF THE SAMPLE AFTER
C     APPLYING REQUIRED TRANSLATION
      DIMENSION YPR(2500),XPR(2500),XPL(2500),YPL(2500)
      COMMON/B1/XR(2500),XL(2500),YR(2500),YL(2500)
      COMMON/B2/XNR,XNL,YNR,YNL,DX,DY,DELTA,STX
      DO 10 I=1,NPR-2
      XPR(I)=XR(I)
      YPR(I)=YR(I)
 10   CONTINUE
      DO 11 I=1,NPL-2
      XPL(I)=XL(I)
      YPL(I)=YL(I)
 11   CONTINUE
      JR=NPR-1
      JL=NPL-1
      MR=0
      ML=0
      IEX=0
      DO 20 I=1,JR
      IF(I.EQ.IEX) GOTO 15
      PAR=ABS(XPR(I)-XNR)
      IF(PAR-DELTA) 80,80,85
 85   IF(XPR(I)-XNR) 90,80,30
 90   IF(I.EQ.JR) GO TO 30
      XR(I)=XPR(I)
      YR(I)=YPR(I)
      GO TO 20
 80   XR(I)=XPR(I)
      XR(I+1)=XR(I)+STX
      YR(I)=YPR(I)
      YR(I+1)=YR(I)+DY*IP
      MR=2
      IEX=JR
      NPR=NPR-1
      GO TO 20
 30           IF(MR.EQ.0) THEN
              XR(I)=XNR
              XR(I+1)=XNR+STX
              YR(I)=YNR
              YR(I+1)=YR(I)+DY*IP
              MR=1
              ELSEIF(MR.EQ.2) THEN
              XR(I+1)=XPR(I)+DX
              YR(I+1)=YPR(I)+DY*IP
              ELSE
              XR(I+1)=XPR(I-1)+DX
              YR(I+1)=YPR(I-1)+DY*IP
              ENDIF
 20   CONTINUE

 15   IEX=0
      DO 60 I=1,JL
      IF(I.EQ.IEX) GOTO 70
      PAR=ABS(XPL(I)-XNL)
      IF(PAR-DELTA) 100,100,105
 105  IF(XPL(I)-XNL) 110,100,40
 110  IF(I.EQ.JL) GO TO 40
      XL(I)=XPL(I)
```

```
      YL(I)=YPL(I)
      GO TO 60
100   XL(I)=XPL(I)
      XL(I+1)=XL(I)+STX
      YL(I)=YPL(I)
      YL(I+1)=YL(I)+DY*IP
      ML=2
      IEX=JL
      NPL=NPL-1
      GO TO 60
40            IF(ML.EQ.0) THEN
              XL(I)=XNL
              XL(I+1)=XNL+STX
              YL(I)=YNL
              YL(I+1)=YL(I)+DY*IP
              ML=1
              ELSEIF(ML.EQ.2) THEN
              XL(I+1)=XPL(I)+DX
              YL(I+1)=YPL(I)+DX*IP
              ELSE
              XL(I+1)=XPL(I-1)+DX
              YL(I+1)=YPL(I-1)+DY*IP
              ENDIF
60    CONTINUE
70    RETURN
      END
```

```
      SUBROUTINE INCAL(IPAR,XMAX,XMIN,DINT,SLP,SL,
     *  CI,NL,NP,NPOS,XI,YI,NSB,NPNUM)
      DIMENSION X(2500),XMAX(1),XMIN(1),DINT(1)
      DIMENSION SL(1),CI(1),XI(1),YI(1),NSB(1)
      COMMON/B2/XNR,XNL,YNR,YNL,DX,DY,DELTA,STX
      N=0
      DO 10 I=1,NP
      DO 20 J=1,NL
      PAR=ABS(SL(J)-SLP)
      IF(PAR-DELTA) 20,20,30
30    X(J)=(DINT(I)-CI(J))/(SL(J)-SLP)
      PAR=ABS(X(J)-XMIN(J))
      IF(PAR-DELTA) 35,35,40
40    IF(X(J)-XMIN(J)) 20,35,35
35    PAR=ABS(X(J)-XMAX(J))
      IF(PAR-DELTA) 45,45,50
50    IF(X(J)-XMAX(J)) 44,45,20
44    IF(IPAR.EQ.1) GO TO 60
45    IF(IPAR.EQ.1) THEN
      PAR=ABS(SL(J+1)-SLP)
      IF(PAR-DELTA) 65,65,70
65    X(J)=XMAX(J+1)
70    GO TO 60
      ENDIF

      PAR=ABS(SL(J+1)-SLP)
      IF(PAR-DELTA) 55,55,60
55    PAR=ABS(X(J)-XMIN(J+1))
      IF(PAR-DELTA) 10,10,60
60    N=N+1
      XI(N)=X(J)
      YI(N)=SLP*XI(N)+DINT(I)
      NSB(N)=I
      GO TO 10
20    CONTINUE
10    CONTINUE
      NPOS=N
      RETURN
      END
```

```
      SUBROUTINE MNCSBC(NPOS,NPMIN,SLP,SLR)
C     THIS SUBROUTINE SELECTS THE SHEAR BANDS WITH MINIMUM NUMBER
C     OF SHEAR BANDS CROSSING THEM
      DIMENSION NP(1250),DIFP(1250),NID(1250)
      COMMON/SB2/NPARA(1250),SBRI(1250,50),YSRMIN(1250,50),
     * YSRMAX(1250,50)
      COMMON/B2/XNR,XNL,YNR,YNL,DX,DY,DELTA,STX
      COMMON/B3/IPRINT,NT,NTR,NPMAX
      COMMON/C1/XNRC(1250),XNLC(1250),YNRC(1250),YNLC(1250)
      COMMON/C2/XNRP(1250),XNLP(1250),YNRP(1250),YNLP(1250)

      DO 100 I=1,NPOS
      XNLP(I)=XNLC(I)
      XNRP(I)=XNRC(I)
      YNRP(I)=YNRC(I)
      YNLP(I)=YNLC(I)
100   CONTINUE
      MF=NPOS
      DO 150 I=1,MF
      DIFP(I)=YNLP(I)-SLP*XNLP(I)
150   CONTINUE
      DO 160  I=1,MF
      NP(I)=0
      DO 170 J=1,NTR
      NBR=NPARA(J)
      DO 180 K=1,NBR
      YSEC=(SLR*DIFP(I)-SBRI(J,K)*SLP)/(SLR-SLP)
      PAR=ABS(YSEC-YSRMIN(J,K))
      IF(PAR-DELTA) 190,190,195
195   IF(YSEC-YSRMIN(J,K)) 180,190,190
190   PAR=ABS(YSEC-YSRMAX(J,K))
      IF(PAR-DELTA) 210,210,200
200   IF(YSEC-YSRMAX(J,K)) 210,210,180
210   NP(I)=NP(I)+1
180   CONTINUE
170   CONTINUE
160   CONTINUE
      NPMIN=NP(1)
      N=1
      NID(1)=1
      IF(MF.EQ.1) GO TO 260
      DO 250 I=2,MF
      IF(NP(I).LT.NPMIN) THEN
      N=1
      NPMIN=NP(I)
      NID(N)=I
      ELSEIF(NP(I).EQ.NPMIN) THEN
      N=N+1
      NID(N)=I
      ENDIF
250   CONTINUE
260   NPOS=N
      DO 300 I=1,NPOS
      J=NID(I)
      XNRC(I)=XNRP(J)
      XNLC(I)=XNLP(J)
      YNRC(I)=YNRP(J)
      YNLC(I)=YNLP(J)
300   CONTINUE
280   RETURN
      END
```

```
      SUBROUTINE ELCAL(NP,X,Y,SL,CI,XMAX,YMAX,XMIN,YMIN)
      DIMENSION X(1),Y(1),SL(1)
      DIMENSION CI(1),XMAX(1),YMAX(1)
      DIMENSION XMIN(1),YMIN(1)
      COMMON/B2/XNR,XNL,YNR,YNL,DX,DY,DELTA,STX
      DO 10 I=1,NP-1
      SL(I)=(Y(I+1)-Y(I))/(X(I+1)-X(I))
      CI(I)=(Y(I+1)+Y(I)-SL(I)*(X(I+1)+X(I)))/2.
      XMIN(I)=X(I)
      XMAX(I)=X(I+1)
      Y1=Y(I)
      Y2=Y(I+1)
      PAR=ABS(Y1-Y2)
      IF(PAR-DELTA) 20,20,25
25    IF(Y1-Y2) 30,20,20
20    YMAX(I)=Y1
      YMIN(I)=Y2
      GO TO 10
30    YMAX(I)=Y2
      YMIN(I)=Y1
10    CONTINUE
      RETURN
      END
```

```
      SUBROUTINE RANNUM(Z)
      INTEGER A,X
      DATA I/1/
      IF(I.EQ.0) GO TO 1
      I=0
      M=2**20
      FM=M
      X=234567
      A=2**10+3
1     X=MOD(A*X,M)
      FX=X
      Z=FX/FM
      RETURN
      END
```

```
      SUBROUTINE SELECT(NPOS,NOPT,NREST)
      DIMENSION ISEL(1250),IOR(1250)
      COMMON/C1/XNRC(1250),XNLC(1250),YNRC(1250),YNLC(1250)
      COMMON/C2/XNRP(1250),XNLP(1250),YNRP(1250),YNLP(1250)
      DO 5 I=1,NPOS
      XNLP(I)=XNLC(I)
      XNRP(I)=XNRC(I)
      YNLP(I)=YNLC(I)
      YNRP(I)=YNRC(I)
 5    CONTINUE
      IF(NPOS.EQ.1) GO TO 280
      IF(NPOS.LE.NREST) GO TO 280
      DO 10 I=1,NPOS
270   CALL RANNUM(Z)
      ICH=INT(Z*NPOS)+1
      IF(ICH.GT.NPOS) GO TO 270
      JCUR=I
      IF(JCUR.EQ.1) GO TO 15
      DO 20 J=1,JCUR-1
      IF(ISEL(J).EQ.ICH) GO TO 270
20    CONTINUE
15    ISEL(I)=ICH
10    CONTINUE
         NTOT=NPOS
         DO 30 I=1,NPOS
         MNUM=ISEL(1)
              DO 40 J=1,NTOT
              IF(ISEL(J).LT.MNUM) THEN
              MNUM=ISEL(I)
              JCUR=J
              ENDIF
40            CONTINUE
         NTOT=NTOT-1
         IOR(I)=MNUM
         IF(NTOT.EQ.1) GO TO 30
         IF(JCUR.GT.NTOT) GO TO 30
         DO 50 K=JCUR,NTOT
         ISEL(K)=ISEL(K+1)
50       CONTINUE
30    CONTINUE
      DO 70 I=1,NPOS
      ICH=IOR(I)
      XNRC(I)=XNRC(ICH)
      YNRC(I)=YNRC(ICH)
      XNLC(I)=XNLC(ICH)
      YNLC(I)=YNLC(ICH)
70    CONTINUE
280   RETURN
      END
```

```
      SUBROUTINE MNCSBC(NPOS,NPMIN,SLP,SLR)
C     THIS SUBROUTINE SELECTS THE SHEAR BANDS WITH MINIMUM NUMBER
C     OF SHEAR BANDS CROSSING THEM
      DIMENSION NP(1250),DIFP(1250),NID(1250)
     COMMON/SB2/NPARA(1250),SBRI(1250,50),YSRMIN(1250,50),
    * YSRMAX(1250,50)
      COMMON/B2/XNR,XNL,YNR,YNL,DX,DY,DELTA,STX
      COMMON/B3/IPRINT,NT,NTR,NPMAX
      COMMON/C1/XNRC(1250),XNLC(1250),YNRC(1250),YNLC(1250)
      COMMON/C2/XNRP(1250),XNLP(1250),YNRP(1250),YNLP(1250)

      DO 100 I=1,NPOS
      XNLP(I)=XNLC(I)
      XNRP(I)=XNRC(I)
      YNRP(I)=YNRC(I)
      YNLP(I)=YNLC(I)
100   CONTINUE
      MF=NPOS
      DO 150 I=1,MF
      DIFP(I)=YNLP(I)-SLP*XNLP(I)
150   CONTINUE
      DO 160  I=1,MF
      NP(I)=0
      DO 170 J=1,NTR
      NBR=NPARA(J)
      DO 180 K=1,NBR
      YSEC=(SLR*DIFP(I)-SBRI(J,K)*SLP)/(SLR-SLP)
      PAR=ABS(YSEC-YSRMIN(J,K))
      IF(PAR-DELTA) 190,190,195
195   IF(YSEC-YSRMIN(J,K)) 180,190,190
190   PAR=ABS(YSEC-YSRMAX(J,K))
      IF(PAR-DELTA) 210,210,200
200   IF(YSEC-YSRMAX(J,K)) 210,210,180
210   NP(I)=NP(I)+1
180   CONTINUE
170   CONTINUE
160   CONTINUE
      NPMIN=NP(1)
      N=1
      NID(1)=1
      IF(MF.EQ.1) GO TO 260
      DO 250 I=2,MF
      IF(NP(I).LT.NPMIN) THEN
      N=1
      NPMIN=NP(I)
      NID(N)=I
      ELSEIF(NP(I).EQ.NPMIN) THEN
      N=N+1
      NID(N)=I
      ENDIF
250   CONTINUE
260   NPOS=N
      DO 300 I=1,NPOS
      J=NID(I)
      XNRC(I)=XNRP(J)
      XNLC(I)=XNLP(J)
      YNRC(I)=YNRP(J)
      YNLC(I)=YNLP(J)
300   CONTINUE
280   RETURN
      END
```

```
      SUBROUTINE FIND(XG,YG,FCAL)
C     THIS PROGRAM CALCULATES THE VALUE OF THE FUNCTION
C     ON A TWO DIMENSIONAL GEOMETRY BY BI-CUBIC SPLINE
C
      COMMON/F1/NX,NY,X(50),Y(50),F(50,50)
      DIMENSION B(50),C(50),D(50),FX(50),FY(50),XP(50),YP(50)
      NXP=NX
      NYP=NY
      DO 10 I=1,NY
      DO 20 J=1,NX
      FX(J)=F(I,J)
      XP(J)=X(J)
 20   CONTINUE
      CALL SPLINE(NXP,XP,FX,B,C,D)
      FY(I)=SEVAL(NXP,XG,X,FX,B,C,D)
      YP(I)=Y(I)
 10   CONTINUE
      CALL SPLINE(NYP,YP,FY,B,C,D)
      FCAL=SEVAL(NYP,YG,Y,FY,B,C,D)
      RETURN
      END
```

```
      SUBROUTINE SPLINE(N,X,Y,B,C,D)
C=====================================================================
C
C          THE COEFFICIENTS B(I),C(I), AND D(I), I=1,2,...,N
C    ARE COMPUTED. FOR A CUBIC SPLINE INTERPOLATION
C
C    S(X) = Y(I) + B(I)*(X-X(I))+C(I)*(X-X(I))**2 + D(I)*(X-X(I))**3
C
C       FOR X(I) .LE. X .LE. X(I+1)
C
C    INPUT...
C
C    N - THE NUMBER OF DATA POINTS (N.GE.2)
C    X - THE ABSCISSAS OF THE DATA POINTS IN STRICTLY INCREASING
C        ORDER.
C    Y       - THE ORDINATES OF THE DATA POINTS.
C
C    OUTPUT...
C
C    B,C,D  - ARRAYS OF SPLINE COEFFICIENTS AS DEFINED ABOVE
C
C       USING P TO DENOTE DIFFERENTION,
C
C       Y(I)  = S( X(I) )
C       B(I)  = SP( X(I) )
C       C(I)  = SPP( X(I) )
C       D(I)  = SPPP( X(I) )/6 (DERIVATIVE FROM THE RIGHT)
C
C       ACCOMPANIYING FUNCTION PROGRAMS SEVAL, DEVAL CAN BE USED TO
C       EVALUATE SPLINE.
C
C       PRECISION - SINGLE
C
C    FROM:     COMPUTER METHODS FOR MATH. COMPUTATIONS
C              FORSYTHE, MALCOLM, AND MOLER
C              PAGE: 77-78
C
C=====================================================================
      INTEGER N,NM1,IB,I
      DIMENSION X(N),Y(N),B(N),C(N),D(N)
C
      NM1 = N - 1
      IF(N.LT.2) RETURN
      IF(N.LT.3) GO TO 50
C
      D(1) = X(2) - X(1)
      C(2) = (Y(2) - Y(1))/D(1)
      DO 10 I=2,NM1
         D(I) = X(I+1) - X(I)
         B(I) = 2.0E00*(D(I-1) + D(I) )
         C(I+1) = (Y(I+1) - Y(I) )/D(I)
         C(I) = C(I+1) - C(I)
10    CONTINUE
C
C
      B(1) = - D(1)
      B(N) = - D(N-1)
      C(1) = 0.0
      C(N) = 0.0
      IF(N.EQ.3) GO TO 15
```

```
      C(1) = C(3)/(X(4) - X(2)) - C(2)/( X(3) - X(1) )
      C(N) = C(N-1)/(X(N) - X(N-2)) - C(N-2)/(X(N-1)-X(N-3))
      C(1) = C(1)*D(1)**2/(X(4)-X(1))
      C(N) = -C(N)*D(N-1)**2/( X(N)- X(N-3) )
CC
15    DO 20 I=2,N
         T = D(I-1)/B(I-1)
         B(I) =  B(I) - T*D(I-1)
         C(I) =  C(I) - T*C(I-1)
20    CONTINUE
C
      C(N) = C(N)/B(N)
      DO 30 IB = 1,NM1
         I = N-IB
         C(I) = (C(I)-D(I)*C(I+1))/B(I)
30    CONTINUE
C
      B(N) = (Y(N)-Y(NM1))/D(NM1)+D(NM1)*(C(NM1)+2.0*C(N))
      DO 40 I=1,NM1
         B(I) = (Y(I+1)-Y(I))/D(I) - D(I)*(C(I+1)+2.0*C(I))
         D(I) = (C(I+1)-C(I))/D(I)
         C(I) = 3.0E00*C(I)
40    CONTINUE
      C(N) = 3.0E00*C(N)
      D(N) = D(N-1)
      RETURN
C
50    B(1) = (Y(2)-Y(1))/(X(2)-X(1))
      C(1) = 0.0
      D(1) = 0.0
      B(2) = B(1)
      C(2) = 0.0
      D(2) = 0.0
      RETURN
      END


      FUNCTION SEVAL(N,U,X,Y,B,C,D)
C=====================================================================
C
C          THIS SUBROTINE EVALUATES THE CUBIC SPLINE FUNCTION.
C
C       SEVAL = Y(I)+B(I)*(U-X(I))+C(I)*(U-X(I))**2+D(I)*(U-X(I))**3
C
C       WHERE X(I) .LT. U .LT. X(I+1) , USING HORNER'S RULE
C
C       IF( U .LT. X(I) ) THEN  I = 1 IS USED.
C       IF( U .GE. X(N) ) THEN  I = N IS USED.
C
C       INPUT...
C
C       N       - THE NUMBER OF DATA POINTS
C       U       - THE ABSCISSA AT WHICH THE SPLINE IS TO BE EVALUATED.
C       X,Y     - THE ARRAYS OF DATA ABSCISSAS AND ORDINATES
C       B,C,D   - ARRAYS OF SPLINE COEFFICIENTS COMPUTED BY SPLINE
C
C
C       PRECISION - SINGLE
C
```

```
C     FROM :   COMPUTER METHODS FOR MATH. COMPUTATIONS
C              FORSYTHE,MALCOLM,MOLER
C     PURPOSE: EVALUATION OF THE CUBIC SPLINE FUNCTIONS
C              B,C,D ARTE COMPUTED BY SPLINE
C=====================================================================
      INTEGER N,I,J,K
      REAL U,X(N),Y(N),B(N),C(N),D(N),DX,SEVAL
      DATA I/1/
C
      IF(I.GE.N) I=1
      IF(U.LT.X(I)) GO TO 10
      IF(U.LE.X(I+1)) GO TO 30
C
10    I= 1
      J = N + 1
20    K = (I+J)/2
      IF(U.LT.X(K)) J=K
      IF(U.GE.X(K)) I=K
      IF(J.GT.(I+1)) GO TO 20
C
30    DX = U - X(I)
      SEVAL = Y(I) + DX*(B(I)+DX*(C(I)+DX*D(I)))
      RETURN
      END


        SUBROUTINE CALINT(A,B,FUN,RES)
        EXTERNAL FUN,SPLINE,SEVAL
C       THIS FUNCTION PERFORMS INTEGRATION OF FUNTION "FUN"
C       ACCORDING TO 8 POINT GAUSSIAN QUADRATURE
C
        COMMON/F2/W(8),XAB(8)
        RES=0.
        DO 10 I=1,8
        Y=(B-A)/2.*XAB(I)+(B+A)/2.
        RES=RES+W(I)*FUN(Y)
 10     CONTINUE
        RES=(B-A)*RES/2.
        RETURN
        END


        FUNCTION FUN1(X)
        COMMON/F3/AVL,SDL
        FUN1=X/2.5066/SDL*EXP(-((X-AVL)/SDL)**2/2.)
        RETURN
        END

        FUNCTION FUN2(X)
        COMMON/F3/AVL,SDL
        COMMON/F4/APAR,TAU,TIME,VELP,VELCO
        BETA=APAR/X/TAU
        TETA=VELCO*TAU**VELP*TIME/X
        CALL FIND(BETA,TETA,SNORM)
        FUN2=X/2.5066/SDL*SNORM*EXP(-((X-AVL)/SDL)**2/2.)
        RETURN
        END
```

```
      BLOCK DATA PARAM
      COMMON/F2/W(8),XAB(8)
      DATA XAB/-0.18343,-0.52553,-0.796666,-0.9602898,0.96028,
     *  0.796666,0.52553,0.18343/
      DATA W/0.36268,0.31370,0.22238,0.1012285,0.1012285,
     *  0.222381,0.31370,0.36268/
      END


     SUBROUTINE GUESS3(F,X,XNEW,INEW,DERR,DERA)
     IMPLICIT REAL(A-H,O-Z)
C=============================================
C  F RIGHT HAND SIDE
C  X
C  XNEW NEW GUESS
C  INEW COMPONENT OF X WHICH HAS THE MAX ERR.
C  DERR REL ERROR MAX X(I),XNEW
C  DERA ABS DMAX1(ABS(F(I)))
C---------------------------------------------
      DIMENSION F(3),X(3)
C      IO6=6
      SMALL = 1.0E-12
      DERR=0.0
      DERA=0.0
      DO 10 I=1,3
         IF(ABS(F(I)).LT.1.E-S) THEN
         XNEW=X(I)
         GO TO 101
         ENDIF
C
         IF(ABS(F(I)).LE.DERA) GO TO 10
         INEW=I
         DERA=ABS(F(I))
 10   CONTINUE
      DX1 = X(1) - X(2)
      DX2 = X(3) - X(1)
      DX3 = X(2) - X(3)
      F12 = F(1)*F(2)*DX1
      F13 = F(1)*F(3)*DX2
      F23 = F(2)*F(3)*DX3
      FFF = F12+F13+F23
      FFT = (F(1)*F(3)-F(2)*F(3))*DX2*DX3
      IF(ABS(FFF).LT.SMALL) GO TO 100
      XNEW = FFT/FFF + X(3)
      DO 20 I=1,3
      DERR=AMAX1(DERR,ABS( (XNEW-X(I))/(XNEW-SMALL) ))
 20   CONTINUE
      GO TO 99
 100  XNEW = (X(1)+X(2)+X(3))/3.0
      WRITE(6,*) 'N/O IN GUESS3',(X(I),I=1,3)
 99   CONTINUE
 101  RETURN
      END
```

```
      SUBROUTINE SHCAL(IS,FRLEN,XLEN,SHDIS,T,NREST,MF)
      EXTERNAL FUN1,FUN2
      DIMENSION XG(3),YG(3)
      COMMON/F3/AVL,SDL
      COMMON/F4/APAR,TAU,TIME,VELP,VELCO
      COMMON/F5/ALP,BURV,PPN,CHV,ERR,SHMAX,SHMIN,DTAU,DELT
      COMMON/F6/SLMIN,SLMAX,XHEIG,ALEN,EPS
      COMMON/F7/ICO,NTOT,SHOLD,DPOLD,SBM,CHOLD,TOLD
      SLN=SLMIN
      SLX=SLMAX
      ALEN=AVL
      ICN=1
      CRITL=TIME*1.5*VELCO*TAU**VELP
      IF(SLN.LT.CRITL) SLN=CRITL
      IF(ALEN.LT.SLN) ALEN=SLN+5.E-3
      IF(SLX.LT.ALEN) SLX=ALEN+5.E-3
      CALL CALINT(SLN,SLX,FUN1,RES)
      DPN=XLEN*FRLEN/RES
      ICM=0
      ICP=0
      IF(NREST.NE.0) GO TO 40
5     IF(IS.EQ.2) THEN
      NTOT=NTOT+1
      GO TO 8
      ENDIF
      ICR=0
8     CH1=CHV/NTOT
      TIME=1.E-3
      DO 10 I=1,3
      TIME=TIME+(I-1)*DELT
      CALL CALINT(SLN,SLX,FUN2,RES)
      CH=BURV*PPN*DPN*RES/XLEN/TIME/SQRT(2.)
      YG(I)=CH1-CH
      XG(I)=TIME
10    CONTINUE
20    CALL GUESS3(YG,XG,XNEW,INEW,DERR,DERA)
      TIME=XNEW
      CALL CALINT(SLN,SLX,FUN2,RES)
      CH=BURV*PPN*DPN*RES/XLEN/TIME/SQRT(2.)
      YG(INEW)=CH1-CH
      XG(INEW)=XNEW
      DO 30 I=1,3
      IF(ABS(YG(I)).LT.ERR) THEN
      CH=CH1-YG(I)
      TIME=XG(I)
      GO TO 25
      ENDIF
30    CONTINUE
      IF(ICM.EQ.5.AND.IS.EQ.2) THEN
      ICM=0
      NTOT=NTOT+1
      GO TO 8
      ENDIF
         ICM=ICM+1
         ICN=ICN+1
         IF(ICN.GE.20) THEN
         WRITE(6,*) '15 TRIALS WITH GUESS3'
         STOP
         ENDIF
      GO TO 20
```

```
25      SHDIS=CH1*TIME*SQRT(2.)
        IF(SHDIS.LT.SHMIN) THEN
        IF(ICO.EQ.0) THEN
        TAOL=TAU
        DELTAU=DTAU*10.
        ELSE
        DELTAU=FTAU
        GO TO 26
        ENDIF
        IF(ICP.EQ.1) THEN
        DELTAU=DTAU*5.
        ENDIF
26      TAU=TAU+DELTAU
        NTOT=NTOT-1
        ICP=1
        GO TO 8
        ENDIF
        IF(ICR.EQ.1) GO TO 35
        IF(TIME.GE.TOLD) THEN
        TAU=TAU+DTAU
        GO TO 8
        ENDIF
35      IF(SHDIS.GT.SHMAX) THEN
        IF(ICP.EQ.1) THEN
        TAU=TAU+DTAU
        GO TO 8
        ENDIF
        NTOT=NTOT+1
        ICR=1
        GO TO 8
        ENDIF
        CHOLD=CH
        NREST=NTOT-1
        SHOLD=SHDIS
        DPOLD=DPN
        SBM=XLEN
        TOLD=TIME
        EPST=EPS+0.032
        WRITE(6,2500) IS,NREST,SHDIS,TAU,CH,TIME,EPST
        IF(ICO.EQ.0) THEN
        FTAU=TAU-TAOL
        ICO=1
        ENDIF
        T=T+TIME
        GO TO 2600
40      SHDIS=SHOLD*DPN/DPOLD*SBM/XLEN
        IF(SHDIS.LT.SHOLD) THEN
        SHOLD=SHDIS
        DPOLD=DPN
        SBM=XLEN
        ENDIF
        NREST=NREST-MF
        DELT=TIME/1.8
2500    FORMAT(2X,I4,1X,I3,1X,E12.6,1X,F8.4
     *  ,1X,E12.6,1X,E12.6,2X,E12.6)
2600    RETURN
        END
```